

Targeting the EGF-receptor and the CD38/NADase in
solid and hematological malignancies with nanobody-
based heavy chain antibodies and AAV vectors

Dissertation

Dissertation with the aim of achieving a doctoral degree
at the Faculty of Mathematics, Informatics and Natural Sciences
Department of Biology,
University Hamburg

submitted by
Natalie Baum
from Nördlingen

Hamburg, November 2020

“Even if it will not work out, even if you fail, it doesn’t matter, because the earth will keep moving and you have the chance to rearrange yourself and redecide over things every single day”.

My favorite quote from my dad, Peter Baum

First examiner

Prof. Dr. Friedrich Koch-Nolte
University hospital Hamburg-Eppendorf (UKE)
Institute of immunology
Martinistr. 52
20246 Hamburg

Second examiner

Prof. Dr. Julia Kehr
University of Hamburg
MIN faculty – Department of biology
Ohnhorststr. 18
22609 Hamburg

Day of disputation: 26.02.2021

Publications and congress contributions

Publications

Baum N, Fliegert R, Bauche A, Hambach J, Menzel S, Bannas P, Koch-Nolte F. Daratumumab and Nanobody-Based Heavy Chain Antibodies Inhibit the ADPR Cyclase but not the NAD⁺ Hydrolase Activity of CD38-Expressing Multiple Myeloma Cells. *Cancers (Basel)*. 2020 Dec; 13 (1):76

Baum N‡, Eggers M‡, Königsdorf J, Menzel S, Hambach J, Staehler T, Fliegert R, Kulow F, Adam G, Haag F, Bannas P‡, Koch-Nolte‡. Mouse CD38-Specific Heavy Chain Antibodies Inhibit CD38 Enzyme Activity and Mediate Cytotoxicity Against Tumor Cells. *Front. Immunol.* 2021 Sept; doi: 10.3389/fimmu.2021.703574

Tintelnot J, **Baum N**, Schultheiß C, Braig F, Trentmann M, Finter J, Fumey W, Bannas P, Fehse B, Riecken K, Schuetze K, Bokemeyer C, Rösner T, Valerius T, Peipp M, Koch-Nolte F, Binder M. Nanobody Targeting of Epidermal Growth Factor Receptor (EGFR) Ectodomain Variants Overcomes Resistance to Therapeutic EGFR Antibodies. *Mol Cancer Ther.* 2019 Apr;18(4):823-833.

Eichhoff M A, Börner K, Albrecht B, Schäfer W, **Baum N**, Buck F, Haag F, Körbelin J, Trepel M, Braren I, Grimm D, Adiouch S, Koch-Nolte F. Nanobody-enhanced targeting of AAV gene therapy vectors. *Mol Ther Methods Clin Dev.* 2019 Dec; 15: 211-220.

Schriewer L,‡, Schütze K,‡, Petry K,‡, Hambach J, Fumey W, Koenigsdorf J, **Baum N**, Menzel S, Rissiek B, Riecken K, Fehse B, Schmid J, Albrecht B, Pinnschmidt H, Ayuk F, Kröger N, Binder M, Schuch G, Hansen T, Stortelers C, Haag F, Adam G, Koch-Nolte F,‡, Bannas P,‡. CD38-specific heavy chain antibodies induce killing of multiple myeloma and other hematological malignancies. *Theranostics.* 2020; 10(6): 2645-2658.

Hambach J, Riecken K, Cichutek S, Schütze K, Albrecht B, Petry K, Röckendorf J L, **Baum N**, Kröger, Hansen T, Schuch G, Haag F, Adam G, Fehse B, Bannas P,‡, Koch-Nolte F,‡. Targeting CD38-Expressing Multiple Myeloma and Burkitt Lymphoma Cells in Vitro with Nanobody-Based Chimeric Antigen Receptors (Nb-CARS). *Cells.* 2020 Feb; 9(2):321.

Congress contributions (poster)

Baum N, Fumey W, Hambach J, Eichhoff A M, Petry K, Röckendorf J, Albrecht B, Schütze K, Körbelin J, Trepel M, Riecken K, Fehse B, Fliegert R, Braig F, Binder M, Rösner T, Peipp M, Börner K, Grimm D, Bannas P, Koch-Nolte F, Targeting the EGF-receptor and CD38 in solid and hematological malignancies with nanobody-based heavy chain antibodies and AAV vectors. European Society for Medical Oncology, Geneva (Dec 2019) → Merit Award

Schäfer W, Eichhoff A, Börner K, Albrecht B, **Baum N**, Haag F, Körbelin J, Trepel M, Grimm D, Adriouch S, Koch-Nolte F. Using nanobodies directed against cell surface proteins to enhance cell-specific targeting of AAV gene therapy vectors. 1st Nanobody Symposium, Bonn (Aug2018)

Table of Contents

Publications and congress contributions	V
Table of Contents	VII
Abstract	X
Zusammenfassung	XI
1. Introduction.....	1
1.1. Overexpressed surface antigens in head-and neck cancer, metastatic colorectal cancer and multiple myeloma	1
1.1.1. Structure and function of the epidermal growth factor receptor (EGFR)	1
1.1.2. Structure and function of the ecto-NADase CD38	3
1.2. Anti-tumor effects mediated by therapeutic mAbs	4
1.2.1. The mode of action of the EGFR-specific mAbs cetuximab and panitumumab	5
1.2.2. The mode of action of the CD38-specific mAbs isatuximab and daratumumab	6
1.3. Nanobody-mediated targeting of Adeno-associated viral (AAV) vectors	7
2. Objectives of this PhD thesis.....	8
3. Materials.....	9
3.1. Laboratory devices	9
3.2. Chemicals	10
3.3. Buffers and solutions	11
3.4. Cell Culture Media	12
3.5. Antibodies	13
3.6. Plasmids	14
3.7. Size standard for proteins and DNA	14
3.8. Enzymes.....	15
3.9. Oligonucleotides	15
3.10. Cell lines	15
4. Methods	17
4.1. Cell lines	17
4.1.1. Murine cell lines	17
4.1.2. Human cell lines and primary patient samples	17
4.2. Llama immunizations and construction of a phage library.....	18
4.3. Phage-panning based selection of nanobodies against mouse CD38	19
4.4. Construction of monospecific heavy chain antibodies (hcAbs)	20
4.4.1. PCR-based amplification of selected VHHs	20
4.4.2. Endonuclease based digestion of inserts and vectors.....	21
4.4.3. Dephosphorylation of vector DNA	21
4.4.4. Agarose gel electrophoresis and PCR-DNA clean up	21
4.4.5. Quantification of DNA	22
4.4.6. Ligation of DNA fragments	22
4.4.7. Transformation of chemically competent <i>E. coli</i> bacteria.....	22

4.4.8. Isolation of plasmid DNA	23
4.4.9. Sequencing of isolated DNA	23
4.5. PCR Mutagenesis	23
4.6. Transient transfection of HEK293-6E cells with recombinant hcAbs	24
4.7. SDS-Polyacrylamide gel electrophoresis and Coomassie staining	24
4.8. Protein purification.....	25
4.9. Calculation of protein concentration from purified hcAbs.....	25
4.10. Fluorochrome conjugation of heavy chain antibodies.....	26
4.11. Cross-blockade analyses on mouse CD38 epitope	26
4.12. Dissociation assay of anti-mouse CD38 hcAbs	26
4.13. Transient transfection of HEK-T cells with mouse- and human CD38	27
4.14. CDC of transiently transfected HEK-T-mCD38 cells	27
4.15. ADCC of mouse thymoma cell lines	28
4.16. Human EGFR-specific antibody and -nanobody binding to EGFR-escape variants	28
4.17. Cellular proliferation assay of human EGFR-escape variant – and WT cells	28
4.18. 3D Spheroid proliferation assay of human EGFR WT- and EGFR R521K cells	29
4.19. Construction of humanized 7D12-E345R-hcAb and 7D12-G236A-S239D- I332E-hcAb	29
4.20. CDC-mediated killing of HNSCC cell lines	29
4.21. ADCC mediated killing of HNSCC cell lines	30
4.22. Fluorometric enzyme assay of mouse thymoma and human myeloma cells	30
4.23. HPLC analysis of a human myeloma- and murine thymoma cell line	31
4.24. Marker expression of primary patient bone marrow cells	32
4.25. CDC and ADCC of primary MM cells from patient bone marrow	32
4.26. Synthesis of recombinant Nanobody-displaying AAV for transduction of primary MM cells.....	33
4.27. Synthesis of antiAAV-antiCD38 bispecific adaptor proteins to mediate AAV transduction of primary MM cells	34
4.28. Data evaluation and statistical analysis.....	34
5. Results	35
5.1. Selection and characterization of mouse CD38-specific nanobodies.....	35
5.1.1. Phage display selection yields 5 families of mouse CD38-specific nanobodies	35
5.1.2. Generation and site directed mutagenesis of heavy chain antibodies	36
5.1.3. Cross blockade analyses reveal three independent epitopes on mouse CD38.....	37
5.1.4. hcAbs of family 4 show the slowest dissociation from mouse CD38, i.e. the highest binding avidity for CD38	38
5.1.5. mCD38-expressing EL4-thymoma cells metabolize NAD ⁺ to ADPR	40
5.1.6. Family 4 and 5 hcAbs strongly inhibit the NGD cyclase activity of mouse CD38.....	41

5.1.7. Fc-engineered hcAbs mediate CDC-dependent lysis of mCD38-transfected human embryonic kidney (HEKT) cells.....	46
5.1.8. CD38-specific hcAbs mediated ADCC against mouse CD38-expressing EL4 thymoma cells	47
5.2. Retargeting of solid and hematological malignancies with hcAbs	49
5.2.1. EGFR-specific hcAb 7D12 inhibits the proliferation of EGFR-escape variant cells	49
5.2.2. Human CD38-specific hcAbs against epitope 2 inhibit the NGD cyclase activity of CD38 expressing human LP1 myeloma cells	51
5.2.3. Fc-engineered EGFR- and CD38-specific hcAbs induce CDC and ADCC of human tumor cell lines	55
5.2.4. Cultivation of primary multiple myeloma cells from patient bone marrow samples may alter their sensitivity toward CDC	56
5.3. Using nanobodies to improve the targeting of tumor cells by AAV.....	60
5.3.1. Display of CD38-specific nanobody on the AAV-capsid specifically enhances the transduction of primary MM cells from a patient bone marrow	61
5.3.2. Bispecific adaptors enhance specific transduction of primary MM cells by AAV.....	62
6. Discussion	63
6.1. Mouse CD38 nanobody discovery and generation of heavy chain antibodies	63
6.2. Targeting EGFR-variants and CD38 with heavy chain antibodies	65
6.2.1. Direct effects of EGFR- and CD38-specific hcAbs	65
6.2.2. Indirect effects of EGFR- and CD38 specific hcAbs	69
6.3. Using αCD38 nanobodies to enhance cell-specific targeting of AAV gene therapy vectors.....	72
7. Conclusion and Outlook.....	74
8. Lists	75
8.1. List of abbreviations	75
8.2. List of figures.....	78
8.3. List of tables.....	79
9. References.....	80
10. Acknowledgements	87
11. Declaration on oath/Eidesstattliche Versicherung.....	88
12. Confirmation on accurate language	89

Abstract

Targeted tumor therapy with monoclonal antibodies (mAbs) is based on targeting mutated, selectively expressed or overexpressed cell surface antigens such as the epidermal growth factor receptor (EGFR) or the NAD-hydrolase CD38. However, not all patients respond to targeted therapy. Moreover, many patients develop resistance towards the therapeutic mAb. Patients with head and neck cancer (HNSCC) or metastatic colorectal cancer (mCRC) may develop mutations of the EGFR that result in loss of binding by the mAbs cetuximab and panitumumab. In patients with Multiple Myeloma (MM), loss of CD38 from the cell surface may render tumor cells inaccessible for the α CD38-specific mAb daratumumab and consequently resistant against antibody-mediated effector functions, such as natural killer cell (ADCC)- and complement-dependent (CDC) lysis.

The goal of this thesis was to improve the targeting of EGFR and CD38 overexpressing tumor cells with nanobody-based heavy chain antibodies (hcAb) and Adeno-associated viral (AAV) vectors. Nanobodies comprise a single variable domain of 15 kilo Dalton (kDa). The results show that nanobody 7D12, in contrast to cetuximab, can bind to EGFR epitope escape variants and subsequently inhibit the proliferation of EGFR variant cells. In case of CD38, some nanobodies inhibited the enzymatic activities of CD38 more effectively than daratumumab. To allow Fc-mediated effector functions, selected α EGFR and α CD38 nanobodies were fused to the hinge, CH2, and CH3 domains of human IgG1. These chimeric llama/human heavy chain antibodies (hcAb) are about half the size of conventional mAbs (75 kDa vs. 150 kDa). The Fc-optimized 7D12-hcAb mediated effective ADCC and CDC also against cells expressing EGFR ECD variants that did not respond to cetuximab or panitumumab. In primary bone marrow samples from MM patients the combination of daratumumab with α CD38 hcAbs mediated more effective CDC than daratumumab alone. Finally, CD38-specific nanobodies mediated more effective transduction of CD38+ MM cells by recombinant AAVs.

The results of this thesis pave the way for novel therapeutic approaches against EGFR or CD38 overexpressing solid and hematological malignancies.

Zusammenfassung

Die zielgerichtete Tumor-Therapie mit monoklonalen Antikörpern (mAbs) bei soliden und hämatologischen Tumoren basiert auf Antikörpern gegen mutierte, selektiv exprimierte oder überexprimierte Zelloberflächenantigene, z.B. dem epidermalen Wachstumsfaktorrezeptor (EGFR) oder der CD38 NAD-Hydrolase. Es sprechen jedoch nicht alle Patienten auf eine zielgerichtete Antikörper Therapie an. Zudem entwickeln viele Patienten eine Resistenz gegenüber dem therapeutischen Antikörper. Bei Patienten mit Kopf-/Halstumoren (HNSCC) und metastasiertem Kolorektalkarzinom (mCRC) können Mutationen im epidermalen Wachstumsfaktorrezeptor (EGFR) die Bindung der mAbs Cetuximab und Panitumumab beeinträchtigen. Beim Multiplen Myelom (MM) könnte der Verlust der Zelloberflächenexpression von CD38 die Zugänglichkeit zum mAb Daratumumab-beeinträchtigen, und folglich auch die Antikörper-abhängige Lyse durch Natürliche Killerzellen (ADCC) und das Komplementsystem (CDC) verhindern.

Ziel dieser Arbeit war es, das Targeting von EGFR und CD38 überexprimierenden Tumorzellen mit Nanobody-basierten Schwerekettenantikörpern (hcAb) und Adeno-assoziierten viralen (AAV) Vektoren zu verbessern. Nanobodies bestehen aus einer variablen Domäne von 15 kDa. Die Ergebnisse zeigen, dass der Nanobody 7D12, im Gegensatz zu Cetuximab, EGFR-Epitop-Escape-Varianten bindet und die Proliferation entsprechender Zellen reduziert. Im Falle von CD38 konnten einige CD38-spezifische Nanobodies die enzymatische Aktivität von CD38 stärker hemmen als Daratumumab. Um Fc-vermittelte Effektorfunktionen zu ermöglichen, wurden ausgewählte α EGFR und α CD38 Nanobodies an die Hinge-, CH2- und CH3-Domänen von humanem IgG1 fusioniert. Die so generierten chimären Lama/Human Schwereketten-Antikörper (hcAb) sind etwa halb so groß wie herkömmliche mAbs (75 kDa gegenüber 150 kDa). Der Fc- optimierte 7D12-hcAb konnte gegenüber Tumorzellen, die EGFR ECD-Varianten exprimieren, effektiv ADCC und CDC auslösen. In primären Knochenmarkproben von MM-Patienten konnte die Kombination von Daratumumab mit α CD38 hcAbs einen stärkeren CDC auslösen als Daratumumab alleine. Schließlich konnten CD38-spezifische Nanobodies die Transduktion von Myelomzellen durch AAV-Vektoren steigern.

Die Ergebnisse dieser Arbeit bahnen den Weg für neuartige therapeutische Ansätze bei EGFR oder CD38 überexprimierenden soliden und hämatologischen Tumoren.

1. Introduction

The immune system has been recognized as a critical regulator of tumorigenesis (1) for both, solid and hematological malignancies. Tumor development can be controlled by the immune system leading to tumor rejection (2). However, tumors often contain immune cell populations that do not mediate tumor destruction (3). These tumor-infiltrating immune cells appear to be suppressed by tumor micro-environmental factors (4). Immune suppression can explain why tumors are not rejected, even in the presence of tumor-specific or tumor-enriched antigens. Therefore, local immunosuppression is a main target for cellular tumor immunotherapy. Thus, successful tumor therapy often requires multifactorial approaches: Targeting the suppressive tumor microenvironment, activating tumor-infiltrating immune cells and immune effector mechanisms, such as NK- and T cell mediated killing and complement activation.

According to the National Cancer Institute, solid tumors are defined as “An abnormal mass of tissue that usually does not contain cysts or liquid areas. Solid tumors may be benign (not cancer), or malignant (cancer). Different types of solid tumors are named for the type of cells that form them (f. e. ovarian cancer, lung cancer). Examples of solid tumors are sarcomas, carcinomas, and lymphomas.” Hematological malignancies are considered to “affect the blood, bone marrow, and lymph nodes. This classification includes various types of leukemia (acute lymphocytic (ALL), chronic lymphocytic (CLL), acute myeloid (AML), chronic myeloid (CML)), myeloma, and lymphoma (Hodgkin's and non-Hodgkin's (NHL)).”

The aim of this work was to explore the use of nanobody-based heavy chain antibodies and nanobody-displaying AAV to target cell surface antigens of head and neck squamous cell carcinoma (HNSCC), metastatic colorectal cancer (mCRC), and multiple myeloma (MM) cells.

1.1. Overexpressed surface antigens in head-and neck cancer, metastatic colorectal cancer and multiple myeloma

Targeted therapy with monoclonal antibodies (mAbs) against solid and hematological malignancies has become one of the mainstays for cancer patients. Antibody therapy is based on targeting mutated, selectively expressed or overexpressed surface antigens and/or immune-checkpoint inhibitors (5), (6). The epidermal growth factor receptor (EGFR) and the ectoenzyme Cluster of Differentiation 38 (CD38) belong to the group of overexpressed surface antigens present in various cancer entities, that may endow tumor cells with certain growth- and survival advantages over non-malignant cells.

1.1.1. Structure and function of the epidermal growth factor receptor (EGFR)

Many solid tumors, such as HNSCC and mCRC, show enhanced cell surface levels of the EGFR, which is an important regulator of growth, survival, proliferation and differentiation of cells.

The Erb-receptor family member EGFR is a transmembranous glycoprotein with the size of 170kDa (7) (Fig. 1.1). The EGFR is composed of a highly glycosylated extracellular N-terminus with ligand binding domain, a transmembrane helix and an intracellular tyrosine kinase domain. The extracellular domain is divided in four sub-domains: domains II and IV are long and cysteine-enriched involved in receptor dimerization; domains I and III consist of β -leaflets and mediate ligand binding. Ligand binding is followed by receptor dimerization, transautophosphorylation and recruitment of signaling proteins (8).

In the inactive state, the EGFR is in a monomeric form with domain II folded onto domain IV; this “tethered” conformation auto-inhibits EGFR dimerization. Upon binding of an EGF-ligand family member to domain I (f.e. EGF, transforming growth factor alpha, heparin binding EGF, amphiregulin), domain rearrangement is induced. The dimerization arm is exposed in domain II, which keeps the EGFR in a stabilized “untethered” conformation, followed by rearrangements in the transmembrane domain (9) (10). Upon homo- or heterodimerization with one of the four ErbB family receptors (11), the C-terminus of the activating kinase inserts into the active site of the receiving kinase, which results in transautophosphorylation of tyrosine residues on the C-terminal tail (12). Phosphorylated tyrosine residues are docking points for proteins with phosphor-tyrosine-binding residues (f. w. SH2, PTB). Depending on ligand and dimerization partner, different downstream signaling pathways are induced that regulate tumor proliferation, growth, differentiation, migration, and inhibition of apoptosis.

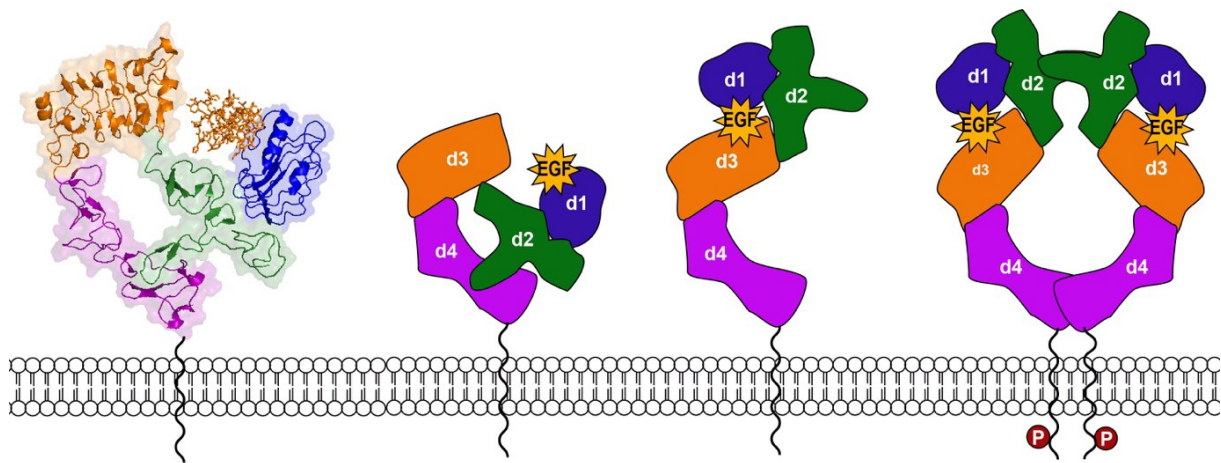


Fig. 1.1: Model of domain architecture and activation of the EGFR.

Upon EGF binding domain I, the tethered conformation of the EGFR (schematic first and second EGFR) rearranges to the extended conformation, and EGF is located between domain I and III (third EGFR). This leads to EGFR dimerization, followed by phosphorylation of intracellular tyrosine residues.

The EGFR can enable tumor cells significant advantages over non-malignant cells by inhibiting apoptosis and promoting proliferation of tumor cells. Hence, the EGFR has become a promising therapeutic target for the chimeric monoclonal antibody cetuximab and the fully humanized antibody panitumumab. These FDA approved mAbs inhibit downstream signaling upon binding, which leads to an increased apoptosis and inhibition of tumor cell proliferation. An aim of this thesis was to generate and to test the use of EGFR-specific heavy chain antibodies based on the published 7D12 nanobody (13) to bind and subsequently inhibit proliferation of HNSCC- and mCRC cells.

1.1.2. Structure and function of the ecto-NADase CD38

Multiple myeloma often show high cell surface levels of CD38, a 45 kDa surface glycoprotein functioning as an ectoenzyme (14) (Fig. 1.2). CD38 is involved in the metabolism of extracellular nicotinamide adenine dinucleotide (NAD^+) and cytoplasmic nicotinamide adenine dinucleotide phosphate (NADP) (15, 16). It has been postulated that the endothelial CD31 might be a ligand for CD38, there acting as a receptor (31).

The main enzymatic reaction of CD38 is NAD glycohydrolase. It has been shown that CD38+ erythrocytes from cancer patients display an increased NAD glycohydrolase activity and higher uptake of ADPR compared to the healthy control group (17). Preoperative ADP-ribosylation and NAD glycohydrolase activity levels were significantly higher in patients with CRC than in the control group (18). Conceivably, high glycohydrolase activity could promote cancer progression by hydrolyzing extracellular NAD^+ to adenosine diphosphate ribose (ADPR) which can be further processed to adenosine monophosphate (AMP) and to anti-inflammatory and immunosuppressive adenosine by CD203 and CD73 (19) (20). An immune-suppressive milieu promoted by CD38 in the TME might be favorable for survival of malignant cells at the tumor side, since most immune effector cells display an exhausted phenotype in an acidic- and anti-inflammatory TME (21), (22), (23). CD38 also functions as an ADPR cyclase, converting NAD^+ to cyclic ADPR (cADPR) and as a cADPR hydrolase that hydrolyzes cADPR to ADPR. CD38 is a very inefficient cyclase, generating approximately 80-fold more ADPR than cADPR. However, even small amounts of cADPR can function as second messenger that regulates intracellular calcium homeostasis (24) and mobilizes intracellular calcium stores and thereby may modulate cell proliferation and differentiation (25).

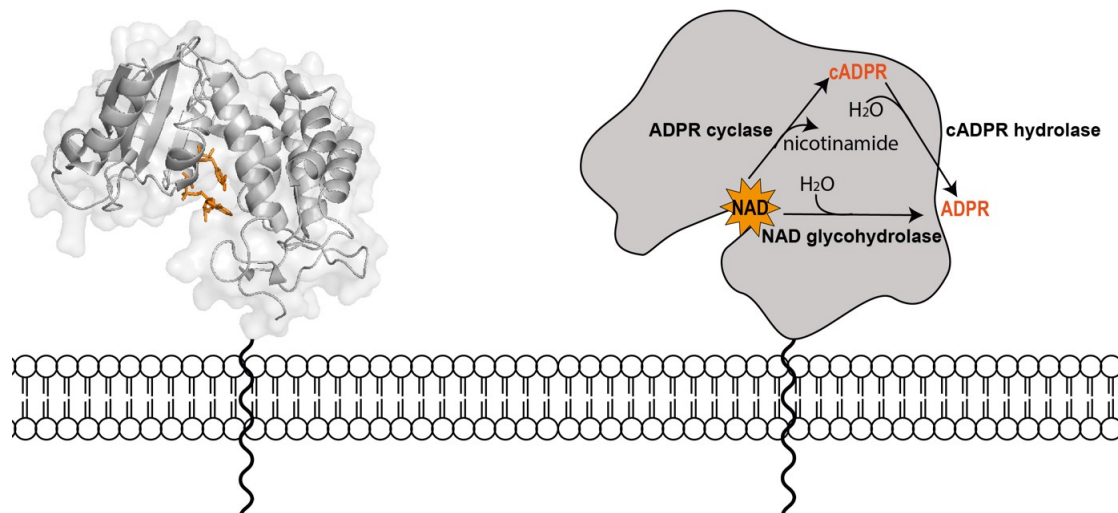


Fig. 1.2: Model of architecture and enzymatic activity of CD38.

CD38 NAD glycohydrolase and ADPR cyclase metabolize NAD^+ to ADPR and cADPR, respectively. cADPR in turn is converted to ADPR by cADPR hydrolase.

In contrast, the structurally related ADPR cyclase from *Aplysia californica* shows a much higher ADPR-cyclase over NAD hydrolase activity than CD38. CD38 has 12 cysteine residues in its extracellular domain, ten of which are conserved in the *Aplysia* ADP-ribosyl cyclase. CD38 contains a sixth disulfide pair between cysteine 119 and cysteine 201 (lysine and glutamic acid,

respectively in the Aplysia cyclase). This extra disulfide bond has been implicated in the reduced cADPR hydrolase activity of CD38 (26).

CD38 has also become a promising therapeutic target for the chimeric monoclonal antibody isatuximab and for the fully humanized monoclonal antibody daratumumab in multiple myeloma (MM). A goal of this thesis was to generate and to test CD38-specific heavy chain antibodies (hcAbs) based on nanobodies previously generated in our lab. We hypothesized that smaller hcAbs might bind to difficult accessible cavities on CD38 and inhibit CD38 enzymatic reactions.

1.2. Anti-tumor effects mediated by therapeutic mAbs

Monoclonal antibodies are composed of two heavy chains and two light chains. Nanobody-based heavy chain antibodies lack light chains and are composed only of two shorted heavy chains (Fig. 1.3).

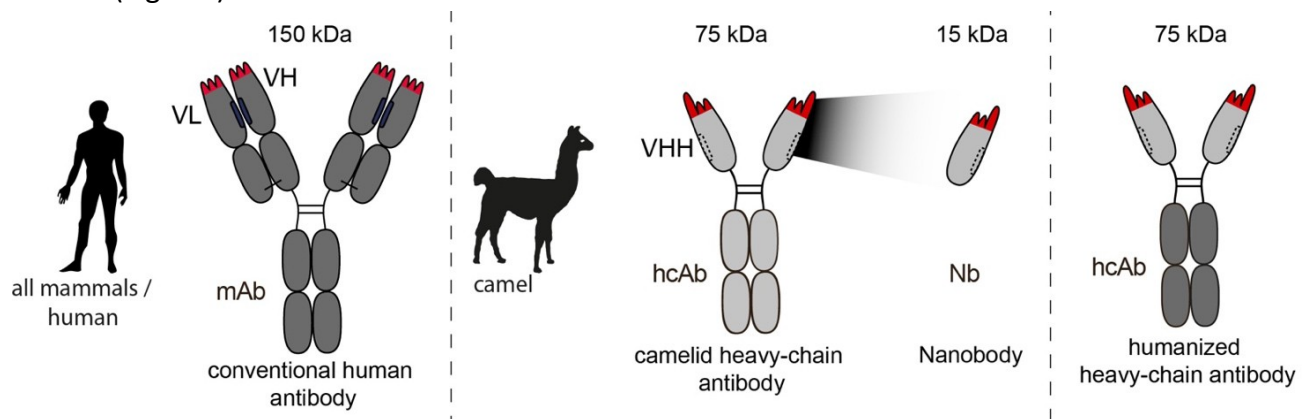


Fig. 1.3: Nanobodies from heavy-chain antibodies.

mAbs contain two heavy and two light chains. A nanobody (Nb) is the variable domain (VHH) of a heavy chain antibody (hcAb) naturally occurring in camelids. Advantages of nanobodies over mAbs include their small size, high solubility and the capacity to target cryptic epitopes.

Therapeutic monoclonal antibodies can display various direct and indirect anti-tumor effects. Direct effects, e.g. blocking of ligand binding, are mediated by binding to the target via the Fab-fragments of the mAb. Indirect effects are mediated by the Fc-portion of the mAb by inducing immune effector functions, such as Antibody-Dependent Cellular Cytotoxicity (ADCC) and Complement-Dependent Cytotoxicity (CDC), and Antibody-Dependent Cellular Phagocytosis (ADCP). Antibody-dependent cellular cytotoxicity is a lytic mechanism mediated by Natural Killer (NK) cells, and other mononuclear cells carrying an Fc-receptor (e.g. CD16) that engage with the Fc-portion of IgG antibodies bound to a tumor antigen (such as EGFR and CD38), thereby triggering the lysis of tumor cells perforins and granzymes. CDC is induced when the Fc-portion of mAbs -that are bound to an overexpressed surface antigen, like EGFR or CD38- binds the C1 complex, which is made up of C1q, C1r, and C1s subunits. Upon binding of C1q to the Fc-portion of a monoclonal antibody, C1r catalyzes the breakage of C1s ester

bond, resulting in its activation. Subsequently, C2 and C4 are cleaved into respective “a” and “b” fragments and formation of C2a4b builds C3 convertase. C3 convertase in turn cleaves C3 into C3a and C3b that binds to other C3 convertases forming C2a4b3b – also known as C5 convertase. C5 cleaves C5 into C5a and C5b. C5b next combines with C6, C7, C8 and C9 to form a pore-like structure called membrane attack complex (MAC). When MACs are incorporated in the plasma membrane, tumor cells undergo osmotic lysis and die (27).

Fc-engineering has been shown to improve ADCC and CDC (5), (28), (29). A further goal of this thesis was to explore the use of such mutations to enhance the effector functions of nanobody-based heavy chain antibodies.

1.2.1. The mode of action of the EGFR-specific mAbs cetuximab and panitumumab

Cetuximab and panitumumab hinder substrate binding and subsequent EGFR dimerization. As a result of that, the pro-cancerogenic downstream RAS-RAF-MEK-ERK-MAPK-, PI3K-AKT-mTOR- and PLC- γ 1-PKC signaling pathways are inhibited and tumor cells do not proliferate anymore and undergo apoptosis (30). In addition to direct downstream effects, the IgG2-Fc part of panitumumab connects with Fc γ RIIa expressed on myeloid cells like neutrophils and monocytes, thereby mediating ADCC (31). In contrast, the IgG1-Fc part of cetuximab induces ADCC by engaging NK cells through the Fc γ RIII (32), resulting in a perforin- and granzyme induced cell death of HNSCC- and mCRC tumor cells. The second indirect mechanism mediated by EGFR-specific mAbs is CDC, which apparently cannot be induced by cetuximab or panitumumab alone, but by combinations of the two different mAbs targeting two non-overlapping epitopes (33). The binding of two mAbs to the same surface antigen mediates a hexameric cross-connection of more Fc parts onto the same C1q molecule, followed by complement cascade and MAC induced osmolytic cell death as described above (34).

Patients diagnosed with mCRC or HNSCC often do not respond to neither cetuximab nor panitumumab therapy due to primary or acquired resistance mechanisms in intracellular signaling molecules, such as RAS (35), (36), (37), or the EGFR ectodomain (EGFR ECD). So far, 10 EGFR ECD mutations – V441, S442, R451, I462, S464, G465, K467, K489, I491, and S492- in mCRC patients have been described that were acquired due to selective pressure during cetuximab and panitumumab therapy (38), (39), (40). Those point mutations -except the R451C- are located in either the cetuximab or panitumumab epitope or in their overlapping epitope, leading to a complete binding or binding abrogation of cetuximab and panitumumab to the EGFR domain III.

In addition to acquired resistance in mCRC, there is evidence of primary resistance mechanisms in HNSCC patients. Braig et al. described a single nucleotide polymorphism (SNP) at the position R521K in the EGFR ECD. HNSCC patients with primary EGFR R521K SNP show a significantly decreased progression free survival compared to patients with a low K-allele frequency (29). This might be mediated by a reduced glycosylation pattern in the EGFR ECD,

causing an attenuated affinity for cetuximab to the EGFR. Hence, the proliferation promoting, anti-apoptotic-EGFR downstream pathway is no longer inhibited.

A goal of this thesis was to determine whether the EGFR-specific nanobody binds to an independent epitope which is not affected by neither the point mutations, nor the SNP, respectively.

1.2.2. The mode of action of the CD38-specific mAbs isatuximab and daratumumab

Daratumumab was described to induce apoptosis of CD38+ MM cells by crosslinking and clustering of cells. Apoptosis is accompanied by phosphatidylserine translocation, loss of mitochondrial membrane potential and loss of membrane integrity (41). Isatuximab strongly, and daratumumab partially also inhibit the cyclase activity of CD38 which might counteract the anti-inflammatory TME (42), (43). The indirect anti-tumor effects of isatuximab and daratumumab are mainly related to their ability in inducing ADCC, CDC and ADCP of CD38+ myeloma cells as described above. CD38 is not only expressed on myeloma cells, but also on regulatory myeloid and lymphoid cells. Daratumumab mediated depletion of CD38+ immunosuppressive cells, such as regulatory T cells (Tregs) and myeloid-derived suppressor cells has been proposed to elevate the anti-tumor activity of immune effector cells (44, 45). Furthermore, daratumumab inhibits *in vitro* osteoclastogenesis and bone resorption activity from BM samples of MM patients by targeting CD38-expressing monocytes and early osteoclast progenitors (46). CD38 expressing microvesicles (MVs) derived from MM cells are also targeted by daratumumab; The CD38/CD39/CD73/CD203 mediated catabolism of ATP, NAD⁺, ADPR and AMP to adenosine was higher in MVs from MM patients compared to MVs from control patients. Hence, daratumumab may counteract the synthesis of adenosine and thereby the anti-inflammatory TME (47).

Daratumumab-treated multiple myeloma patients often show disease relapse independent of first-, second- or third line therapy. Disease progression and drug resistance might be either due to intrinsic mediated mutational changes, or extrinsically by the tumor micro-environment (TME) (48). Genetic abnormalities in myeloma disease progression include translocation of chromosome 14 (t[14;16] and t[14;4]), MYC amplification, constitutive activation of NRAS and KRAS, mutations in FGFR3, and inactivation of cyclin-dependent kinase inhibitors CDKN2A and CDKN2C (49), (50).

Since multiple myeloma is dependent on the bone marrow microenvironment promoting tumor proliferation, survival and migration, TME-mediated resistance mechanisms have been postulated. One is a metabolic shift in MM cells from oxidative phosphorylation towards anaerobic glycolysis – termed the Warburg effect. This shift favors the accumulation of NAD⁺ and H⁺, which can lead to an increased extracellular acidity (51). This acidic pH is hypothesized to deteriorate the therapeutic efficacy of daratumumab by affecting an aspartic acid residue in the complementarity-determining region (CDR) of the mAb. Binding of daratumumab to its

epitope on CD38 might be subsequently decreased (52). Moreover, CD8⁺ T cells, Tumor-associated Macrophages (TAMs), Dendritic Cells (DC) and Natural Killer (NK) cells can lose their anti-tumor functions at an acidic pH (21), (53), (54), (55). Moreover, immune-suppressive cell types like myeloid-derived suppressor cells (MDSCs) and regulatory T cells (Treg) can proliferate in an acidic TEM, thereby boosting tumor outgrowth (56). In addition, CD38 is also expressed on other non-malignant cells that are involved in anti-tumor activity, such as NK cells, B cells and activated T cells. Hence, an off-target effect of daratumumab by depleting NK cells could impede ADCC and antibody-dependent cellular phagocytosis (ADCP) of tumor cells (Cherkasova E, et. al, blood, 2015). Furthermore, upregulation of complement inhibiting proteins CD55 and CD59 may reduce the sensitivity of MM cells to CDC (57).

A goal of this thesis was to evaluate the capacity of nanobody-based hcAbs to inhibit CD38 enzymatic activities and to induce Fc-mediated CDC and ADCC effector functions.

1.3. Nanobody-mediated targeting of Adeno-associated viral (AAV) vectors

AAV (adeno-associated viral vectors) are being used with increasing success for gene therapy (58), (59), (60). More than 100 clinical studies are currently focusing on the use of AAV to correct rare hereditary diseases. After transduction of target cells, the AAV genome is expressed episomally, i.e. without integration into the genome of the target cell. A limiting factor for the use of AAV vectors in gene therapy is the broad tropism of AAV serotypes, i.e. the parallel infection of several cell types (61). Previous work in the Koch-Nolte lab showed that nanobodies targeting cell surface proteins can enhance the transduction of target-expressing cells, when these nanobodies were fused either to the VP1 capsid protein of AAV2 or to an AAV-specific nanobody (61), (Eichhoff A, dissertation MIN faculty, Hamburg, 2018).

A goal of this thesis was to assess the utility of CD38-specific nanobodies to enhance AAV-transduction of CD38-overexpressing primary myeloma cells from a patient bone marrow.

2. Objectives of this PhD thesis

Targeted therapy with monoclonal antibodies has become a mainstay for cancer patients. Cetuximab and panitumumab, and daratumumab have been shown to improve progression free survival and overall survival in head and neck cancer patients, metastatic colorectal cancer patients and multiple myeloma patients, respectively. Despite this progress, many patients still show disease relapse due to primary and acquired resistance mechanisms. The main goals of this PhD work were 1) to analyze the use of nanobody-based heavy chain antibodies targeting the EGFR and CD38 to mediate direct (Fig. 2A, left panel) and indirect (Fig. 2B) anti-tumor effects and 2) to explore the use of nanobodies to promote the transduction of primary myeloma cells by AAV (Fig. 2A, right panel).

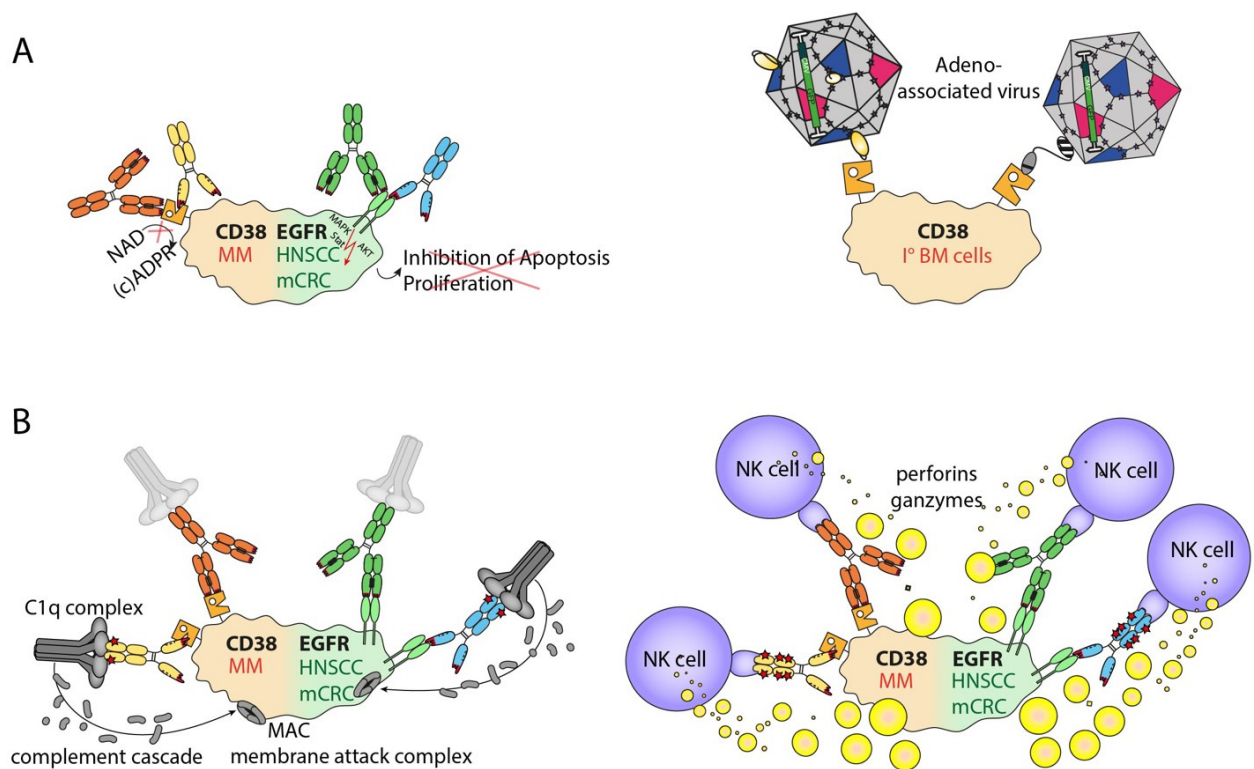


Fig. 2: Graphical abstract illustrating the goals of this thesis.

Targeting of the EGFR in HNSCC, mCRC, and of CD38 in MM with heavy chain antibodies. (A) The schematic on the left panel depicts direct effects mediated by hcAb and mAbs. (B) The illustration shows indirect effects mediated by the Fc-part of hcAbs and mAbs inducing complement dependent (A) and NK-cell dependent (B) killing of tumor cells. (A, right panel) Using direct effects of α CD38 Nbs to enhance cell-specific targeting of AAV gene therapy vectors. The schematic depicts the strategies used to increase the specificity of AAVs targeting CD38-overexpressing myeloma cells from a patient bone marrow. Left AAV: fusion of the nanobody to the VP1 capsid protein of AAV (blue). Right AAV: engage AAVs with CD38-expressing target cells via bispecific AAV-Nb adaptors composed of a CD38-specific nanobody fused to an AAV-specific nanobody.

3. Materials

3.1. Laboratory devices

Table 3.1: Used laboratory devices and the corresponding manufacturer

Laboratory device	Model	Manufacturer
Analytical scale	Analytical Plus	Ohaus
Autoclave	Modell 2540 EL	Tuttnauer Europe
Autoclave	Evo 130 Typ II	MediTech Service GmbH
Incubator for bacteria	Biotherm 37	Julabo
Incubator for bacteria	Multitron Pro	Infors HT
Incubator for bacteria	Ecotron	Infors HT
CO ₂ incubator	MCO-20AIC	Sanyo Electric Co.
C ₁₈ -HPLC column	Multohyp BDS C18	Langerwehe
Flow cytometer	FACS Canto II	BD Biosciences
Heating block	Thermomixer kompakt	Eppendorf
Chambers for Agarose- Gel electrophoresis	Modell 40-0708	PEQLAB Biotechnology
Chambers for SDS-PAGE	XCell SureLock MiniCell	Thermo Fisher Scientific
Micro pipettes	Modell Research	Eppendorf
Microtiter plates-	Infinite M200 with Software	
Fluorescence-photometer	i-control, Tecan	Grödig
pH-Meter	Toledo MP220	Mettler
Photometer	Nanodrop 2000c	PEQLAB Biotechnology
Photometer	Ultraspec 2000	Pharmacia Biotech
Roller	Mixer SRT6	Stuart
Voltage device agarose- Gel electrophoresis		Biometra GmbH
Voltage device SDS-PAGE	PowerPac 200	BioRad
Sterile bench	Gelaire Typ BSB4	Gelman
Thermocycler	T3/T Gradient	Biometra
Table centrifuge	5424	Eppendorf
Table scale	Scout Pro	Ohaus
UV-Transilluminator	Typ TI1	Biometra
Vivaspin2	10 kDa size filter	Sartorius Stedim
Water bath	Modell 1007	Society for Lab technique
Centrifuge	Rotana 460 R	Hettich

3.2. Chemicals

The used standard chemicals for production of buffers and solutions were obtained from the companies BD Biosciences, Carl Roth GmbH + Co. KG, GE Healthcare, Merck or Thermo Fisher Scientific. Special chemicals or chemicals obtained from other companies are listed below.

Table 3.2: Used chemicals and the corresponding manufacturer

Chemical	Manufacturer
3,3',5,5'-Tetramethylbenzidin (TMB)	Pierce™/Thermo Fisher Scientific
Amersham ECL Western Blotting Detection R.	GE Healthcare
Aqua ad iniectabilia	B. Braun Melsungen AG
BSA	Sigma-Aldrich/Merck
Blasticidin	InvivoGen
Carbenicillin	Sigma-Aldrich/Merck
Dimethylsulfoxid (<i>DMSO</i>)	Sigma-Aldrich/Merck
DMEM (<i>dulbecco's modified eagle medium</i>)	Gibco™/Thermo Fisher Scientific
DNA Gel Loading Dye (6x)	New England Biolabs
eFluor450	eBioscience™/Thermo Fisher Scientific
FastStart Essential DNA Green Master Mix	Roche
FCS (<i>fetal calf serum</i>)	Gibco™/Thermo Fisher Scientific
G418	Gibco™/Thermo Fisher Scientific
Geneticin	Gibco™/Thermo Fisher Scientific
HIS-Select Nickel Affinity Gel	Sigma-Aldrich/Merck
IgG Elution buffer pH 2.8	Thermo Fisher Scientific
Kanamycin	Sigma-Aldrich/Merck
Methanol LiChrosolv Hypergrade	Merck
Tetrabutylammonium-phosphat	Sigma-Aldrich
NuPAGE™ LDS Sample Buffer (4x)	Invitrogen/Thermo Fisher Scientific
NuPAGE™ Sample Reducing Agent (10x)	Invitrogen/Thermo Fisher Scientific
Phosphate buffered saline (PBS)	Gibco™/Thermo Fisher Scientific
Pluronic F-68	Gibco™/Thermo Fisher Scientific
Polyethylenglycol (PEG) MW 8000	Carl Roth GmbH + Co.
Polyethylenimin (PEI), MW25000	Polysciences, Inc.
Protein G Sepharose 4 Fast Flow	GE Healthcare
TAE-Puffer (50x) UltraPure DNA Typing Grade	Thermo Fisher Scientific
Triton X-100	Sigma-Aldrich/Merck
Tryptone N1	Organo Technie
Tween-20	Sigma-Aldrich/Merck

3.3. Buffers and solutions

Table 3.3: Composition of used solutions and buffers

Buffer	Composition
<i>Buffer for SDS-PAGE:</i>	
NuPAGE™ Sample Reducing Agent (10x)	500 mM Dithiothreitol (DTT)
NuPAGE™ LDS Sample Buffer (4x)	Lithiumdodecylsulfat (pH 8.4)
MES-running buffer	50 mM MES, 50 mM TrisBase, 1% SDS, 1 mM EDTA (pH 7.3)
<i>Buffer for Transfection/AAV production:</i>	
PEI (Polyethylenimin)	7.5 mM 25kDa linear Polythylenimine (Polyxciences Inc.), 0.333 mg/ml solved in H ₂ O at 60°C, sterile filtered
NaCl 300mM	300 mM NaCl in H ₂ O, sterile filtered
PBS-MK (10x)	PBS (10x), 10 mM MgCl ₂ , 25 mM KCl, sterile filtered
<i>Buffer used for purification of recombinant proteins based on chromatography:</i>	
Elution buffer Ni-NTA	50 mM Sodium phosphate, 0.3 M NaCl, 250 mM Imidazol (pH 8.8)
IgG Elution Buffer (Protein G)	Thermo Fisher Scientific (pH 2.8)
Neutralizing buffer (Protein G)	1 M Tris (pH 9)
<i>Buffer for agarose-gel electrophoresis:</i>	
Tris-Acetate-EDTA-buffer (50x)	2 M Tris-Acetate, 50mM EDTA
Loading dye (6x)	2.5% Ficoll-400, 11mM EDTA, 3.3mM Tris-HCl, 0.017% SDS, 0.015% Bromphenolbue (pH 8)
FACS-Buffer	0.02% BSA in PBS
<i>RP-HPLC buffer:</i>	
Calcium-buffer	140 mM NaCl, 5 mM KCl 1 mM MgSO ₄ , 1 mM CaCl ₂ , 20 mM HEPES, 1 mM NaH ₂ PO ₄ , 5 mM D-Glucose, pH 7,4)
HPLC-Buffer A	20 mM KH ₂ PO ₄ , 5 mM Tetrabutylammonium-phosphate, pH 6)
HPLC-Buffer B	50% HPLC-Buffer A, 50% Methanol, LiChrosolv Hypergrade

HPLC-Buffer C	30% HPLC-Puffer A, 70% Methanol, LiChrosolv Hypergrade
Phosphate buffer	9,1 mM NH_2PO_4 , pH 5, Triethanolamin buffer (TEA, pH 9)
<i>NGD-Fluorometric assay buffer</i>	
Calcium buffer	140 mM NaCl, 5 mM KCl 1 mM M, 1 mM CaCl_2 , 20 mM DEA-Puffer (1 M DEA, 1 mM MgCl_2 , pH 9,8)

3.4. Cell Culture Media

Table 3.4: Composition of the used media

Media	Composition
<i>Media for eukaryotic cell culture:</i>	
DMEM complete medium	DMEM (Gibco TM), 1 mM Sodium-pyruvate, 2 mM L-Glutamine, 10 mM HEPES, 1x non-essential Amino Acids, 10% FCS
RPMI medium	1 mM Natrium-pyruvate, 2 mM L-Glutamine, 10% FCS
aMem medium	12.5% FCS (Gibco), 12.5% horse serum (Gibco), 100 IU/mL IL-2 (Proleukin), 2 mM L-Glutamine (Gibco) \pm EGF (5 ng/ml)
F17 complete medium	FreeStyle TM F17 Expression media (Gibco TM), 4 mM L-Glutamine, 1% FCS, 0.5 % G418
F17 transfection medium	FreeStyle TM F17 Expression medium (Gibco TM), 4 mM L-Glutamine, 0.1% Pluronic
F293 medium	FreeStyle TM 293 Expression medium (Gibco TM)

All antibodies -commercially obtained or self-produced- used during this work are listed below.

Antigen	Clone	Host	Conjugate	Manufacturer
CD38, human	MU370-hFc	Lama	-	AG Nolte
CD38, human	MU1057-hFc	Lama	AF647	AG Nolte
CD38, human	WF211-hFc	Lama	AF647	AG Nolte
CD38, human	JK36-hFc	Lama	AF647	AG Nolte
CD38, human	JK2-hFc	Lama	-	AG Nolte
CD38, human	ST52-hcFc	Lama	-	AG Nolte
CD38, human	Daratumumab	Mouse	-	UKE pharmacy
CD45, human	HI30	Mouse	BV785	BioLegend
CD19, human	HIB19	Mouse	PeCy5	BD Biosciences
CD269, human	19F2	Mouse	PeCy7	BioLegend
CD138, human	MI15	Mouse	FITC	BD Pharmingen
CD319, human	162.1	Mouse	PeCy7	BioLegend
CD229, human	30CO7	Rat	FITC	BD
CD56, human	MEM-188	Mouse	PeCy7	BD
CD55, human	IA10	Mouse	FITC	BD
CD59, human	P282 (H19)	Mouse	FITC	BD
C1q, human	F0254	Rabbit	FITC	eBio
C3b, human	7636	Mouse	PE	CEDERLANE
CD38, mouse	JK3-mlgG2c	Lama	AF647	AG Nolte

CD38, mouse	JK5-mIgG2c	Lama	AF647	AG Nolte
CD38, mouse	JK13-mIgG2c	Lama	AF647	AG Nolte
CD38, mouse	JK3-mIgG2c	Lama	AF647	AG Nolte
CD38, mouse	NB32-mIgG2c	Lama	AF647	AG Nolte
CD38, mouse	NB11-mIgG2c	Lama	AF647	AG Nolte
PacO, human/mouse	-	-	-	ThermoFisher
Propidiumiodide m/h	-	-	-	ThermoFisher

3.6. Plasmids

Table 3.6: Plasmids, origin and reference

Name	Manufacturer	Reference
pCSE2.5_rblgGfc	Thomas Schirrmann, IHK Braunschweig, pCSE2.5 with <i>rabbit</i> IgG-Fc sequence between <i>NotI</i> and <i>XbaI</i>	Jäger <i>et al.</i> , 2013
pcDNA6.2	Invitrogen	

3.7. Size standard for proteins and DNA

Table 3.7: Size standards used for proteins and double-stranded DNA

Name	Manufacturer
<i>Size standards for DNA:</i>	
GeneRuler 1Kb DNA ladder	Thermo Fisher Scientific
GeneRuler 100bp DNA ladder	Thermo Fisher Scientific
<i>Size standards for proteins:</i>	
Supermarker (1x and 4x)	AG Nolte (1x = 75 µg/ml IgG, 100 µg/ml BSA, 10 µl/ml Lysozyme)
MagicMark™ XP Western Standard	Invitrogen/Thermo Fisher Scientific

3.8. Enzymes

Table 3.8: Enzymes for cloning and PCR

Name	Manufacturer
<i>Restriction enzymes:</i>	
NotI	New England Biolabs
NotI HF	New England Biolabs
XbaI	New England Biolabs
XbaI HF	New England Biolabs
Nco	New England Biolabs
Nco HF	New England Biolabs
Pci	New England Biolabs
Pci HF	New England Biolabs
<i>Ligation enzyme:</i>	
T4 ligase	New England Biolabs
<i>DNA Polymerase:</i>	
<i>PfuUltra</i> HF DNA Polymerase	New England Biolabs

3.9. Oligonucleotides

All oligonucleotides were synthesized by Sigma-Aldrich and Eurofins. The corresponding sequences are attached to this thesis.

3.10. Cell lines

Table 3.9: Prokaryotic and eukaryotic cell lines

Name	Source
<i>Prokaryotic cells:</i>	
XL-1 Blue E. coli	Stratagene
XL-10 Gold E. coli	Agilent Technologies
C2925 <i>dam</i> ^{-/-} E. coli	New England Biolabs

Eukaryotic cells:

HEK293-6E		obtained from Dr. Yves Durocher (licensed by NRC Canada)
HEK-T		obtained from Carol Stocking, HPI, Hamburg
LP1		obtained from the Leibniz-Institute DSMZ-German Collection of Microorganisms and Cell Cultures
EL4 NOD		EL4 R were cells stably transfected with ARTC2.2, Nolte lab (62)
EL4 R		obtained from Carol Stocking, HPI, Hamburg
EL4 alt	EL4	ATCC [®] TIB-39 [™]

4. Methods

4.1. Cell lines

4.1.1. Murine cell lines

Mouse CD38 and ARTC2.2 expressing EL4 R thymoma cells were generated in the Koch-Nolte lab (62). CD38 gene of EL4 alt cell line was inactivated using CRISPR/Cas9 technology (sc-401117-NIC, Santa Cruz Biotechnology). EL4 NOD, EL4 R and EL4 alt cell lines were cultured in a RPMI-1640 medium (Gibco, Life Technologies, Paisley, UK) supplemented with 2 mM sodium pyruvate (Gibco), 2 mM L-glutamine (Gibco) and 10% (v/v) fetal calf serum (Gibco). All experiments shown in this thesis were performed with EL4-NOD cells. Hence, EL4 NOD cells are referred to mCD38 EL4-thymoma cells in the following.

NK-92, a human NK cell line, was obtained from DSMZ. Prior to this work, NK-92 cells stably co-expressing GFP and human or murine CD16 were obtained by retroviral transduction using the pSF91 retroviral vector. The sequence for CD16, i.e. the ectodomain of FcγRIII fused to the transmembrane and cytosolic domains of FcεRI, was kindly provided by B. Clémenceau (Nantes, France). The CD38 gene was inactivated in these cells using CRISPR/Cas9 technology (sc-401117-NIC, Santa Cruz Biotechnology). NK-92-CD16-GFP cells and NK-92-CD16-GFP-CD38ko cells were FACS-sorted and grown in an alpha MEM culture medium (Gibco) supplemented with 10% FCS (Gibco), 10% horse serum (Gibco), 100 IU/mL IL2 (Proleukin, Novartis, Nürnberg, Germany) and 2 mM L-glutamine (Gibco).

4.1.2. Human cell lines and primary patient samples

The human HNSCC cell lines SAT (EGFR R521K) and UTSCC14 (EGFR WT) were kindly provided by M. Baumann (2006, University of Dresden, Germany) and R. Grenman (2011, University of Turku, Finland), respectively. Both lines were cultivated in DMEM (Life Technologies) supplemented with 10% (v/v) FBS (Merck Millipore) and 1% (v/v) penicillin/ streptomycin (Gibco/Life Technologies) at 37°C in a humidified atmosphere with 5% CO₂.

Ba/F3 cells (CSC-C2045, Creative Bioarray) were kindly provided by S. Horn (2014, UKE) and were maintained in RPMI medium containing 10% (v/v) FBS, 1% (v/v) penicillin/ streptomycin, and 10 ng/mL recombinant murine IL3 purchased from PeproTech. Prior to this work, different EGFR expression constructs, the complete human wild-type (WT) EGFR, the respective full-length cDNA was inserted into a third-generation, self-inactivating (SIN) lentiviral gene ontology vector LeGO-iG3-Puro+/eGFP as well as LeGO-iG3-Puro+/mCherry (Braig-Karzig F, dissertation MIN faculty, Hamburg, 2016). The EGFR mutants S492R, K467T, G465R, S464L and R451C were generated from the WT construct in the pcDNA3.1(+) vector with the QuikChange XL Site-Directed Mutagenesis Kit (Agilent Technologies). The respective EGFR mutant was amplified using individually designed oligonucleotides and cloned into the LeGO-iG3-Puro+/eGFP vector by In-Fusion HD Cloning Plus (Takara Bio). Ba/F3 cells were lentivirally

transduced with a WT or mutant *EGFR* encoding vector. Effectively transduced cells were sorted based on their selectable fluorescent marker by fluorescence-activated cell sorting (FACS) on a FACS Aria IIIu (Becton Dickinson), and transduction efficiency was determined. Ba/F3 cell lines stably expressing EGFR WT or EGFR S492R, K467T, G465R, S464L or R451C mutants were established by puromycin (1 µg/mL; InvivoGen) and Ba/F3 EGFR WT cells by puromycin and zeocin (100 µg/mL; InvivoGen) selection.

The human multiple myeloma cell line LP-1 was obtained from the Leibniz-Institute DSMZ-German Collection of Microorganisms and Cell Cultures (Braunschweig, Germany). LP1 cells were cultured in a RPMI 1640 medium (Gibco, Life Technologies, Paisley, UK) supplemented with 2 mM sodium pyruvate (Gibco), 2 mM L-glutamine (Gibco) and 10% (v/v) fetal calf serum (Gibco).

The human cell line NK-92 obtained from DSMZ was stably co-transfected with human CD16 and GFP as described in 1. for mCD16-NK92 cells. Cells were grown in alpha MEM culture medium (Gibco) supplemented with 12.5% FCS (Gibco), 12.5% horse serum (Gibco), 100 IU/mL IL2 (Proleukin, Novartis, Nürnberg, Germany), and 2 mM L-glutamine (Gibco). The CD38 gene was inactivated in these cells using CRISPR/Cas9 technology (sc-401117-NIC, Santa Cruz Biotechnology) and subsequently FACS-sorted.

Bone marrow aspirates of patients were kindly provided by T. Hansen (2018-2020, Hematology-Oncology Institute Altona, Germany) and K. Weisel (2018-2020, UKE, Germany) after written informed consent as approved by the ethics committee (Ethikkommission der Ärztekammer Hamburg, PV4767). Human bone marrow mononuclear cells were prepared by Ficoll-Paque density gradient centrifugation of bone marrow aspirates and subsequent depletion of remaining erythrocytes using red blood cell lysis buffer (NH₄Cl, KHCO₃, EDTA). BMMCs were subsequently analyzed and further cultivated up to 21 days in alpha MEM culture medium (Gibco) supplemented with 12.5% FCS (Gibco), 12.5% horse serum (Gibco), 100 IU/mL IL2 (Proleukin, Novartis, Nürnberg, Germany), 2 mM L-glutamine (Gibco) with/without recombinant human EGF, -IL6, -IL1β and -VEGF. All cytokines and growth factors were added in 5ng/ml and were obtained from BioLegend.

4.2. Llama immunizations and construction of a phage library

Prior to this thesis, two llamas (designated 538 and 539) were immunized subcutaneously by ballistic cDNA immunization with the full-length open reading frame of CD38 cloned into the pEF-DEST51 expression vector. The humoral immune response was monitored in serially diluted serum by ELISA on microtiter plates (Nunc MaxiSorp, Thermo Fisher Scientific, Waltham, MA) coated with recombinant CD38, using monoclonal antibodies directed against llama IgG2 and IgG3 kindly provided by Dr. Judith Appelton, Cornell University, NY. Blood from the animals was taken 4–18 days after the 3rd or 4th boost.

4.3. Phage-panning based selection of nanobodies against mouse CD38

Phage libraries from *E. coli* glycerol stocks of Llamas 538 and 539 were thawed from -80°C. 15 µl of glycerol stocks were mixed with 5 ml of 2YT-2%Glucose-Carbenicillin containing medium and incubated at 37°C, 200 rpm for 1 hour. Then, the bacteria-suspension was centrifuged at 4500 rpm for 10 minutes and resuspended in a 10 ml 2YT-2%Glucose-Carbenicillin containing medium and grown until the optical density (OD) was 0.4. In the next step, culture supernatants of *E. coli* transformants were infected with a 10-fold excess of M13K07 helper phage (GE Healthcare, Chalfont St Giles, UK) for 30 minutes at 37°C, and shook at 150 rpm. After two washing steps at 4500 rpm for 10 minutes with 2YT-carb, followed by 2YT-Carbenicillin-canamycin medium, the suspension was shook at 220 rpm, 28°C for 6 hours. Phage particles were precipitated with polyethylene glycol from bacterial supernatants over night at 4°C. The next day, the supernatants were discarded, and precipitated phages were resuspended in 1 ml PBS and centrifuged at 14000 rpm for 1 minute. A second precipitation was performed with polyethylene glycol and NaCl for 30 minutes at 4°C, followed by centrifugation again at high speed 14000 rpm for 5 minutes at 4°C. The supernatant was discarded, and the phage pellet was resuspended in 1 ml PBS, and centrifuged at 13000rpm for 4 minutes. After centrifugation, the supernatant was transferred into a new Eppendorf tube; this was repeated until there was no visible pellet anymore. The next day, phages were titrated; therefore, the TG1 *E. coli* cells (Stratagene, La Jolla, CA) from glycerol stocks were grown in 20 ml 2YT-medium until an OD of 0.5 was reached. Phages were diluted from 1:10³ to 1:10¹² in PBS+1% BSA, then were added to TG1 cells (OD= 0.5) and incubated for 30 minutes at 37°C. In the last step, 5µl of each cell-phage mix was plated on Carbenicillin containing agar (1:1000) and incubated overnight. To calculate the titer, the dilution was multiplied by 4000 and the number of clones.

For phage panning, three CD38 wildtype (WT) Black6 (B6) and three CD38 knock-out (ko) B6 mice were killed. Spleens were transferred into a Falcon-tube with a RPMI medium, and then shredded and filtered with subsequent centrifugation (1600 rpm, 10 minutes, 4°C). The supernatant was discarded, and the pellet was resuspended in an erythrocyte-lysis buffer for 3 minutes on ice. The reaction was neutralized with 40 ml PBS and splenocytes were centrifuged again for 5 minutes at 1300 rpm, 4°C. The splenocytes were resuspended in 2 ml RPMI medium and split into 2 tubes according to two immunized 538 and 539 Llamas. Panning of specific phages was started with a negative panning round using CD38-ko splenocytes by adding 20 µl of 538 or 538 phage libraries to 975 µl CD38-ko splenocytes. Cell-phage suspension were rolled for 1 hour at 4°C, followed by centrifugation at 1500 rpm at 4°C. Thereby, unspecific binders were removed. The supernatant from negative selection was further incubated and rolled with CD38-WT-splenocytes for 1 hour at RT. To remove unbound proteins, cells were washed 20 times in 10 ml PBS and transferred to a new tube every other time (1300 rpm, 5 minutes, 4°C). After extensive washing, splenocytes were resuspended in 250 µl Trypsin for 10 minutes at RT to elute bound phages from CD38-WT-splenocytes. After centrifugation, the supernatant with phages was added onto AEBSF to stop the trypsin-mediated digestion. Eluted phages were titrated and subjected to one or two more rounds of

panning, following the same procedure. Phage titers were determined at all steps by infection of TG1 *E. coli* cells. 5 ml of TG1 *E. coli* cells were infected with 250 µl of eluted phages for 30 minutes at 37°C and 150 rpm. Infected TG1 *E. coli* cells (1:1000) were distributed on two 2YT-carbenicillin agar plates and grown overnight at 37°C. The next day, 24 clones of each plate were picked in 5 ml 2YT-carb-medium at 37°C, overnight at 200 rpm. Lastly, plasmid DNA was isolated from single colonies using QIAprep Spin Miniprep Kit from Qiagen (4.8.) and subjected to sequence analyses using pHEN2-specific forward and reverse primers (4.9.). To clone selected VHHs from pHEN2-vector into the expression vector pCSE2.5, the VHH coding region was amplified by polymerase chain reaction (PCR) (4.1.) using degenerate VHH-specific primers. PCR products were purified from agarose gels (4.3.), digested sequentially with PciI and NotI (NEB, Ipswich, MA) (4.2.) and cloned into the pCSE2.5 vector downstream of a mouse IgG2c Fc-portion. Another round of phage panning as described above was done with CD38-ko EL4 alt cells for negative absorption and mouse CD38 expressing EL4-thymoma cells for positive absorption.

4.4. Construction of monospecific heavy chain antibodies (hcAbs)

4.4.1. PCR-based amplification of selected VHHs

The coding regions of selected nanobodies found during phage panning (JK3, JK5, JK13, JK16, NB3, NB7, NB11, NB22, NB24, NB28, NB32, NB38, NB40 and NB42) were subcloned using restriction enzymes NcoI/PciI and NotI upstream of the hinge coding region of mouse IgG2c in pCSE2.5 vectors (kindly provided by Thomas Schirrmann, Braunschweig). Those VHHs with an internal NcoI cutting site were PCR amplified to exchange the NcoI site with a PciI cutting side upstream of the VHH. The three-step PCR was performed to amplify specific DNA-fragments. First, the double stranded (ds) DNA was denaturized at 95°C, followed by flanked annealing of specific oligonucleotides (primer) onto their complementary DNA-fragments. The annealing step was performed at the corresponding melting temperatures ranging from 50°C to 68°C. In the last step, the complementary DNA strand was synthesized from dNTPs by DNA-Polymerase (PfuUltra Polymerase) at 70°C. The sequential repetition of all three steps in various cycles enabled exponential amplification of the specific DNA-fragment.

Table 4.1: Reagents used for endonuclease mediated digestion of pCSE2.5 vectors

Reagents	Volume	Final concentrations
10x Puffer für <i>PfuUltra</i> Polymerase	5 µl	1x
dNTPs (2 mM each)	5 µl	0,2 mM each
forward-Primer 'TE#155_fwd' (100 ng/µl)	1.25 µl	125 ng
reverse-Primer 'fdSeq1_rev' (100 ng/µl)	1.25 µl	125 ng
<i>PfuUltra</i> HF DNA Polymerase (2.5 U/µl)	1 µl	0,05 U/µl
Plasmid-DANN (10 ng/µl)	1 µl	
ddH2O	35.5 µl	

To purify PCR products from substances involved in PCR, PCR products were loaded onto an agarose gel for gel electrophoresis as described in 4.4. Subsequently, PCR products were sequentially digested with Pci and NotI (NEB, Ipswich, MA) and cloned into the pCSE2.5 expression vector upstream of the hinge region and mIgG2c C220S Fc-portion (4.2).

4.4.2. Endonuclease based digestion of inserts and vectors

To clone a new hcAb, exchanging the Fc-portion and not the VHH region is often easier. Instead of exchanging the VHH using PciI and NotI with PCR-based insertion of a PciI cutting site, the Fc-portion was directly exchanged with XbaI and NotI without preliminary PCR. All endonucleases with corresponding buffers to digest DNA-fragments and plasmid-DNA used for cloning were obtained from New England Biolabs (NEB). Endonucleases are enzymes that cut dsDNA in palindrome-sequences. Every reaction was performed in a total volume of 30 μ l. Therefore, 1 Unit of endonuclease was used to digest 1 μ g DNA for 3 hours at 37°C with subsequent heat inactivation of enzymes at 65°C for 20 minutes.

Table 4.2: Reagents used for endonuclease mediated digestion of pCSE2.5 vectors

Reagents	Volume/concentration
3.1 buffer	3 μ l
NotI	1 μ l
XbaI or PciI	1 μ l
DNA	1 μ g
H ₂ O	Fill up to a total volume of 30 μ l

4.4.3. Dephosphorylation of vector DNA

After endonuclease-mediated digestion, vector-based DNA fragments were dephosphorylated to prevent unspecific reformation into cyclic DNA. Therefore, 1 μ l of Antarctic phosphatase (New England Biolabs) and 3 μ l of the tenfold Antarctic concentrated buffer were added to the reaction mixture and incubated at 37°C for 1 hour. The enzyme was heat inactivated at 65°C for 10 minutes.

4.4.4. Agarose gel electrophoresis and PCR-DNA clean up

After endonuclease mediated digestion and dephosphorylation of pCSE2.5 vectors, agarose gel electrophoresis was performed to separate and isolate DNA-fragments based on their size. Therefore, 1% agarose was dissolved in TRIS-Acetate-EDTA-(TAE)- buffer. Then, the solution was poured into a gel chamber and 5 μ l Roti®-GelStain (Carl Roth GmbH + Co. KG) was added to a 100ml agarose solution and a comb was placed. Roti®-GelStain is a substance to visualize DNA bands under UV light. After the gel was hardened, it was placed into a running chamber,

which was filled up with TAE-buffer. Into the first and last gel pocket two different DNA ladders (1 kb and 100 bp, Invitrogen™) were pipetted to later assign different DNA bands to size standards. DNA samples were mixed with 6x loading dye (Thermo Scientific™) and added into the gel pockets in between the DNA ladder. The loading dye contained the dyes Bromphenolblue and Xylencyanol FF to visually observe the progress of gel electrophoresis. On average, for big gels with 100 ml, gel electrophoresis was performed at 100V for 1 hour and 30 minutes for small gels with 50 ml. Validation was done using a UV light transilluminator and a Video-Image-System (BioVision 3000 WL). To extract DNA fragments for further cloning, the gel was placed on the UV- Transilluminator (Type TI1, Biometra) and DNA-bands were cut out in accordance to reference DNA standards. DNA from gel pieces were subsequently purified using the Nucleospin Extract II kit (Macherey-Nagel) according to the manufacturer protocol.

4.4.5. Quantification of DNA

To check for concentration and purity of dsDNA, samples were analyzed using the spectral photometer Nanodrop 2000c. Therefore, the absorption of samples was measured at the wavelength of 260nm and converted concentration using $A_{260} = 1 = 50 \mu\text{g/ml}$ for DNA. The relation of A_{260}/A_{280} was used to determine sample purity. Values between 1,8-2,0 were defined to be pure.

4.4.6. Ligation of DNA fragments

To lastly ligate the inserted DNA fragment with the vector backbone, 100 ng of enzymatically digested, purified plasmid DNA (vector backbone) was mixed with the DNA-insert in a relation of 1:3. DNA fragments were ligated by complementary nucleotide overhangs. The ligase is an ATP-dependent enzyme catalyzing the formation of phosphodiester bonds between 5'-phosphate- and 3'-hydroxygroups of DNA. Ligation was done using vector backbone DNA and DNA-insert in a ratio of 3 to 1 with 1 μL of T4-Ligase (New England Biolabs) in a total volume of 20 μL 1x ligase buffer. Ligation was done in the Thermocycler for 16 hours at 14 °C and the reaction was stopped at 65°C for 10 minutes and paused at 4°C.

4.4.7. Transformation of chemically competent *E. coli* bacteria

To transform chemically competent *E. coli* bacteria with newly cloned DNA, bacteria were heat shocked. DNA from cloning performed with the enzyme combination of PciI/NotI or NcoI/NotI was transformed into XL1-blue *E. coli* bacteria (NEB), whereas DNA digested with XbaI/NotI was transformed into C2925 non-methylating *E. coli* bacteria (NEB). Amplification of DNA in C2925 *E. coli* bacteria enables later digestion with XbaI/NotI, since XbaI can only cut non-methylated sites. Therefore, 100 μL bacteria aliquots stored at -80°C were thawed on ice. In

case of retransformation, 50 µl of bacteria were mixed with 10 ng plasmid-DNA. For new cloning, 50 µl of bacteria was mixed with 2 µl of the ligation preparation. Bacteria and DNA were inverted and incubated on ice for 20 minutes. Then, bacteria were heat-shocked for 30 seconds in a 42°C warm water bath and subsequently incubated on ice for another 2 minutes. Next, a 450 µl pre-warmed SOC-medium was added and cells were incubated for 1 hour at 37°C shaking. In the last step, 400 µl of bacteria transformed with ligation-based DNA or 50 µl of re-transformed bacteria were distributed on carbenicillin containing 2YT-agar plates (1:1000) in a sterile environment. Agar plates were incubated overnight at 37°C.

4.4.8. Isolation of plasmid DNA

In the next step, individual bacteria colonies were picked in 2YT-medium containing carbenicillin (1:1000) and incubated over night at 37°C and 240 rpm. Plasmid-DNA was isolated either using the QIAprep Spin Miniprep Kit from Qiagen or the EndoFree Plasmid Maxi Kit from Qiagen according to the manufacturer protocol.

4.4.9. Sequencing of isolated DNA

To check for successful cloning, DNA was sequenced using the Dideoxy method according to Sanger. Sequencing was performed by Eurofins (Ebersberg). Therefore, 75 ng/µl of DNA was mixed with 2 µl forward or reverse sequencing primer (10µM) and filled with deionized water to a total volume of 17 µl. Evaluation of sequencing data was done with 4Peaks.

4.5. PCR Mutagenesis

In conventional antibodies, the first free Cysteine within the mouse Fc-portion interacts with a free Cysteine in the light chain. Since nanobodies lack the light chain, the free Cysteine can form complexes with other nanobodies. To avoid this, the free Cysteine in mIgG2c at position 220 and mIgG2a at position 224 were exchanged with Serine by PCR mutagenesis. Primers were designed as following:

mIgG2c_C220S_fwd

5'CCAGCGGCCGCTCCATCTCCTCCACTCAAAGAGTG 3'

mIgG2c_C220S_rev

5'CACTCTTTGAGTGGAGGAGATGGAGCGGCCGCTGG 3'

mIgG2a_C224S_fwd

5'CCGACGATTAAGCCGTCTCCGCCGTGTAAGTGTCC 3'

mIgG2a_C224S_rev

5'GGACACTTACACGGCGGAGACGGCTTAATCGTCGG 3'

Table 4.3: Reagents used for PCR

Reagents	Volume (mIgG2c #435)	Volume mIgG2a (#935)
DNA	1.79 µg/µl	1 µg/µl
Reaction Buffer 10x	5 µl	5 µl
DNA Template	1 (of 1 µl DNA + 86.5 µl H ₂ O)	1 (of 1 µl DNA + 49 µl H ₂ O)
125 ng Primer fwd	1.21 µl	1.25 µl
125 ng Primer rev	1.19	1.15
dNTP	1 µl	1 µl
H ₂ O	40.6 µl	40.6 µl
PfuUltra HF Polymerase	1 µl	1 µl
Overlay Mineral Oil	30 µl	30 µl

PCR was performed 1 h at 37°C. PCR products were purified according to the manufacturer's protocol using the PCR Purification Kit described above. Supercoiled dsDNA was digested using 1 µl of DpnI at 37°C for 1 hour. Then, 2 µl of each PCR product were transformed as described in 4.7 and DNA was isolated as described in 4.8-4.9 and the DNA was sequenced.

4.6. Transient transfection of HEK293-6E cells with recombinant hcAbs

Selected nanobodies (7D12 (EGFR), JK3, JK5, JK13, JK16, NB3, NB7, NB11, NB22, NB24, NB28, NB32, NB38, NB40 and NB42) with different Fc-portions (rbFc WT, hIgG1 WT, hIgG1-E, hIgG1-T, hIgG1-TE, mIgG2c WT, mIgG2a WT C224S, mIgG2a ADS, mIgG2a LALAPG) were subcloned behind the hinge region into the pCSE2.5 vector using NotI and XbaI as described in 4.2.

Transfection of HEK293-6E cells was done using 7.5 mM (0.333 mg/ml) of PEI (Polysciences Inc.) was used. Depending on the volume to be transfected, either 10 µg DNA, 40 µg PEI (124 µl) and 250 µl ddH₂O were prepared for a transfection volume of 10 ml (T75 culture flask) or 30 µg DNA, 80 µg PEI (248 µl) and 750 µl ddH₂O were mixed for a transfection volume of 30ml. All DNA/PEI mixes were vortexed in 1:1 with 300 mM NaCl (150 mM NaCl in final volume) for 10 seconds. Then, the PEI-mix was added drop by drop to the DNA/NaCl-mix, and vortexed for another 10 seconds with a subsequent incubation of 20 minutes at RT. The DNA/PEI Mix was added very slowly to the corresponding cell culture flask directly onto HEK293-6E cells cultivated in F17 transfection medium. 24 hours post transfection, 0.1-0.2 mg Tryptone N1 were added to prevent cells from starving. Six days post transfection, supernatants were harvested and cleared by centrifugation, 4000 rpm for 10 minutes.

4.7. SDS-Polyacrylamide gel electrophoresis and Coomassie staining

Recombinant proteins in HEK293-6E cell supernatants were quantified by SDS-PAGE (sodium dodecyl sulfate polyacrylamide gel electrophoresis) and Coomassie staining relative to marker

proteins of known quantities: 10 µl samples of the supernatant were size fractionated side by side with standard proteins: m/M (amount loaded per lane in µg) bovine serum albumin (1/4), IgH (0.5/2), IgL (0.25/1), hen egg lysozyme (0.1/0.4). Therefore, samples were mixed with Loading dye (4x), NuPAGE™ reducing agent (10x) and deionized water and denaturated at 70°C for 10 minutes. Electrophoresis was done in 10 % Bis-Tris NuPAGE™ gels (Thermo Fisher Scientific) in MES-running buffer at 200 V for 45 minutes. Bands were visualized using Coomassie-blue staining solution from the Collidial Blue Staining Kit (Invitrogen™). Yields of recombinant hcAbs typically ranged from 0.5–3 µg/10 µl. For pilot assays supernatants containing hcAbs were used; in case of potentially good killing hcAbs or enzyme modulating hcAbs, hcAbs were purified by affinity chromatography using protein G or A sepharose (GE healthcare) as described in the following.

4.8. Protein purification

Heavy chain antibodies were purified from HEK293-6E cells via affinity chromatography. Thereby, constant domains of the hcAbs were bound to Protein G, which was immobilized as a ligand of the Sepharose matrix. 60-90 ml culture supernatant of transiently transfected HEK293-6E cells were loaded onto Protein G Sepharose 4 Fast Flow (GE Healthcare) columns, and unbound proteins were eluted using 20 ml PBS after the supernatant was flown through. The elution of bound hcAbs was performed with a low pH-IgG elution buffer pH 2.8 (Thermo Fisher Scientific) in three fractions (eluate 1: 1.2 ml, eluate 2 and 3: 2.5 ml each). The acidic pH was neutralized with a tenth volume of 1M Tris at pH9. Via PD-10 columns, the buffer of eluates with the highest protein concentration (E2 and E3) was exchanged to PBS+/+. To increase the concentration of the purified protein, Amicon centrifugation filters with a 10.000 cut off were used. Purified heavy chain antibodies were stored with 0.02% sodium azide at 4 °C.

For flowcytometric analysis, purified hcAbs were conjugated with fluorochrome Alexa Fluor 647 (AF647) as described in 10. and stored at 4°C.

4.9. Calculation of protein concentration from purified hcAbs

To determine the concentration of purified hcAbs, the Thermo Scientific™ Pierce™ BCA Protein Assay Kit was used. The assay is based on bicinchoninic acid (BCA) enabling a colorimetric detection and quantitation of total protein. Bovine gamma globulin (BGG) standard proteins of known concentrations were diluted as described in the manufacturer protocol. Standards were assayed alongside the purified hcAbs; therefore, hcAbs were diluted 1:10 and 1:5 in duplicate wells and a pre-mixed solution of A:B (50:1) was added to a total volume of 200 µl for 30 minutes at 37°C. The assay was then analyzed in a spectrophotometer (VIKTOR3) at 562 nm and concentrations of hcAbs were calculated using the standards.

4.10. Fluorochrome conjugation of heavy chain antibodies

For flow cytometric assays, a part of purified hcAbs was conjugated with a fluorochrome. For conjugation of the fluorochrome Alexa Fluor 647 (AF647) with hcAbs, the Kit Molecular Probes Alexa Fluor 647 Kit from Thermo Fisher Scientific was used. To prepare the matrix for column chromatography, columns were prepared using Sephadex G-50 Fine (GE Healthcare) was mixed with PBS-/ to get 10 ml of matrix. To prepare the conjugation, the fluorochrome was resuspended in 100 µl Dimethylformamid (DMF, 10 mg/ml) and vortexed for 5 minutes at RT. 25 µl of the DMF/Fluorochrome-mix was added to 1 mg hcAb and incubated for 1 hour at RT rolling. After 1 hour, the conjugated-hcAbs were pipetted onto the prepared column, followed by the addition of 500 µl elution buffer (PBS-/) until two blue bands, separated by a colorless band, were detectable. The first band for elution were the conjugated hcAbs, the second colorless band was unconjugated protein and the third band was unconjugated fluorochrome. As soon as drops of the first band arrived at the bottom line of the column, conjugated hcAbs were collected. The conjugation was validated by photometric measurement (Ultraspec 2000); therefore, the absorption of the sample at 650 nm was calculated compared to the absorption at 280 nm. HcAbs-AF647 were stored in brown Eppendorf tubes at 4°C.

4.11. Cross-blockade analyses on mouse CD38 epitope

For epitope analyses, mCD38 EL4-thymoma cells were preincubated with a saturating concentration (100 nM) of unconjugated hcAbs with mIgG2c Fc portion for 30 minutes at 4°C. CD38-negative EL4 alt cells were used as a control. Then, mCD38 EL4-thymoma cells stained with Alexa⁶⁴⁷-conjugated CD38-specific hcAbs (500 ng in 0.5 µl PBS) with pre-defined epitopes for 20 minutes at RT and analyzed by flow cytometry on a BD-FACS Canto. Data was analyzed using the FlowJo software (Treestar). The percentage of cross-blockade was then calculated from mean fluorescence intensities (MFI) as follows:

$$\frac{\text{MFI in absence of competing Abs} - \text{MFI in presence of competing Abs}}{\text{MFI in presence of competing Abs}} \times 100.$$

4.12. Dissociation assay of anti-mouse CD38 hcAbs

To analyze binding affinities and relative dissoziation rates of hcAbs, two separate aliquots of mouse CD38-expressing EL4 thymoma cells were incubated either with Cell Proliferation Dye eFluor 450 (eBioscience) or with were incubated with 100 nM Alexa⁶⁴⁷-conjugated hcAbs for 30 minutes at 4°C. Control staining was performed with CD38-negative EL4 alt cells. Cells were thoroughly washed (1600 rpm, 5 minutes at 4°C) and then mixed at a 1:1 ratio with eFluor

450-tagged mCD38 EL4-thymoma cells and further incubated at 4 °C for 0.5, 1, 2, 3 and 6 hours before FACS analyses. The dissociation of hcAbs from EL4-thymoma cells and association with the eFluor 450 labeled cells was analyzed using the FlowJo software (Treestar).

4.13. Transient transfection of HEK-T cells with mouse- and human CD38

mCD38, hCD38 and eGFP subcloned into the pcDNA.6 vector were used to transiently transfect HEK-T cells. Therefore, HEK-T cells were seeded into DMEM (Gibco™) complete medium (1 mM Natrium-pyruvate, 2 mM L-Glutamine, 10 mM HEPES, 1 x non-essential Amino Acids, 10% FCS) at 40% confluency 24 hours prior to transfection. Transfection was prepared as described in 6. To evaluate transfection efficacy, 1.5 µg of eGFP was co-transfected with hCD38 and mCD38. DNA/PEI Mix was then added very slowly directly onto HEK-T cells cultivated in a DMEM complete medium. 24 hours post transfection, successful transfection was controlled GFP-signal in a fluorescence microscope (EVOS). Right after, the transfection medium was exchanged with a DMEM complete medium, since PEI might be cell toxic. 48 hours post transfection, cells were harvested and used for further FACS analysis of binding assays, blockade assays and CDC assays.

4.14. CDC of transiently transfected HEKT-mCD38 cells

To analyze the complement-dependent cytotoxicity (CDC) mediated by hcAbs binding to two different epitopes, CDC assays were performed. mCD38 EL4-thymoma cells were incubated for 10–20 minutes at 4 °C with mIgG2a-Fc-based hcAbs before addition of pooled human serum (15% v/v) as a source of complement before 90 minutes incubation at 37 °C. As a negative control, heat inactivated serum (30 minutes at 56 °C) was used to verify complement dependency. Cells were washed and resuspended in PBS/0.2% BSA/propidium iodide before FACS analysis. The CDC assay was quantified by flow cytometry measuring propidium iodide (PI) uptake. The percentage of lysed cells was defined as percentage of PI-positive cells.

The experimental set up had to be changed, since mCD38-expressing EL4 thymoma cells showed 98% lysis without addition of hcAbs, due to autoreactive IgG or IgM antibodies naturally occurring in human serum. Therefore, we next used HEKT cells and transiently co-transfected them with mouse CD38 (in pcDNA vector) or human CD38 (pcDNA vector) and GFP using the Jet-PEI transfection protocol (described in 13.). 48 hours post transfection, HEKT-mCD38- and HEKT-hCD38-cells were then used for CDC as described above.

4.15. ADCC of mouse thymoma cell lines

To determine NK-cell mediated lysis of mCD38 EL4-thymoma cells, ADCC assays were performed. mCD38 EL4-thymoma cells were incubated for 10–20 minutes at 4°C with 10 µl supernatants of the hcAbs JK3, JK5, JK13 and JK16 with an mIgG2a WT C224S and mIgG2a mADS Fc-portion As a negative control, the ADCC and CDC abrogating mutations LALAPG were inserted into in the mIgG2a Fc-portion of the corresponding hcAbs. To distinguish the effector NK-92 murine- or human-CD16 cells from target thymoma cells, NK92-CD16 cells were tagged with eFluor450 for 10 minutes at 4°C, washed 3 times (1600 rpm, 5 minutes, 4°C) and then were added at an effector to target ratio [E:T] of 3:1. Cells were co-incubated for 3 hours at 37°C, followed by a 2 times washing step. Cells were then resuspended in 1:500 Propidium Iodid (PI) in PBS+ 0,2% BSA before flowcytometric measurement. The percentage of dead cells was defined as percentage of PI-positive cells.

4.16. Human EGFR-specific antibody and -nanobody binding to EGFR-escape variants

Ba/F3 cells stably transduced with either EGFR WT or EGFR S492R, K467T, G465R, S464L and R451C (cloned in LEGO.puro-IG vector) were stained for 30 minutes at RT with a polyclonal EGFR antibody (R&D Systems), the therapeutic antibodies cetuximab or panitumumab, or heavy-chain antibodies 7D12- or 9G8-hIgG1. After washing cells twice (1600 rpm, 5 minutes) in PBS/BSA 0.2%, primary staining was followed by appropriate fluorescently labeled secondary antibodies (R&D Systems) for 30 minutes, RT in the dark. Then, cells were washed twice again with subsequent flow cytometric analysis on a FACSCanto (Becton Dickinson). Percentages of stained cells of total EGFR-positive cells were determined with FlowJo v.10.4 (Tree Star).

4.17. Cellular proliferation assay of human EGFR-escape variant – and WT cells

Ba/F3 cells expressing either the *EGFR* WT or *EGFR* G465R were seeded in triplicates at a density of 1×10^6 cells/mL. Cells were treated every 24 hours with 5 µg/mL cetuximab (Merck, obtained from the UKE hospital pharmacy), 2.5 µg/mL panitumumab (Amgen, hospital pharmacy UKE), or 2.5 µg/mL 7D12-hcAb or in the corresponding absence of therapeutics as controls, without or in combination with EGF (5 ng/ml). The average number of viable cells in a total volume of 500 µl was measured daily for 7 days after trypan blue staining using Vi-CELL Cell Viability Analyzer (Beckman Coulter).

4.18. 3D Spheroid proliferation assay of human EGFR WT- and EGFR R521K cells

UTSCC14 or SAT cells were washed and resuspended in ice cold DMEM medium containing 10% FCS, 1% penicillin/streptomycin, 5 ng/mL EGF, and 2% Matrigel Growth Factor Reduced (GFR) Basement Membrane Matrix or without GFR as control. Matrigel was thawed on ice for 2 hours. Tips used for pipetting and cell culture plates were stored at -80°C for 3 hours prior to the experiment in order to avoid rapid polymerization of the GFR Matrigel. Cell suspension (1×10^4 cells/mL) was seeded in a 96-well Greiner Bio-One CELLSTAR™ Cell-Repellent Surface Cell Culture Multiwell Plates (Fisher Scientific) and centrifuged at $1000 \times g$ for 10 minutes at 4°C. After 7 days of culture, 100 μ L medium with 5 μ g/mL cetuximab, 2.5 μ g/mL panitumumab, 2.5 μ g/mL 7D12-hcAb or medium alone as control were added. The medium was changed every other day, and spheroid size was calculated until day 13 was reached. Pictures were taken daily with $10 \times$ magnification using Axiovert 25 microscope and AxioCamMRc (Carl Zeiss). Cell size was calculated using AxioVision v4.9. (Carl Zeiss).

4.19. Construction of humanized 7D12-E345R-hcAb and 7D12-G236A-S239D-I332E-hcAb

The previously published (Roovers et al., 2011) coding sequence of 7D12 was cloned via NcoI and NotI into the pCSE2.5_IgG1 expression vector upstream of the hinge, CH2 and CH3 domains of human IgG1 (kindly provided by Thomas Schirrmann, Yumab, Braunschweig, Germany) as described in 4.; The CDC-enhancing E345R mutation was introduced into the 7D12-E-hcAb by PCR-mediated mutagenesis as described in 5. The mutation was confirmed by sequencing. In order to ensure that no other mutations were introduced into the vector, the hIgG1 Fc-portion encoding the E345R mutation was recloned into the pCSE2.5 vector using flanking restriction sites (NotI and XbaI). The coding sequence of G236A-S239D-I332E (Triple, T) 7D12-T-hcAb mutated hIgG1 Fc-portion was generated by Integrated DNA Technologies (IDT) and cloned into the pCSE2.5 vector downstream of the hinge region. Recombinant anti-EGFR hcAbs were expressed in HEK293-6E cells and purified by protein A chromatography as described in 6. And 8., respectively.

4.20. CDC-mediated killing of HNSCC cell lines

To analyze the cytotoxic potential of the EGFR-hcAb, UTSCC14 and SAT cells were washed and resuspended in PBS containing 0.2% BSA. Cells were seeded at a density of 50.000 in a total volume of 200 μ L in 96-well plate and 5 μ g/mL cetuximab, 2.5 μ g/mL panitumumab, 2.5 μ g/mL 7D12-hcAb, 7D12-E-hcAb, or 7D12-T-hcAb were added. 15 minutes post incubation with therapeutic constructs, 50 μ L of human serum as a source for complement or 50 μ L of control complement-inactivated human serum (preheated 30 minutes at 56°) were added. Cells were incubated for 3 hours at 37°C in a humidified atmosphere with 5% CO₂. Then, cells were

washed twice in PBS/BSA 0.2% (1600 rpm, 5 minutes, 4°C) and resuspended in PBS with propidiumiodid (PI) (1:500) to stain dead cells that were quantified on a FACSCanto (Becton Dickinson).

4.21. ADCC mediated killing of HNSCC cell lines

The effector cell-mediated cytotoxicity of 7D12-hcAb, 7D12-T-hcAb, or 7D12-E-hcAb and antibodies cetuximab and panitumumab was analyzed in a standard 4 hours ^{51}Cr release assay using human effector mononuclear cells (MNC) from healthy donors. MNCs were isolated from whole blood using two layers of 70% Percoll and 63% Percoll. After a 20 minutes centrifugation at 2.500 rpm at RT, no break, a white layer of MNCs was isolated. In case of many erythrocytes, 1-2 times erythrocyte lysis was performed. In the meantime, HNSCC target cells were tagged with chromium (50 μL ^{51}Cr chrom per 600.000 cells) and incubated with a slightly opened lid for 2 hours at 37°C in a humidified atmosphere with 5% CO_2 . Then, target cells were washed 3 times in R10+ medium. A 40:1 effector-to-target ratio was used in these experiments. The ADCC assay was performed in 96-well microtiter plates in a total volume of 200 μL . 5 $\mu\text{g}/\text{mL}$ cetuximab, 2.5 $\mu\text{g}/\text{mL}$ panitumumab, 2.5 $\mu\text{g}/\text{mL}$ 7D12-hcAb, 7D12-E-hcAb, or 7D12-T-hcAb were mixed with cells at an 40:1 effector-to-target ratio, followed by a 3 hours incubation at 37°C. Rituximab and Fc-optimized rituximab-IgG1-DE (S239D and I332E) were used as control at indicated concentrations. After the incubation, plates were centrifuged at 2.000 rpm for 5 minutes and 25 μL of supernatant was mixed with scintillation solution supermix (Applied Biosystems) and incubated for 15 minutes with agitation. ^{51}Cr release from triplicates was measured in counts per minute (cpm). Percentage of cellular cytotoxicity was calculated using the formula: % specific lysis = (experimental cpm – basal cpm)/(maximal cpm – basal cpm) \times 100. Maximal ^{51}Cr release was determined by adding Triton X-100 (1% final concentration) to target cells, and basal release was measured in the absence of sensitizing proteins and effector cells using a scintillation counter device.

4.22. Fluorometric enzyme assay of mouse thymoma and human myeloma cells

To determine the inhibitory or stimulatory effect of our anti-mouse and -human CD38 hcAbs on the enzymatic CD38 cyclase activity, a fluorometric enzyme assay using nicotinamide guanine dinucleotide (NGD⁺) as substrate was performed. NGD⁺ is converted to cyclic GDP-ribose (cGDPR) and nicotinamide followed by a very slow hydrolysis of cGDPR to GDPR, leading to accumulation of the fluorescent product cGDPR. Enzymatic production of cGDPR from NGD⁺ (50 μM , Sigma, St Louis, MO) was monitored continuously for 50 minutes at 410 nm (emission wavelength) with the excitation wavelength set to 300 nm, using a Tecan Infinite M200 microplate fluorimeter. As a source for CD38, mouse CD38-expressing EL4 thymoma cells or LP1 cells expressing human CD38 were resuspended in calcium-containing buffer and

seeded at a cell density of 1×10^5 cells/well at 37°C in the dark. 15 minutes prior to starting the fluorescence measurement, hcAbs or the CD38-inhibitor araF-NAD (BioLog, Bremen) were added to hCD38-LP1- or mCD38-EL4 thymoma cells at 37°C in a concentration of 10 µg/ml or 1 µg/ml; For some inhibitory selected hcAbs, a dilution series from 10 µg/ml down to 0.01 µg/ml was performed in duplicates. After recording 20 cycles, 500 µM NGD⁺ was added, followed by further incubation in the dark at 37°C for another 50 minutes. Readings (EX300/EM410) from wells without CD38 were subtracted from all sample readings and were plotted for each hcAb concentration in Relative Fluorescence Units (RFU) vs. time. The rate of cGDPR production was calculated as the slope of these curves (RFU/s) during the linear phase of the reaction, i.e. between t=500 seconds and t = 1200 seconds.

4.23. HPLC analysis of a human myeloma- and murine thymoma cell line

Metabolism of NAD⁺ and cADPR by the ectoenzyme CD38 on the surface of mCD38 EL4-thymoma cells and hCD38 LP1 cells was analyzed by HPLC. When NAD⁺ is added as a substrate the ADP-ribosyl cyclase activity and NAD glycohydrolase activity of CD38 can be followed, whereas addition of cADPR as substrate exhibits the cADPR hydrolase activity of CD38. To determine the kinetics of turnover of NAD⁺ and cADPR by LP1 cells (expressing human CD38), 1×10^5 cells were incubated with NAD⁺ (500 µM) or cADPR (500 µM) for 0 (without cells), 5-, 10-, 20-, 60-, 180 minutes and 24 hours at 37°C, shaking at 600 rpm. After incubation cells were removed by centrifugation (2300 rpm for 5 minutes at 4°C) and the supernatants passed through a centrifugal filter device with 10 kDa cut off (Vivaspin at 10000 rpm for 15 minutes at 4°C) to remove proteins shedded or released from the cells. These samples were then analyzed by reversed-phase HPLC with or without ion-pair reagent on 1200 and 1260 Series systems from Agilent Technologies. Due to the better separation and resolution cADPR was analyzed by reversed-phase HPLC on a C-8 Luna column (Phenomenex) with buffer A (20mM KHPO₄, pH 6), a flow rate of 0.8 ml/minutes and the following gradient 0 minutes, 0% MeOH; 5 minutes, 0% MeOH; 27,5 minutes, 50% MeOH; 30 minutes, 50% MeOH; 32 minutes, 0% MeOH; and 43 minutes, 0% MeOH. All other metabolites were analyzed by reversed-phase HPLC with the ion-pair reagent tetrabutylammonium dihydrogen phosphate (TBAHP) on a Multohyp BDS C18 column (250 mm, 4.6 mm, particle size 5 µm; Chromatographie Service) with buffer A (20 mM KHPO₄, 5 mM TBAHP, pH 6) and the following gradient: 0 minutes, 15% MeOH; 3.5 minutes, 15% MeOH; 11 minutes, 31.25% MeOH; 15 minutes, 31.25% MeOH; 25 minutes, 50% MeOH; 27 min, 50% MeOH; 29 min, 15% MeOH; and 38 min, 15% MeOH. In both cases the flow rate was 0.8 ml/minutes. Absorbance was measured at 260 nm using the DAD detector of the Agilent systems and data were processed using the ChemStation (Rev. C.01.05; Agilent Technologies). Peaks were identified by comparing their retention time to known standards. For NAD⁺, ADPR, cADPR and AMP standard curves were constructed by plotting the “area under the curve” against amount of substance for at least three standards

with different concentrations. Using the slope from these standard curves the amount of the nucleotides in the samples was determined.

Furthermore, the effect of different reducing agents (TCEP, DTT and GSH) on NAD glycohydrolase and ADPR cyclase on LP1 cells was analyzed. LP1 cells were preincubated with a dilutional series of the respective reducing agents (10 μ M – 5 mM) at 37°C, 15 minutes prior to addition of 500 μ M NAD⁺. The reaction was stopped 60 minutes later. Samples were then further processed as described above.

4.24. Marker expression of primary patient bone marrow cells

Fresh primary MM cells were obtained from bone marrow aspirates after IRB-approved consent was obtained from all patients. Experiments were performed in accordance with the ethical standards of the responsible committee on human experimentation and with the Helsinki Declaration. The study was approved by the local IRB committee (PV5505). Bone marrow mononuclear cells (BMMCs) were prepared by Ficoll-Paque density gradient centrifugation of bone marrow aspirates. Therefore, the bone marrow aspirate was diluted 1:2 with NaCl and carefully pipetted onto 15 ml Ficoll with subsequent centrifugation at 4000 rpm for 40 minutes at 4°C without brake. After gradient centrifugation, the white/yellowish layer of MNCs was transferred into a new Falcon tube and diluted with NaCl (1:2) and centrifuged again at 1600 rpm for 5 minutes at 4°C. Supernatant was discarded and the cell pellet was resuspended in 5 ml red blood cell lysis buffer (NH₄Cl + KHCO₃ + EDTA) for 5 minutes. Lysis reaction was stopped by adding 15 ml of PBS/BSA (0.2%) and centrifuged again for 5 minutes at 1600 rpm at 4°C. Thereafter, the cell pellet was resuspended in alpha-Mem medium for further culture and PBS/BSA (0.2%) for subsequent marker analysis, ADCC and CDC assays. To analyze the marker expression profile, BMMCs were incubated with directly labeled antibodies against CD38, CD138, CD229, CD269, CD319, CD56, CD55, CD59, CD19 and CD45 for 30 minutes in the dark at 4°C. Then cells were washed twice (1600 rpm, 5 minutes at 4°C) and resuspended in PBS/BSA (0.2%), followed by flow cytometric analysis. MM cells were further used for CDC and ADCC analysis if the CD38/CD138 double positive population was larger than 2% of total alive single cells.

4.25. CDC and ADCC of primary MM cells from patient bone marrow

For CDC assays, patient BMMCs were incubated in PBS/BSA (0.2%) and 100 nM CD38-specific hcAbs, isotype control (L-15-hcAb), or daratumumab and 12.5% pooled human serum as a source of complement for 90 minutes.

For ADCC assays, BMMCs were incubated in alpha MEM and 100 nM CD38-specific hcAbs, isotype control, or daratumumab and NK92 cells stably transduced with CD16 and GFP at an effector to target ratio [E:T] of 3:1 for 3 h.

For both assays, cells were washed twice with PBS/BSA (0.2%) after the corresponding incubation time. Then, cells were stained with a panel of commercially available antibodies (CD38, CD45, CD138, CD229, CD55, CD59, CD269, CD319, CD56, CD19) that allow the differentiation of MM cells from stroma cells or lymphocytes and analyzed via flow cytometry. Staining of CD38 was achieved with Alexa⁶⁴⁷-conjugated hcAbs that bind independently of the hcAb/mAb used for CDC/ADCC: JK36⁶⁴⁷ or MU523⁶⁴⁷ for daratumumab and WF211-hcAb, MU523⁶⁴⁷ for JK36-hcAb, and JK36⁶⁴⁷ or WF211⁶⁴⁷ for MU1067-hcAb. Staining was performed for 30 minutes in the dark at RT, followed by two washing steps (1600 rpm, 5 minutes at 4°C). Cells were resuspended in PBS/BSA (0.2%) and subsequently analyzed at a FACS Celesta. To exclude debris, an FSC threshold was set in a way that the population of small CD19+ B cells were still included. In case of ADCC, GFP-expressing NK-92 cells were excluded by gating on GFP-positive vs. negative cells. MM cells in both assays were identified by high co-expression of CD38 and CD138.

As described above, we cultivated primary MM cells up to 21 days. Flow cytometric analysis of expression markers were performed at d0, d3, d6, d9 and d15. CDC assays were performed at day 6, day 9 and day 15 (in this thesis only day 6 is shown). CDC- assays were performed according to the description above.

4.26. Synthesis of recombinant Nanobody-displaying AAV for transduction of primary MM cells

Nanobody-displaying AAV used for this thesis were kindly provided by Dr. Anna Marai Eichhoff (Eichhoff A, dissertation MIN faculty, Hamburg, 2018).

In this work here, Nanobody-displaying AAV were analyzed on their potential to transduce multiple myeloma patient bone marrow cells. Primary MM cells that had been cultivated for 7 days after isolation were seeded in 96 well culture plate (3×10^5 cells/well) in aMem medium with 12.5% FCS (Gibco), 12.5% horse serum (Gibco), 100 IU/mL IL2 (Proleukin) and 2 mM L-Glutamine (Gibco). Then, 2000 – 0 viral genomes of Nanobody-displaying AAV were diluted in alpha Mem medium and were added to the cells in triplicates. Transduction efficacy was first analyzed after 24 hours using the fluorometric microscope EVOS (ThermoFisher). After 48 hours, transduction efficacy was evaluated by flow cytometric analysis (FACSCelesta, BD Biosciences) of the yellow fluorescent protein (YFP) expression in primary MM cells. To distinguish primary MM cells from BMMCs, cells were stained with an CD38-nanobody that binds independently from the nanobody used in the CD38-Nb-displaying AAV (JK36), CD138, CD56, CD319, CD19 and CD45 for 30 minutes in the dark at RT. Then, cells were washed twice with PBS/BSA (0.2%) and were subsequently FACS-analyzed. AAV-Nb transduction of MM cells was quantified using FlowJo software (Treestar).

4.27. Synthesis of antiAAV-antiCD38 bispecific adaptor proteins to mediate AAV transduction of primary MM cells

Bispecific AAV-nanobody adaptors used for this thesis were kindly provided by Dr. Anna Marai Eichhoff (Eichhoff A, dissertation MIN faculty, Hamburg, 2018).

For this thesis, antiAAV-antiCD38 bispecific adaptor proteins were analyzed on their potential to transduce multiple myeloma patient bone marrow cells. Primary MM cells that had been cultivated for 7 days after isolation from a MM patient were co-incubated with bispecific adaptor proteins MU1067-AAV2 and MU370-AAV2 at different concentrations ranging from 0 to 500 vg/cell for 30 minutes at RT. Adaptors that had not bound were removed in three following washing steps using complete alpha Mem medium. BMMCs were seeded in a-Mem medium with 12.5% FCS (Gibco), 12.5% horse serum (Gibco), 100 IU/mL IL2 (Proleukin) and 2 mM L-Glutamine (Gibco) at a concentration of 3×10^5 cells/well in triplicates. Lastly, 0 - 500 viral genomes of AAV2RA were added to the cells. Transduction efficacy was first analyzed after 24 h using the fluorometric microscope EVOS. 48 hours post transfection, transduction efficacy was evaluated by flow cytometric analysis (FACSCelesta, BD Biosciences) of the yellow fluorescent protein (YFP) expression in primary MM cells. (Treestar). The following staining and washing steps were performed according the protocol described above for Nanobody-displaying AAV.

4.28. Data evaluation and statistical analysis

Data were depicted using GraphPad Prism version 7.00 (GraphPad Software). For statistical evaluation, unpaired student *t*-test, one-way or two-way ANOVA (multiple comparison) were used with *P*-values being calculated using two-sided tests. Results were considered statistically significant for $P < 0.05$ (*), very significant for $P < 0.01$ (**), and highly significant for $P < 0.001$ (***). In all experiments, data represent mean \pm SD of representative or combined experiments.

5. Results

5.1. Selection and characterization of mouse CD38-specific nanobodies

5.1.1. Phage display selection yields 5 families of mouse CD38-specific nanobodies

The molecular mechanisms of a multiple myeloma (MM) are still barely understood. Hence, we aim to long term establish a syngraft MM mouse model that can be targeted with anti-mouse CD38 hcAbs. We therefore in this thesis aimed to select and characterize mouse CD38-specific heavy chain antibodies (hcAbs). To do so, two llamas had been immunized with cDNA expression vectors for CD38. Phage libraries were established, and negative and positive selection panning rounds were performed on primary mouse splenocytes from CD38 WT and CD38 ko BL/6 mice and CD38-expressing EL4 mouse thymoma cell line. The results revealed a selection of clones derived from 5 distinct nanobody families, with CDR3 lengths ranging from 3 to 13 amino acid residues (Fig. 5.1). Sequences of the characteristic VHH motif in framework region 2 (FR2) and of the complementarity determining region 3 (CDR3) are shown.

clone	family	FR2	CDR3	length
JK3	1	QREL	YIVPYGTGSAYTV	13
NB11	1	QREL	YIVPYGTGSAYTS	13
JK5	2	EREF	DLFDRLVIPREST	13
NB32	3	QREV	LNy	3
JK13	4	EREF	WPPRAASWDDYDY	13
JK16	4	EREF	WPQRSASWDDFDY	13
NB3	4	EREF	WPPRAASWDEYDY	13
NB7	4	EREF	WPPRSASWDDYDY	13
NB22	4	EREF	WPPRSASWDDYDY	13
NB24	4	EREF	WPPRAANWDEYDY	13
NB38	5	QREL	DVVDSRGLGFDDY	13
NB40	5	QREL	DVVDDRGLGFDDY	13
NB42	5	QREL	DVVDDRGLGFDDY	13

Fig. 5.1: Alignment of anti-mouse CD38 VHHs revealed five new nanobody families.

Two llamas (538 and 539) were immunized with a cDNA expression vector encoding full length CD38. Phage display libraries were generated by PCR- amplification of the VHH-repertoire from blood lymphocytes obtained 4–10 days after the last boost immunization. Mouse CD38-specific nanobodies had previously been selected by binding of phages to CD38 positive EL4 thymoma cell line (JK VHHs). Another round of mouse CD38-specific nanobody selection was performed in the work for this thesis using CD38 KO mice for a negative selection (preabsorption), followed by positive selection on splenocytes derived from CD38 WT BL/6 mice (NB VHHs). Selected clones were sequenced and clones that share the same framework and highly similar CDR3 sequences were defined as a family, i.e. family 1 – family 5, from top to bottom. The four amino acids listed under FR2 correspond to the characteristic VHH motif of hydrophilic residues in framework region 2.

5.1.2. Generation and site directed mutagenesis of heavy chain antibodies

To allow Fc-mediated effector functions in later assays, including antibody dependent cell-mediated cytotoxicity (ADCC) and complement dependent toxicity (CDC), nanobodies depicted in Figure 5.1 were fused to the hinge, CH2 and CH3 domains of various IgGs: rabbit IgG, mouse IgG2c, mouse IgG2a, and human IgG1. Moreover, mutations were introduced by site directed mutagenesis to enhance or ablate Fc-mediated effector functions, including mutations to enhance CDC (E345R or E430S) or to ablate ADCC and CDC (L234A L235A, P329G). Successful mutagenesis was verified by DNA sequencing (Fig. 5.2).

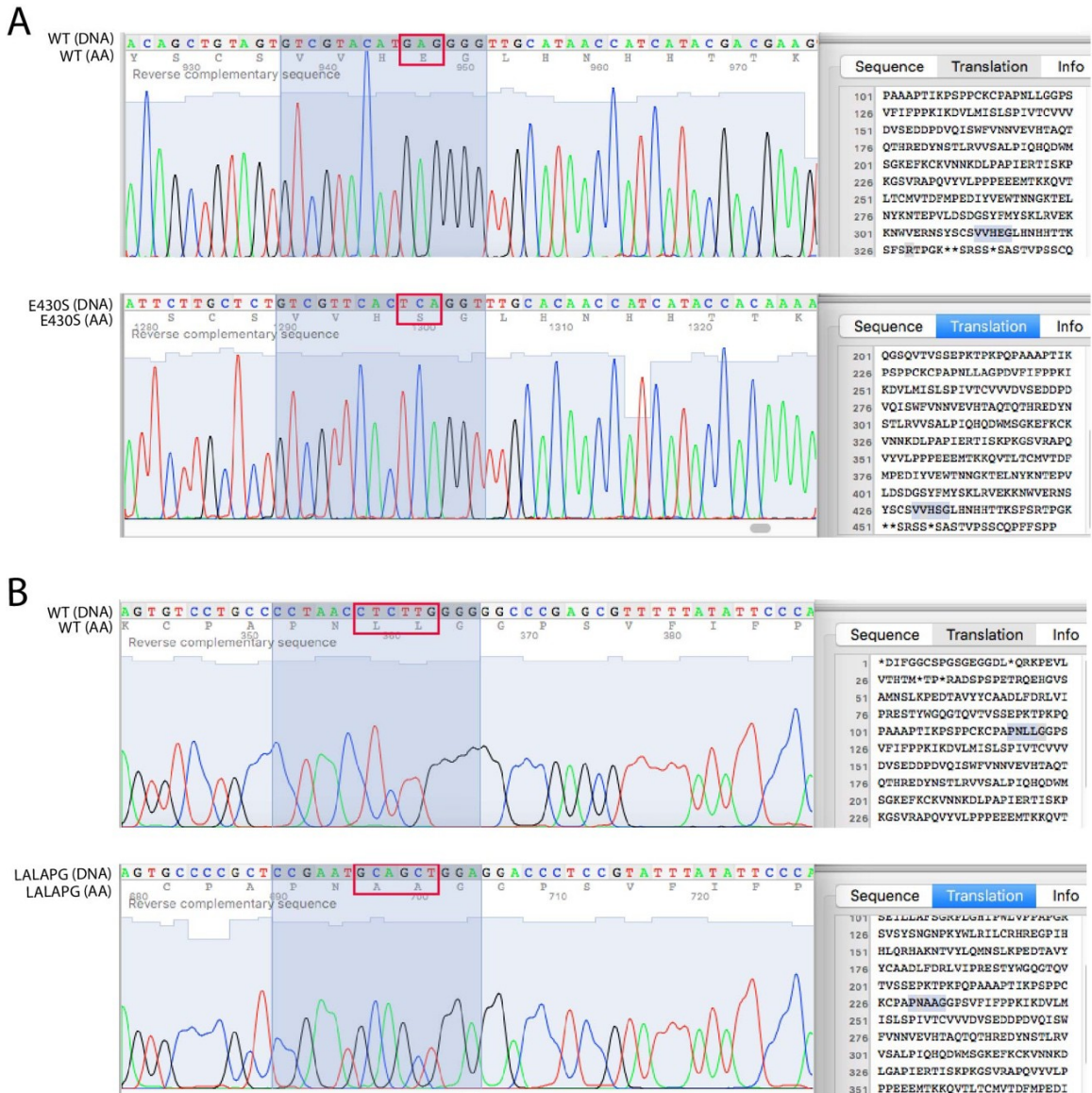


Fig. 5.2: Sequence alignment of wildtype mouse IgG2a and two Fc-engineered mutants for enhanced (ADS, G236A S239D) and reduced (LALAPG, L234A L235A) Fc-mediated effector function.

Fc engineered hcAbs were generated by site-specific PCR mutagenesis. Mutated sequences were confirmed using Sanger sequencing. (A) shows WT vs. CDC-enhanced Fc-portion, (B) shows WT vs. CDC-abrogating mutations. Exchanged amino acids are highlighted in red.

The production of mouse CD38-specific heavy chain antibodies (hcAbs) was done by transient transfection of HEK293-6E cells. Supernatants containing the hcAbs were harvested 6 days post transfection. To control for integrity and amount of recombinant protein in HEK cell supernatants, an SDS-PAGE was performed (Fig. 5.3). Marker proteins (SM) of known concentration served as a reference to quantify protein concentration in supernatants. All hcAbs were typically produced at a concentration of 1-2 $\mu\text{g}/10\ \mu\text{l}$. Thereafter, hcAbs were purified via Protein A based affinity chromatography, protein concentrations were determined, and some hcAbs were conjugated to fluorochromes for use in flow cytometry.

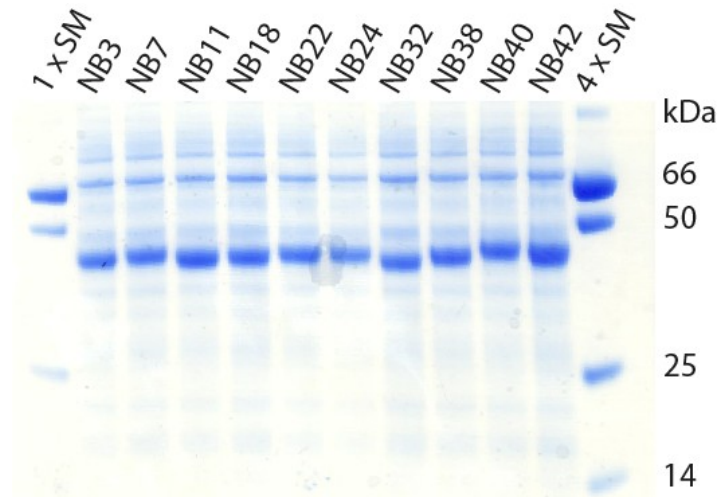


Fig. 5.3: SDS PAGE analyses confirms high level expression and secretion of recombinant mCD38-specific hcAbs by HEK-6E cells.

Expression constructs for VHHs fused to the desirable Fc-portion (here mIgG2c) were transiently transfected into HEK-6E cells using the Jet-PEI transfection method. Supernatants were harvested 6 days post transfection and production of hcAbs was verified using size fractionation of proteins by SDS-PAGE (10 μl HEK-cell supernatant per lane) and subsequent Coomassie staining. The prominent bands at ~45kD correspond to hcAbs.

5.1.3. Cross blockade analyses reveal three independent epitopes on mouse CD38

In order to assign the binding epitopes of the selected nanobodies, a cross blockade flow cytometry analysis was performed (Fig. 5.4). Therefore, Alexa⁶⁴⁷conjugated JK3-mIgG2c, JK5-mIgG2c, JK13-mIgG2c and JK16-mIgG2c were used to analyze, which of the CD38-specific nanobodies (9 NBs and 4 JKs) could block binding of the Alexa⁶⁴⁷conjugated hcAbs. The results allow assignment of the selected nanobodies into three distinct, non-overlapping epitope binning groups. Bold boxes in the diagonal (JK3 - JK16) show that binding is effectively blocked when pre-incubation is performed with the same hcAb used for subsequent staining in Alexa⁶⁴⁷conjugated form. NB11 blocked binding of JK3 hcAb by 74%, but only marginally affected binding of JK5, JK13 or JK16 and, thus was assigned to the same binning group (e1) as JK3. Similarly, NB32 blocked binding of JK5 and was thus assigned to the same binning epitope as JK5 (e2). Remarkably NB32 seemed to enhance binding of the other three hcAbs (JK3, JK13 and JK15). All members of family 4 (JK13, JK16, NB3, NB7, NB22, NB24) and of family

5 (NB38, NB40, NB42) blocked binding of JK13 and JK16 by at least 65%. Members of family 4 and family 5 were thus assigned to a 3rd non overlapping binning group (e3). Note that JK13 and JK16 also blocked binding of JK3, suggesting that binding of these Nbs may either sterically interfere with binding of JK3 or alter the conformation of CD38 so as to inhibit binding of JK3.

ep	fam	name	JK3	JK5	JK13	JK16
1	1	JK3	98	17	27	18
1	1	NB11	74	5	17	29
2	2	JK5	29	97	33	5
2	3	NB32	-58	82	-22	-8
3	4	JK13	55	-5	99	100
3	4	JK16	79	25	95	98
3	4	NB3	-19	4	72	78
3	4	NB7	-22	0	71	82
3	4	NB22	-5	3	66	65
3	4	NB24	-27	0	75	79
3	5	NB38	6	15	79	83
3	5	NB40	0	14	75	77
3	5	NB42	12	13	76	75

Fig. 5.4: Cross blockade analysis reveals binding of hcAbs to three independent epitopes on mouse CD38.

mCD38 HEK-T cells and mCD38 EL4-thymoma cells were preincubated for 30 minutes at 4 °C with unconjugated hcAbs (indicated on the left) before addition of Alexa⁶⁴⁷-conjugated hcAbs (indicated on top). Cells were further incubated for 30 minutes at 4 °C, washed twice and analyzed by flow cytometry. Numbers indicate the degree of inhibition of binding. Negative numbers indicate enhanced binding of the fluorochrome conjugated hcAb in the presence of the unlabeled hcAb. Efficiency of inhibition is indicated by different shades of grey (dark grey: > 80% inhibition, light grey: 50–80% inhibition). Self-blockade by the hcAb used for labelling is indicated by highlighted dark-grey boxes in the diagonal. hcAbs that blocked binding of each other were assigned to the same epitope (ep 1-3).

5.1.4. hcAbs of family 4 show the slowest dissociation from mouse CD38, i.e. the highest binding avidity for CD38

Relative dissociation rates of fluorochrome-conjugated heavy chain antibodies from mouse CD38 expressing EL4 thymoma cells were analyzed to assess their suitability for further assays. Relative binding avidity of AF⁶⁴⁷-fluorochrome-conjugated hcAbs was determined by observing changes in the mean fluorescence intensity over time due to the dissociation from EL4 cells. Efluor450-labeled EL4 cells were added as a sink for the dissociated hcAbs. Results show the slowest dissociation, i.e. strongest binding for hcAbs JK16 and JK13 (family 4), followed by JK5, NB32, JK3 and NB11 (Fig. 5.5). The difference could best be observed after 0.5 hours. At this time point, hcAbs JK3 and NB11 had already largely dissociated onto Efluor450 tagged cells, whereas only a small fraction of Alexa⁶⁴⁷ conjugated JK13- and JK16 hcAbs had dissociated onto Efluor450 mCD38 EL4-thymoma cells.

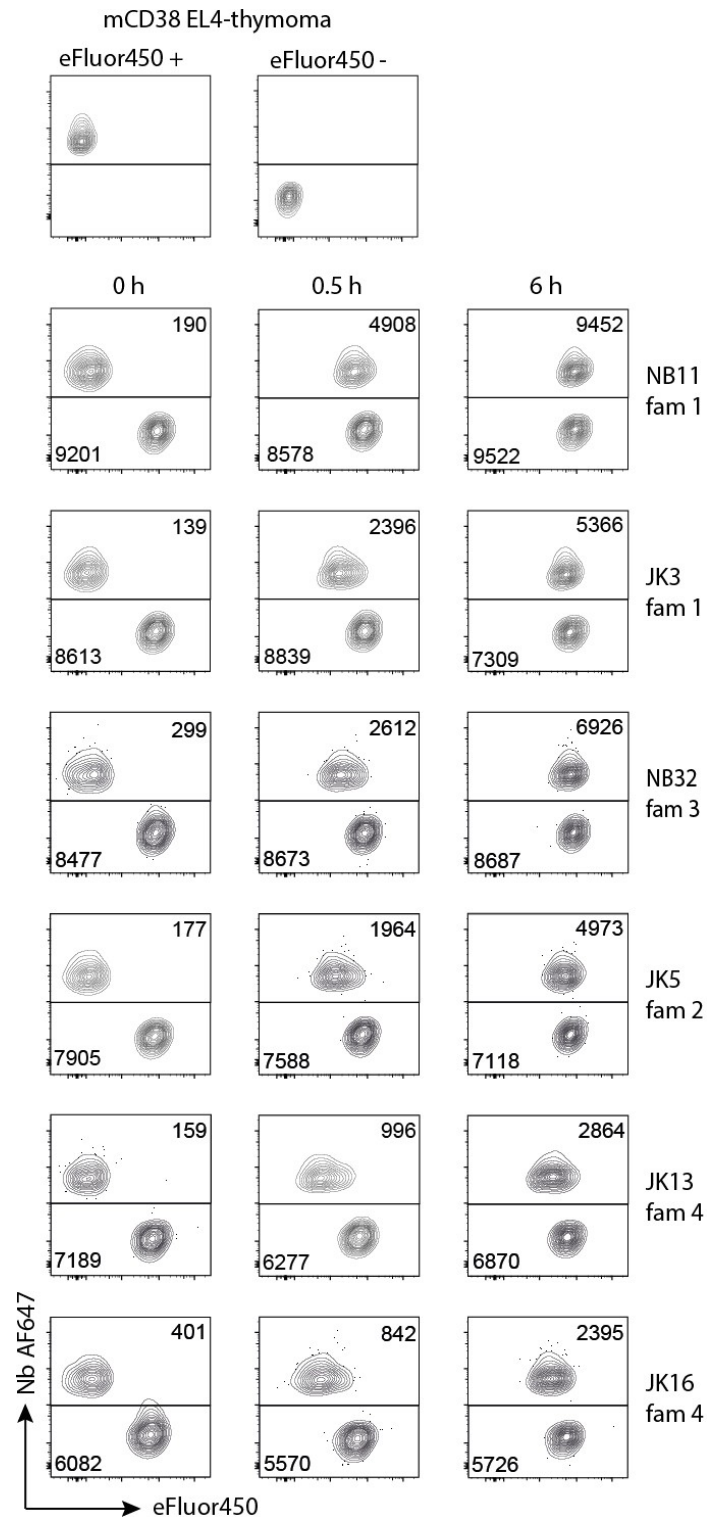


Fig. 5.5: Nbs JK13 and JK16 (family 4) show the slowest, Nb NB11 (family1) the fastest dissociation from mCD38 EL4-thymoma cells.

Dissociation of fluorochrome-conjugated hcAbs was analyzed by monitoring changes in the mean fluorescence intensity over time of two mixed aliquots of mouse CD38-expressing EL4 thymoma cells. One aliquot was incubated with the cell-tracking dye eFluor450 the other aliquot with Alexa⁶⁴⁷-conjugated hcAbs for 30 min at 4 °C. Cells were washed three times, mixed at a 1:1 ratio and further incubated at 4 °C for 0, 0.5 or 6 hours. The eFluor450 labelled cells acted as a sink for dissociated Alexa⁶⁴⁷ conjugated hcAbs. The dissociation of nanobodies from the target cells and association with the eFluor450 labelled cells correlates with binding affinity. Numbers within blots indicate mean fluorescence intensity (MFI).

5.1.5. mCD38-expressing EL4-thymoma cells metabolize NAD⁺ to ADPR

CD38 catalyzes three distinct enzymatic reactions: First, NAD glycohydrolase hydrolyzes NAD⁺ to ADP-ribose (ADPR); second, ADPR cyclase converts NAD⁺ to cyclic ADP-ribose and third, cADPR hydrolase hydrolyzes cADPR to ADPR. CD38 activity may increase the concentration of the anti-inflammatory and immunosuppressive adenosine in the tumor environment that might lead to a favorable survival of malignant cells at the tumor site. Hence, we wanted to check whether the selected hcAbs have a modulatory effect on CD38 enzyme activities.

EL4 thymoma cells express high levels of cell surface CD38. To monitor enzymatic activity by these cells, NAD⁺ metabolites were measured using a reversed-phase HPLC on a Multohyp BDS C18 column (Fig. 5.6). For this, mCD38 EL4-thymoma cells were incubated with a high concentration of NAD⁺ (500 μ M) for 15 minutes. For maximal inhibition of CD38, one sample was incubated with the potent CD38 inhibitor ara-F-NAD for 20 minutes prior to addition of NAD⁺. Results are depicted in three chromatograms in Figure 5.6 A. HPLC-chromatogram of standards (on top) show retention times (R_T) of the nucleotides cADPR, NMN, NAD⁺, Ado, AMP, ADPR and ADP that allow assignment of metabolic products according to their R_T . Results of the 2nd chromatogram show that CD38 expressing EL4 cells metabolize NAD⁺ to ADPR (blue curve); and that this reaction was strongly inhibited by ara-F-NAD (red curve). The 3rd chromatogram confirms that little if any ADPR is produced in control samples without mCD38 EL4-thymoma cells (green and purple curves). Calculation of the areas under the curve of standards allowed to quantify nucleotide concentration of NAD⁺ and ADPR (Fig. 5.6 B). The reduction in the concentration of NAD⁺ by 1.3 nmol (left panel) in the presence of EL4 cells is mirrored by a corresponding increase in the concentration of ADPR (right panel). Treatment of cells with ara-F-NAD strongly inhibited the conversion of NAD⁺ into ADPR by EL4 cells.

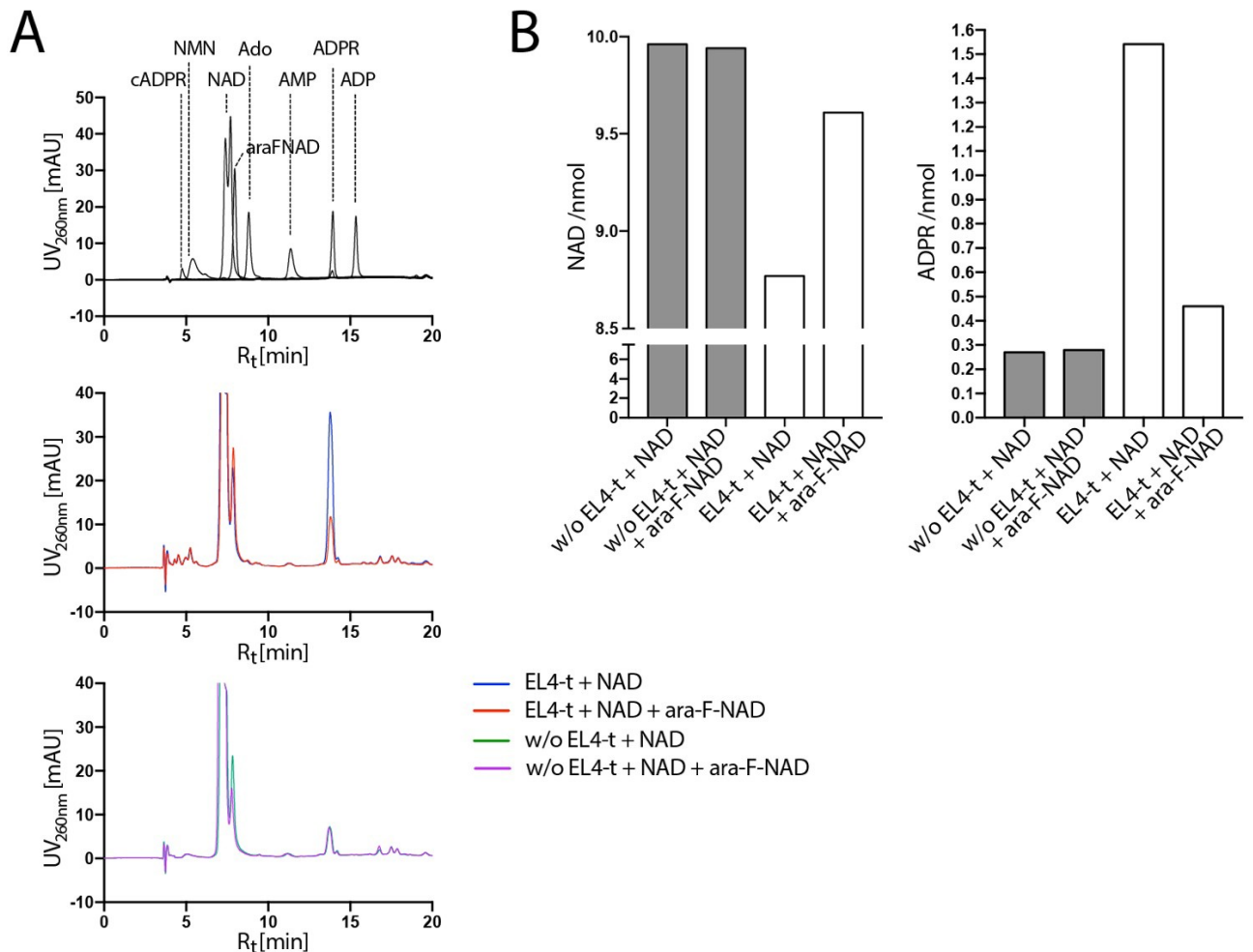


Fig. 5.6: mCD38 EL4-thymoma cells metabolize NAD^+ to ADPR.

mCD38 EL4-thymoma cells (EL4-t) (3×10^5 cells/ well) were incubated with $100 \mu M$ NAD^+ for 15 minutes at $37^\circ C$. One sample was incubated with the potent CD38 inhibitor araF-NAD ($1 \mu M$) for 20 minutes at $37^\circ C$ prior to addition of NAD^+ . The reaction was stopped by centrifugation at $4^\circ C$ and supernatant was loaded onto a Vivaspin column. The flow through was mixed 1:1 with HPLC buffer and products were measured at $4^\circ C$ using a reversed-phase HPLC on a Multohyp BDS C18 column. Detection of nucleotides was performed at $\lambda = 260$ nm. (A) HPLC-chromatograms of standards (top), supernatants of EL4 cells (middle) and control samples without cells (bottom). (B) To quantify ADPR production, standards from the first chromatogram were used for calibration.

5.1.6. Family 4 and 5 hcAbs strongly inhibit the NGD cyclase activity of mouse CD38

The ability of CD38-specific nanobodies to modulate the enzymatic activity of the CD38 cyclase was measured by a colorimetric assay using NGD^+ (nicotinamide guanine dinucleotide) and mouse CD38 expressing EL4 cells. CD38 is known to catalyze the conversion of NGD^+ to cyclic GDP-ribose (cGDPR). Since the latter can be monitored conveniently by fluorimetry, this GDP-ribose-cyclase assay was used to analyze potential inhibitory or stimulatory effects of anti-mouse CD38 nanobodies. Therefore, cells were pre-incubated with CD38 specific hcAbs for 15 min before addition of NGD^+ .

Figure 5.7 depicts three diagrams corresponding to individual nanobody families. In each diagram, maximal production of cGDPR is depicted with the green curve (cells + NGD⁺), the maximal inhibition of CD38 with ara-F-NAD is depicted with the red curve and the black curve shows only cells. The results show that JK3 (family 1), JK5 (family 2) and NB32 (family 3) do not affect the activity of CD38 EL4 cells (Fig. 5.7 A, B, C, respectively). In contrast, all tested members of families 4 and 5 (D, nanobodies JK13, NB3, NB7, NB22 and NB24 and E, NB38, NB40 and NB42) strongly inhibited cyclase activity of EL4 cells.

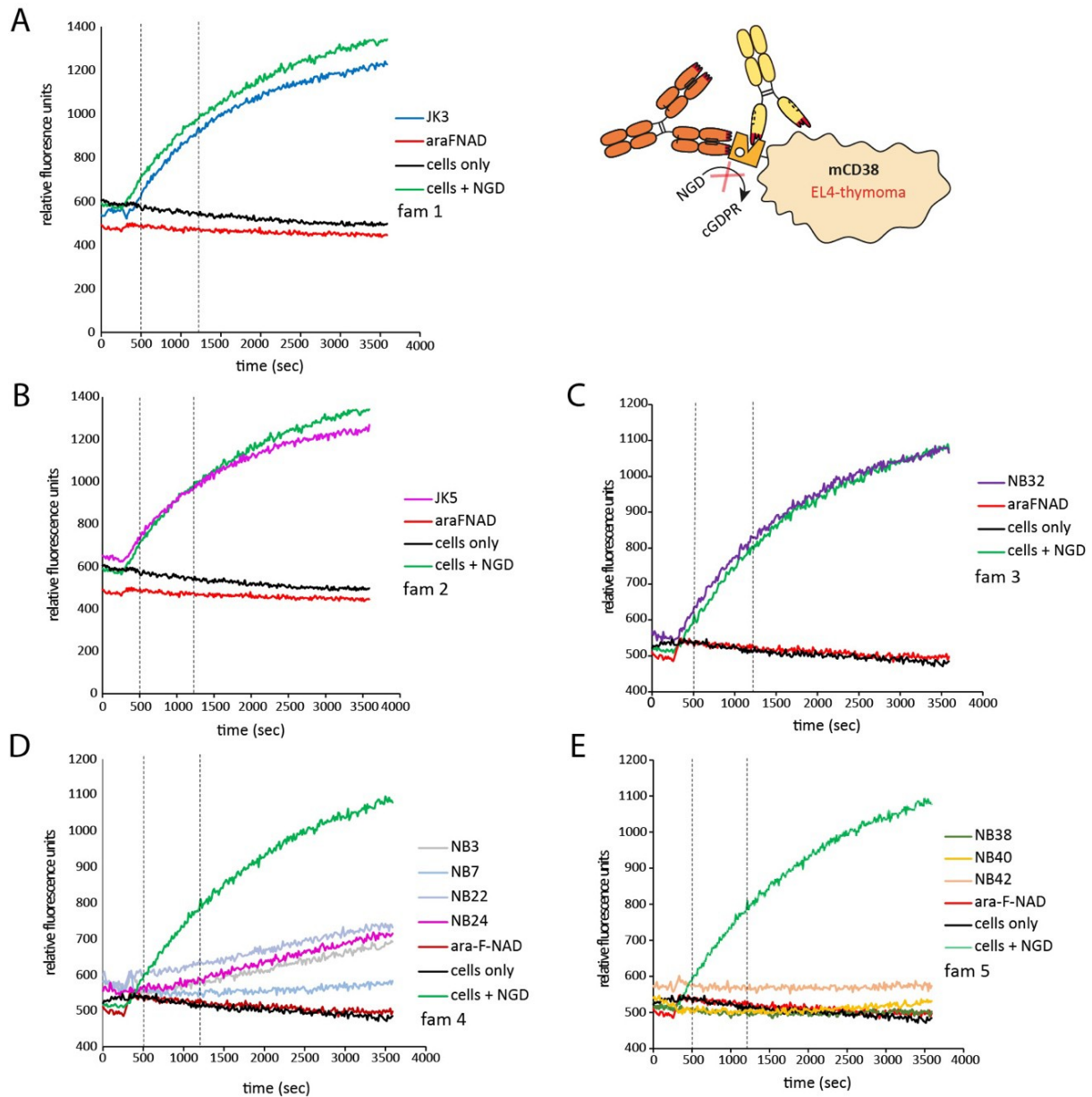


Fig. 5.7: Family 4 and 5 hcAbs inhibit NGD cyclase activity of mCD38 EL4-thymoma cells.

mCD38 EL4-thymoma cells (3×10^5 cells/well) were incubated with 10 $\mu\text{g}/\text{ml}$ mouse hcAbs or 10 μM ara-F-NAD for 15 minutes at 37°C before starting the measurement with an Infinite M200 PRO microplate reader (Tecan). After the first 20 cycles, 50 μM NGD⁺ was added and kinetic fluorescence reading (ex/em: 300/410 nm) was continued for 50 minutes. Controls are depicted in all three curves: ara-F-NAD (red), cells + NGD⁺ (green) and cells only (black) together with hcAbs of (A) JK3 (family 1), (B), JK5 (family 2), (C) NB32 (family 3), (D) NB3, NB7, NB22, NB24 (family 4) and (E) NB38, NB40 and NB42 (family 5). Vertical dotted lines at 500 seconds and 1200 seconds depict the time range quantified in Figure 5.8, 5.9 and 5.10.

For better quantitative comparison, the slope of the curves in Figure 5.7 during the linear phase, e.g. from $t=500$ seconds to $t=1200$ seconds were calculated. The results are depicted as dots in Figure 5.8. The assay was performed according to Figure 5.7, except that triplicate analyses were performed with two concentrations -10 $\mu\text{g/ml}$ or 100 $\mu\text{g/ml}$ - of nanobodies. The results show that hcAbs of family 4 and family 5 significantly inhibited mCD38 cyclase at both concentrations, whereas family 1, 2 and 3 (JK3, JK5, NB32) did not have any detectable effect on cyclase activity of EL4 cells. Family 5 showed the strongest inhibition of 100% at both concentrations. 100 $\mu\text{g/ml}$ of family 4 hcAbs also achieved a complete inhibition of CD38 cyclase, whereas at 10 $\mu\text{g/ml}$, a remaining CD38 cyclase activity between 10 % and 30 % could still be observed. Family 1, 2 and 3 had no effect on cyclase inhibition and hence, CD38 cyclase activity was still at 100%

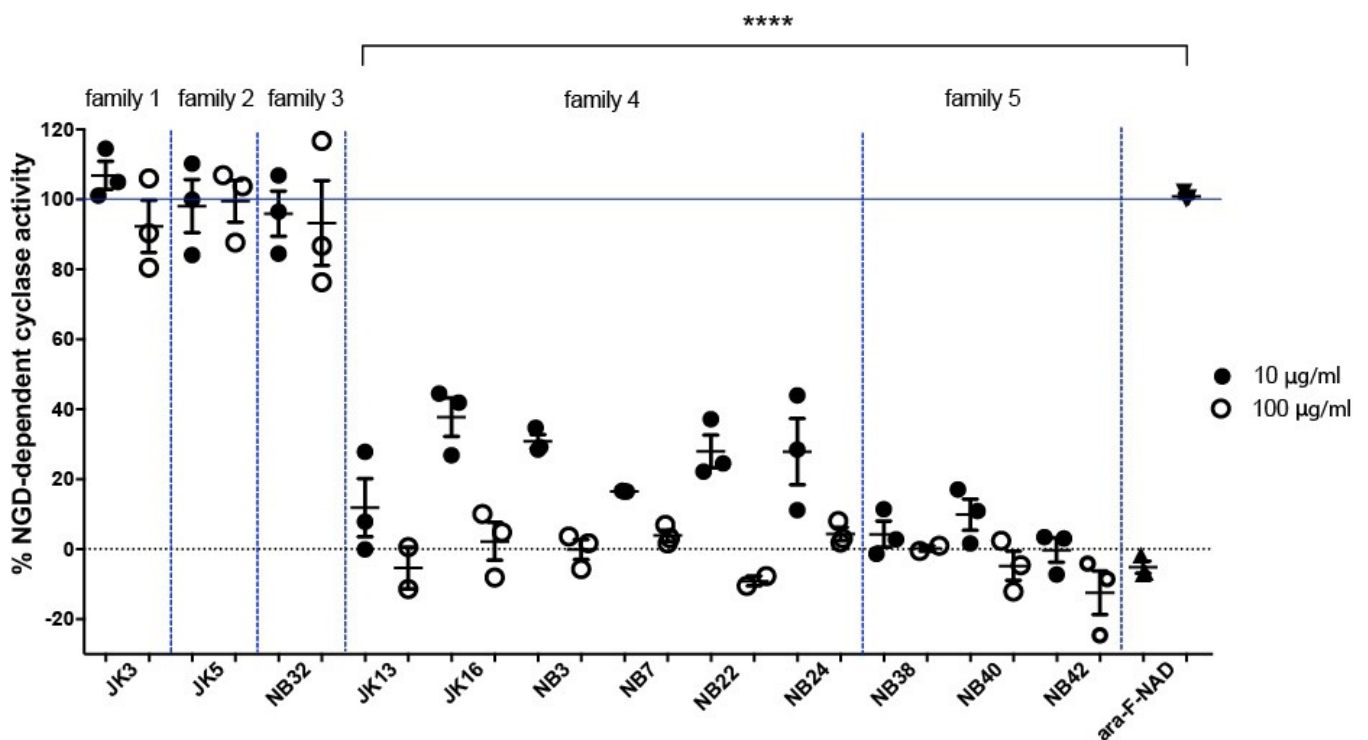


Fig. 5.8: Family 4 and 5 hcAbs inhibit mouse CD38 cyclase activity.

NGD⁺ cyclase assays were performed according to Fig. 5.7 using an Infinite M200 PRO microplate reader (Tecan). Dots indicate the slope of curves during the linear phase, e.g. from $t = 500$ seconds to $t = 1200$ seconds ($n = 3$). Statistical significance was calculated using an one-way ANOVA followed by a Bonferroni *post hoc* test for multiple comparisons. ****, $P < 0.0001$.

In order to determine the IC_{50} of the inhibitory effect of hcAbs NB38 and NB42 another colorimetric NGD⁺ assay was performed with a dilutional series of NB38 or NB42 (Fig. 5.9). The results reveal a slightly stronger inhibition by NB38 compared to NB42, especially at doses between 1 μ g/ml and 100 μ g/ml with similar IC_{50} values for both hcAbs of ~ 10 nM.

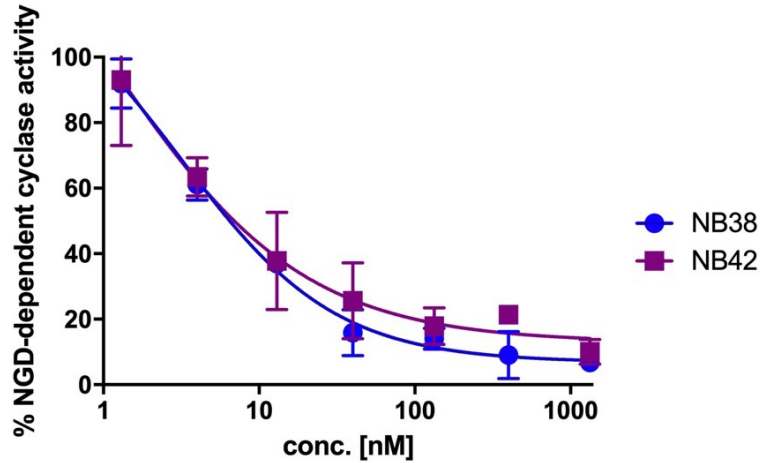


Fig. 5.9: hcAbs NB38 (family 4) and NB42 (family 5) inhibit mouse CD38 cyclase activity with similar IC_{50} values of ~ 10 nM.

IC_{50} values for the inhibition of NGD⁺ cyclase activity by hcAbs NB38 and NB42 was determined by titration in a colorimetric NGD⁺ assay. mCD38 EL4-thymoma cells (1×10^5 cells/well) were incubated with a dilutional series of hcAbs NB38 or NB42 (100 μ g/ml, 30 μ g/ml, 10 μ g/ml, 3 μ g/ml, 1 μ g/ml, 0.3 μ g/ml, 0.1 μ g/ml) for 15 minutes at 37°C before starting the measurement with a Tecan reader (90 μ g/ml of a 90 kD hcAb correspond to a concentration of 1 μ M). After the first 20 cycles, 50 μ M NGD⁺ was added and kinetic fluorescence reading (ex/em: 300/410 nm) was continued for 50 minutes as in Fig. 5.7. Slope curves were evaluated as in Fig. 5.8, i.e. during the linear phase, e.g. from $t = 500$ seconds to $t = 1200$ seconds. Statistical analyses were performed using a nonlinear regression with four parameters for a sigmoid course of curve.

Next we wanted to determine whether the combination of hcAbs from two Nb families could achieve an additive inhibitory effect. Hence, hcAbs NB38 (family 4) and NB42 (family 5) were applied in combination with other members of the other Nb family. The results confirmed the potent inhibitory effects of hcAbs NB38 and NB42 (Fig. 5.10). However, the results do not show any significant additive inhibitory potential for any combination of hcAbs of families 4 and 5.

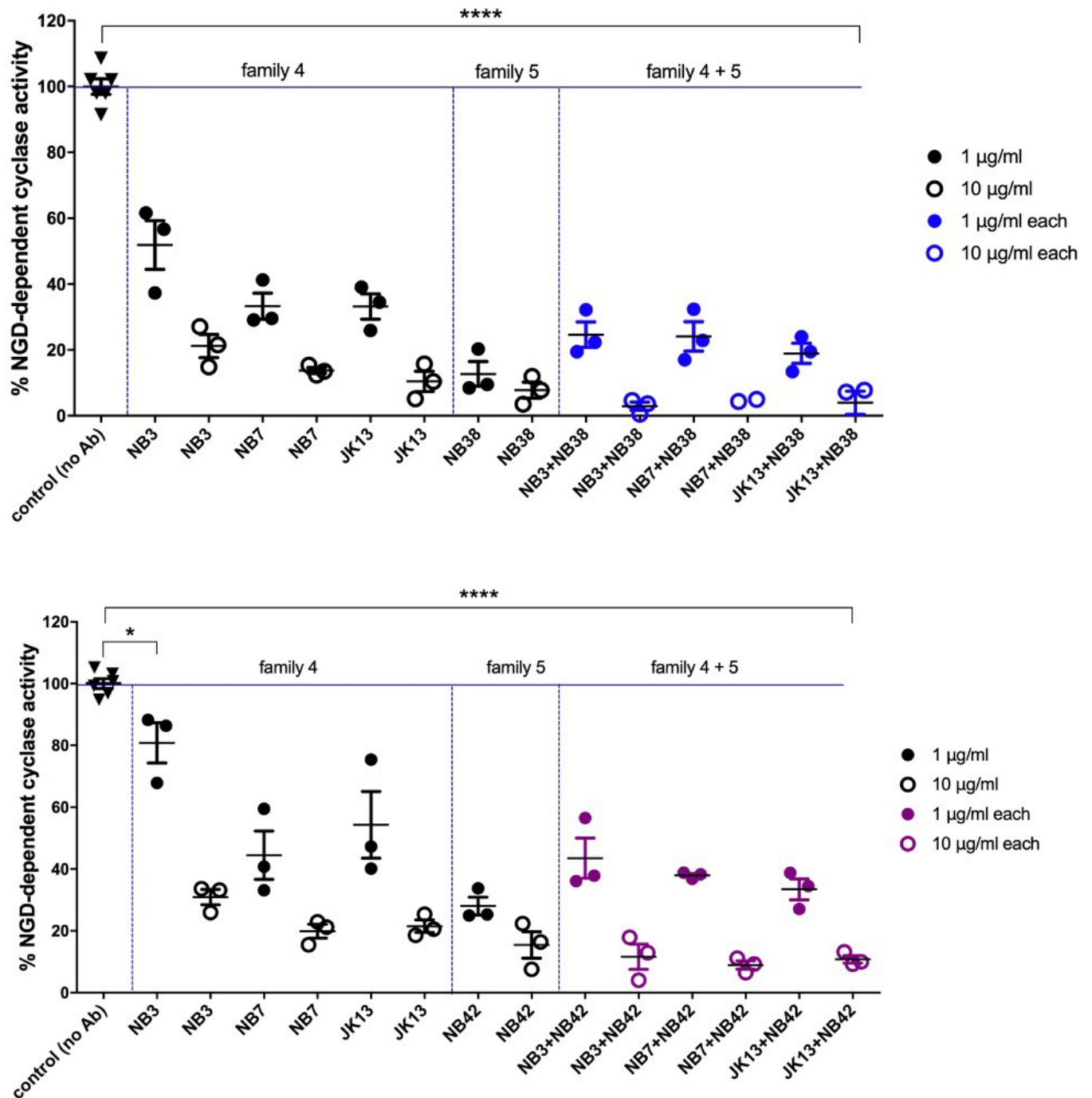


Fig. 5.10: The inhibitory effects of hcAbs NB38 (family 4) and NB42 (family 5) is not enhanced by combination with hcAbs from the other family.

NGD assays were performed according to Fig. 5.7, except that cells were incubated with single or combinations of hcAbs. Dots indicate the slope of curves during the linear phase, e.g. from $t=500$ seconds to $t=1200$ seconds ($n=3$). Statistical significance was calculated using an one-way ANOVA followed by a Bonferroni *post hoc* test for multiple comparisons. ****, $P<0.0001$. *, $P<0.05$.

5.1.7. Fc-engineered hcAbs mediate CDC-dependent lysis of mCD38-transfected human embryonic kidney (HEKT) cells

To analyze the potential of hcAbs to induce complement-dependent cytotoxicity (CDC), human embryonic kidney (HEK) cells were transiently co-transfected with expression constructs for mouse CD38 and green fluorescent protein (GFP). 48 hours post transfection, cells were incubated with saturating amounts of hcAbs, human serum was added for 1.5 hours as a source of complement and CDC-dependent uptake of propidium iodide by lysed cells was monitored using flow cytometry (Fig. 5.11). For a negative control, an aliquot of the serum was treated for 30 min at 56°C in order to inactivate the enzymatic components of the complement system. As a further control, hcAbs (SB112) directed against an irrelevant target (CD39) not expressed by HEK cells were used (Fig. 5.11B, panels 1 and 8). The capacity to activate complement can be abolished by introducing three other amino acid substitutions into human IgG1 (L234A L235A P329G) (63). The samples with the negative controls and samples incubated with the LALAPG mutant hcAb show a similar low level of background cell death (~20% PI+ cells) (Fig. 5.11A panels 5 and 7, Fig. 5.11B panels 1 - 7). Incubation with hcAbs from resulted in increased numbers of PI+ cells, ranging from 30% for hcAb JK3 (Fig. 5.11B panel 9) to 60% for hcAb NB38 (Fig. 5.11B panel 14). Substitution of a single amino acid (E340S) has been shown to enhance the CDC-potency of human IgG1 mAbs and hcAbs, by favoring formation of hexameric IgG complexes on the cell surface, thereby promoting stable binding of the C1q complement component, and subsequent activation of the complement cascade (64). In order to determine whether such mutations had comparable effects on the CDC potency of CD38-specific hcAbs, we introduced comparable mutations into the conserved positions of mouse IgG2a. The results reveal only a moderately enhanced killing of hcAbs carrying the E430S mutation (Fig. 5.11B panels 15-17).

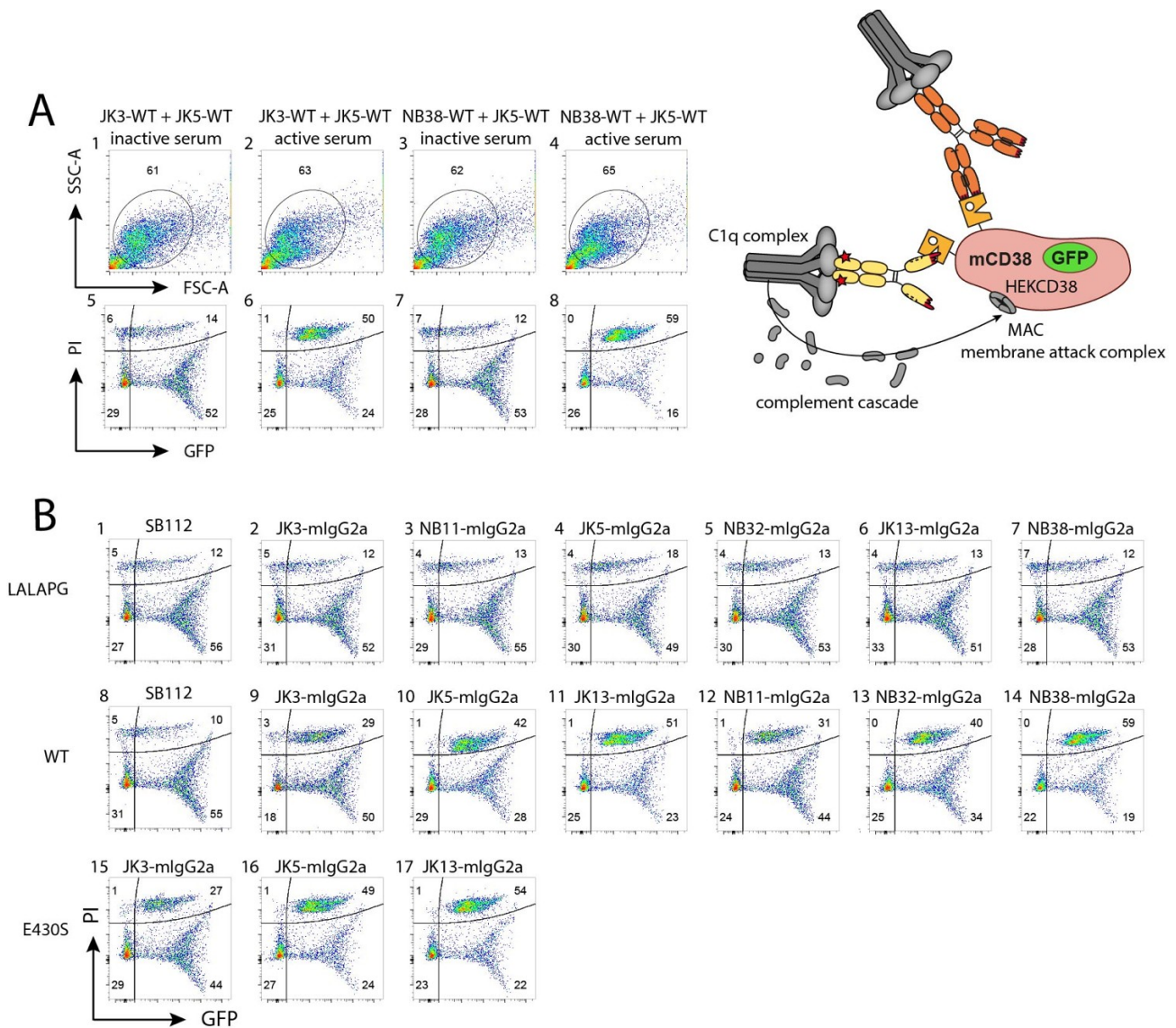


Fig. 5.11: CD38-specific hcAbs mediate complement-dependent cytotoxicity (CDC) of mCD38-transfected HEK-293T cells.

HEK-293T cells were transiently (48 hours) co-transfected with expression constructs for mouse CD38 and GFP using the Jet-PEI transfection method. 48 hours post transfection, cells (1×10^6 cells/well) were incubated at 37°C for 90 min with the indicated hcAbs (100 nM) and human serum (12.5% v/v) as a source of complement (active serum). Serum that had been preincubated for 30 min at 56° to inactivate enzymatic complement components was used as control (inactive serum). Cells were washed twice and incubated for 15 min at RT with propidium iodide (PI) before analysis by flow cytometry. Cells lysis is evidenced by loss of GFP and uptake of PI.

5.1.8. CD38-specific hcAbs mediated ADCC against mouse CD38-expressing EL4 thymoma cells.

To analyze the capacity of CD38-specific hcAbs to induce antibody dependent cell-mediated cytotoxicity, mouse CD38-expressing EL4 thymoma cells were used as target cells and human NK-92 cells stably transfected with the mouse Fc-receptor III (CD16) were used as effector cells. Flow cytometry analyses confirmed high expression of mouse CD38 by EL4 cells and of mouse CD16 by NK-92 cells (Fig. 5.12A). To monitor ADCC, EL4 cells pre-loaded with hcAbs

were incubated with eF450 labeled mCD16 NK92 cells for 3 hours at 37°C at a ratio of 1:3 ratio before analysis by flow cytometry (Fig. 5.12B). Dead cells were identified by loss of forward scatter and uptake of propidium iodide. The results show that the three hcAbs (JK3, JK5 and JK13) mediated effective killing (90 %) of EL4 target cells. In contrast, only background levels (17%) of cell death were observed when incubations were performed in the presence of the LALAPG mutants of the hcAbs.

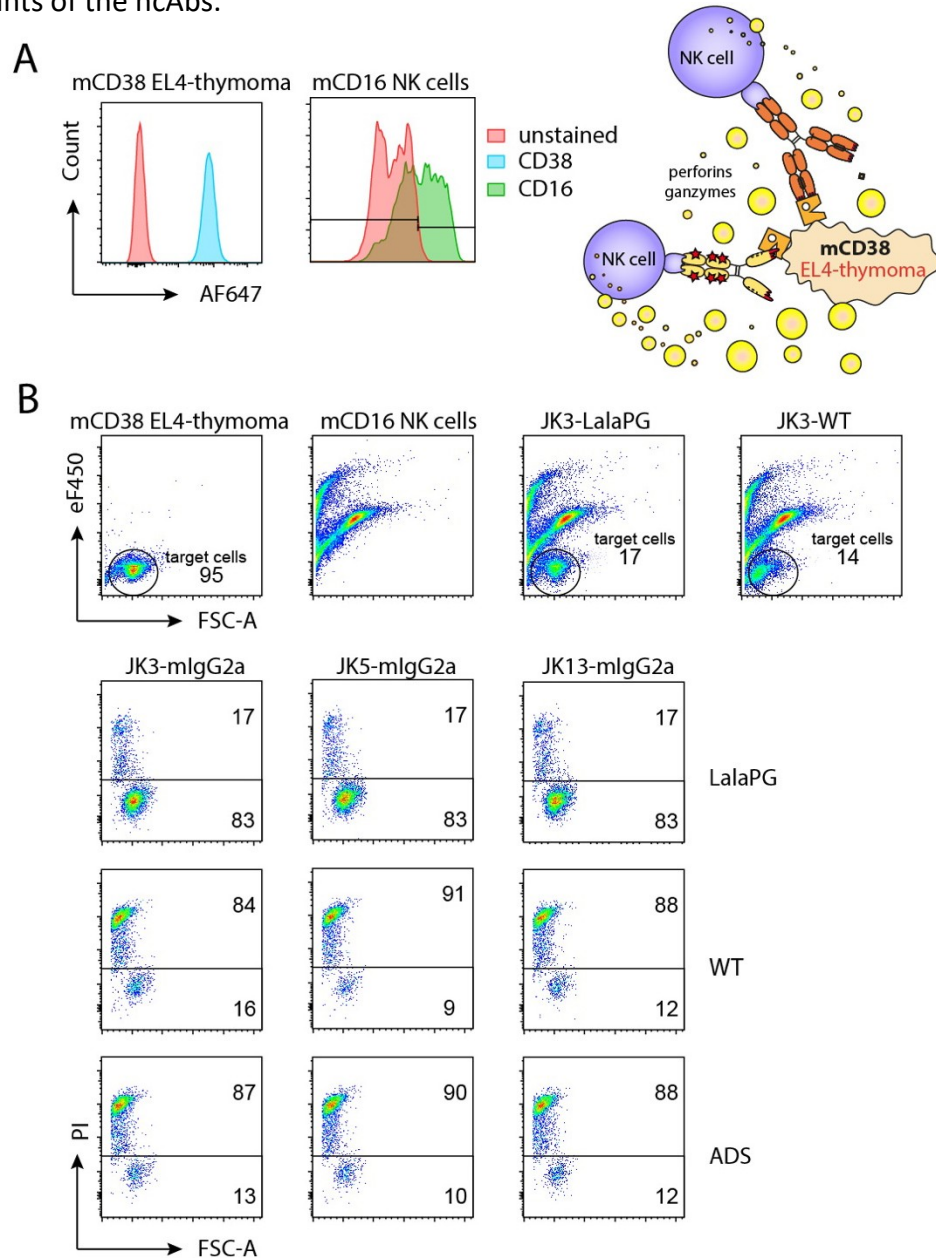


Fig. 5.12: CD38-specific hcAbs mediate antibody dependent cellular cytotoxicity (ADCC) of mCD38 EL4 thymoma.

(A) Mouse CD38 EL4 thymoma target cells were analyzed for their cell surface expression of CD38 and human NK92 effector cells stably transfected with mouse CD16 (FcγRIII) were analyzed for their cell surface expression of mCD16. The schematic illustrates the set-up of the ADCC assay. (B) mCD38 EL4-thymoma cells (1×10^6 cells/well) were pre-incubated for 10 minutes at 4°C with 100 nM hcAbs-mFc. mCD16 NK92 cells were labelled with the cell tracking dye Efluor450 for 15 minutes at 4°C. Efluor-labeled mCD16 NK cells (3×10^6 cells/well) were added to the target cells to achieve a 1:3 ratio followed by a 3 hour incubation time at 37°C. Then, cells were washed twice, and dead cells were stained with propidium iodide (PI) for 15 minutes at RT before analysis by flow-cytometry. Gating was performed on target cells (Efluor-negative cells). Cell lysis is indicated by a decrease in forward scatter (FSC) and uptake of PI.

5.2. Retargeting of solid and hematological malignancies with hcAbs

5.2.1. EGFR-specific hcAb 7D12 inhibits the proliferation of EGFR-escape variant cells

Mutations of the human EGFR-receptor (*inter alia* S492R, G465R, S464L, R451C) have been described in patients with metastatic colorectal cancer (mCRC) that are acquired during therapy and that inhibit binding of the therapeutic monoclonal antibodies (mAbs) cetuximab and panitumumab. In order to generate EGFR-specific hcAbs, we genetically fused the published EGFR-specific Nb 7D12 (13) to the hinge, CH2, and CH3 domains of human IgG1. Moreover, as in case of mouse CD38-specific mAbs, we used site directed mutagenesis to introduce known mutations to enhance or abrogate CDC and ADCC.

To determine whether the anti-EGFR hcAb 7D12 also binds to the EGFR with acquired mutations, Ba/F3 cells transduced with wildtype EGFR or EGFR mutants were stained with 7D12-hcAb, cetuximab, or panitumumab and analyzed by flow cytometry (Fig. 5.13A). The results show that 7D12-hcAb binds to the four EGFR mutant Ba/F3 cells, albeit with reduced efficacy to the EGFR-R451C mutant. In contrast, binding of panitumumab was abrogated in case of mutants G456R and S464L, binding of cetuximab was abrogated for the S492R, G465R and S464L mutants.

To analyze effects of EGFR-specific mAbs and hcAbs on the proliferation of Ba/F3 WT and G465R-mutant cells, proliferation assays using the Vi-CELL Cell Viability Analyzer were performed (Fig. 5.13B). Cells were stimulated with EGF for four days and then proliferation was determined for EGFR WT (left panel) and EGFR G465R (right panel) transduced Ba/F3 cells. The increase of viable cells after mAb or hcAb treatment was compared to EGF treatment alone. The results show that 7D12-hcAb blocks proliferation of both, EGFR WT- and EGFR G465R Ba/F3 cells. Cetuximab and panitumumab also blocked proliferation of EGFR-WT Ba/F3 cells. However, cetuximab had no inhibitory effect on proliferation of EGFR-G465R mutant cells and panitumumab only slightly reduced proliferation of EGFR-G465R Ba/F3 mutant cells.

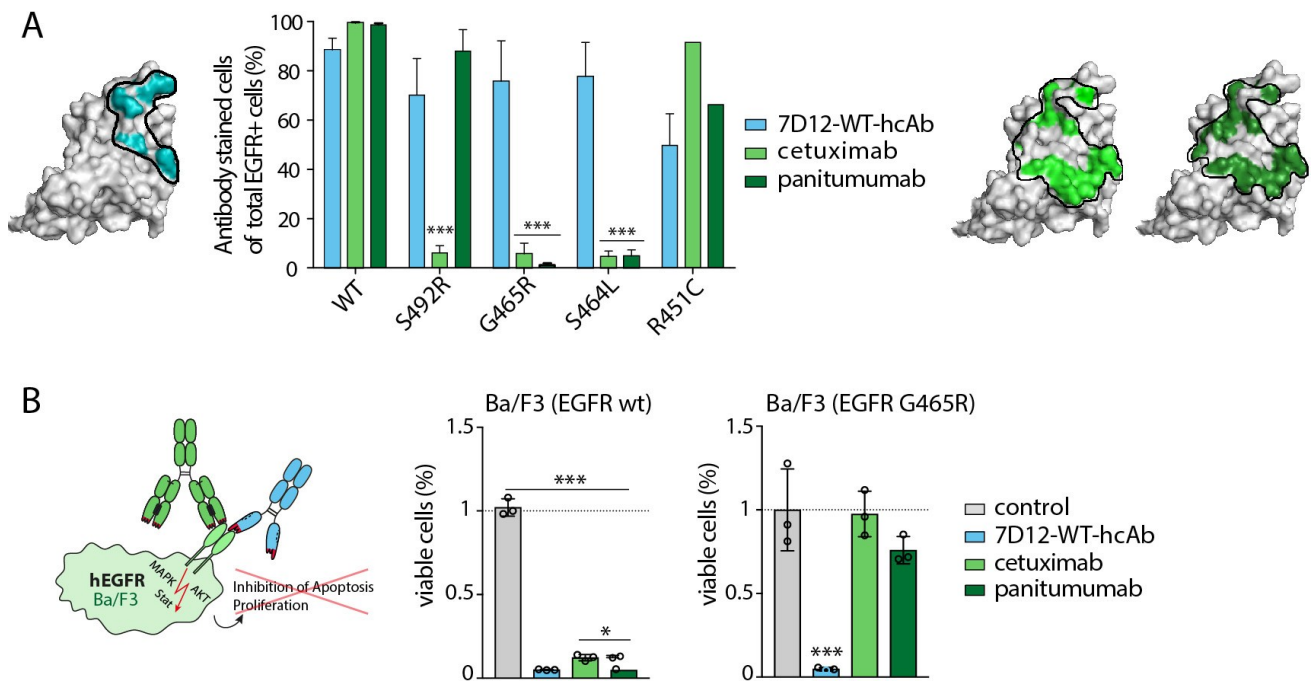


Fig. 5.13: EGFR-specific hcAb 7D12 binds to and reduces the proliferation of cells carrying acquired EGFR escape variants.

(A) Binding of EGFR-specific hcAb 7D12 and mAbs cetuximab and panitumumab to acquired EGFR escape variants was analyzed by flow cytometry. EGFR WT or EGFR mutant transduced Ba/F3 cells (1×10^6) were incubated with hcAb 7D12-hlgG1 (blue) or cetuximab (light green) or panitumumab (dark green) for 30 minutes at 4°C. Cells were washed twice and stained with a fluorochrome conjugated secondary antibody against hlgG1 for another 30 minutes in the dark at RT, followed by flow-cytometric analysis. Relative amount of EGFR+ cells were determined by gating on EGFR-positive cells followed by gating on antibody/nanobody labelled cells. The putative binding sites of the three antibodies are projected onto a 3D space fill model of the extracellular domain of EGFR (pdb code). (B) To assess the effects of EGFR hcAb and mAbs on cell proliferation, Ba/F3 EGFR WT- or EGFR G465R cells were treated every 24 hours with 32.8 $\mu\text{mol/l}$ cetuximab (light green), 17 $\mu\text{mol/l}$ panitumumab (dark green), or 60 $\mu\text{mol/l}$ 7D12-hlgG1 (light blue) or in the absence of Abs as controls. After four days of EGF stimulation (5 ng/ml), proliferation was determined for EGFR WT (left panel) and EGFR G465R (right panel) transduced Ba/F3 cells. The increase of viable cells post antibody or hcAb treatment was compared to EGF treatment alone. Statistics were calculated using an one-way ANOVA with a Tukey post hoc test for multiple comparisons. *, $P < 0.05$; ***, $P < 0.001$.

The primary SNP R521K in the EGFR ectodomain III has also been reported to result in resistance to mAb targeting. To analyze the effects of 7D12-hcAb on the proliferation of human head and neck squamous cell carcinoma (HNSCC) cell lines UTSCC14 (EGFR WT) and SAT (EGFR R521K), a 3D cellular spheroid model was used (Fig. 5.14). Cells were grown for 7 days before mAbs or 7D12-hcAb were added at every second day and growth was monitored until day 13 by microscopy. The results show that the growth of EGFR WT UTSCC14 spheroids relative to control was inhibited upon the first treatment with 7D12-hcAb as well with cetuximab and panitumumab (Fig. 5.14A). Relative spheroid size was not reduced over time but remained the same until the last treatment at day 13. The effect of hcAb and mAbs on SAT EGFR R521K spheroids are depicted in Fig. 5.14B. Growth of SAT spheroids was slowed but not stopped upon treatment with each of the therapeutic constructs.

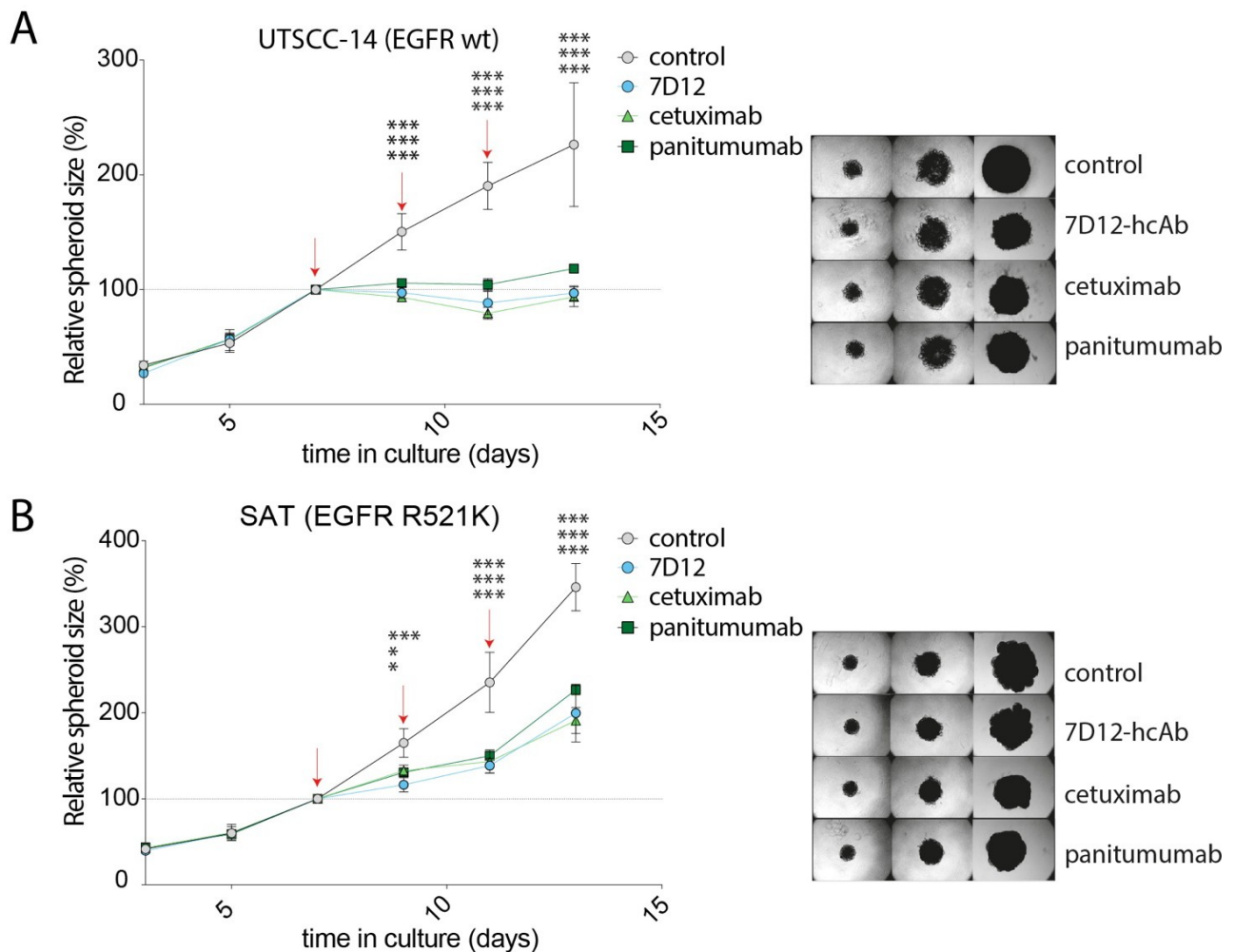


Fig. 5.14: EGFR-specific hcAb 7D12 inhibits the growth of 3D spheroids of UTSCC14 and SAT human head and neck cancer cell lines.

HNSCC cell lines (A) UTSCC14 (EGFR WT) or (B) SAT (EGFR SNP 521K) cells were resuspended in ice cold DMEM complete medium with 2% Matrigel Growth Factor Reduced (GFR) Basement Membrane Matrix or without GFR as control. Cells were seeded in a 96-well Cell-Repellent Surface 96-well plate (1×10^4 cells/well) and centrifuged at $1000 \times g$ for 10 minutes at 4°C . After 7 days of culture, 100 μL medium with 5 $\mu\text{g}/\text{mL}$ cetuximab, 2.5 $\mu\text{g}/\text{mL}$ panitumumab, 2.5 $\mu\text{g}/\text{mL}$ 7D12-hcAb or medium alone as control were added (red arrows). The medium was changed every other day, and spheroid size was calculated until day 13. Pictures were taken daily with $10 \times$ magnification using Axiovert 25 microscope and AxioCamMRC and cell size was calculated using AxioVision v4.9. Statistical analysis was calculated using an one-way ANOVA followed by a Tukey post hoc test for multiple comparisons. *, $P < 0.05$; ***, $P < 0.001$.

5.2.2. Human CD38-specific hcAbs against epitope 2 inhibit the NGD cyclase activity of CD38 expressing human LP1 myeloma cells

The Koch-Nolte lab had previously isolated (65) 22 families of human CD38-specific nanobodies and had assigned these to three distinct binding epitopes. Members that bound to epitope 2 inhibited the NGD cyclase activity of recombinant CD38 protein. Using the fluorometric NGD assay on living cells described for mouse CD38 (see Fig. 5.7), we wanted to analyze the effects of human CD38-specific hcAbs and the therapeutic conventional mAb daratumumab on the NGD cyclase activity of the human myeloma cell line (LP1) which

expresses high levels of cell surface CD38. LP1 cells were incubated with CD38-specific hcAbs, daratumumab or ara-F-NAD before addition of NGD⁺ (Fig. 5.15). The results show that daratumumab, which binds epitope 1, did not have any detectable effect on cyclase activity. JK36-hlgG1 against epitope 3 reduced cyclase activity slightly, whereas all hcAbs against epitope 2 (MU523, MU1067 and ST52) showed a significant inhibition of NGD cyclase activity. The remaining NGD cyclase activity of LP1 cells was ~ 20 % for MU523 and 55 % for ST52. The combination of ST52 and daratumumab enhanced the inhibition of NGD cyclase activity.

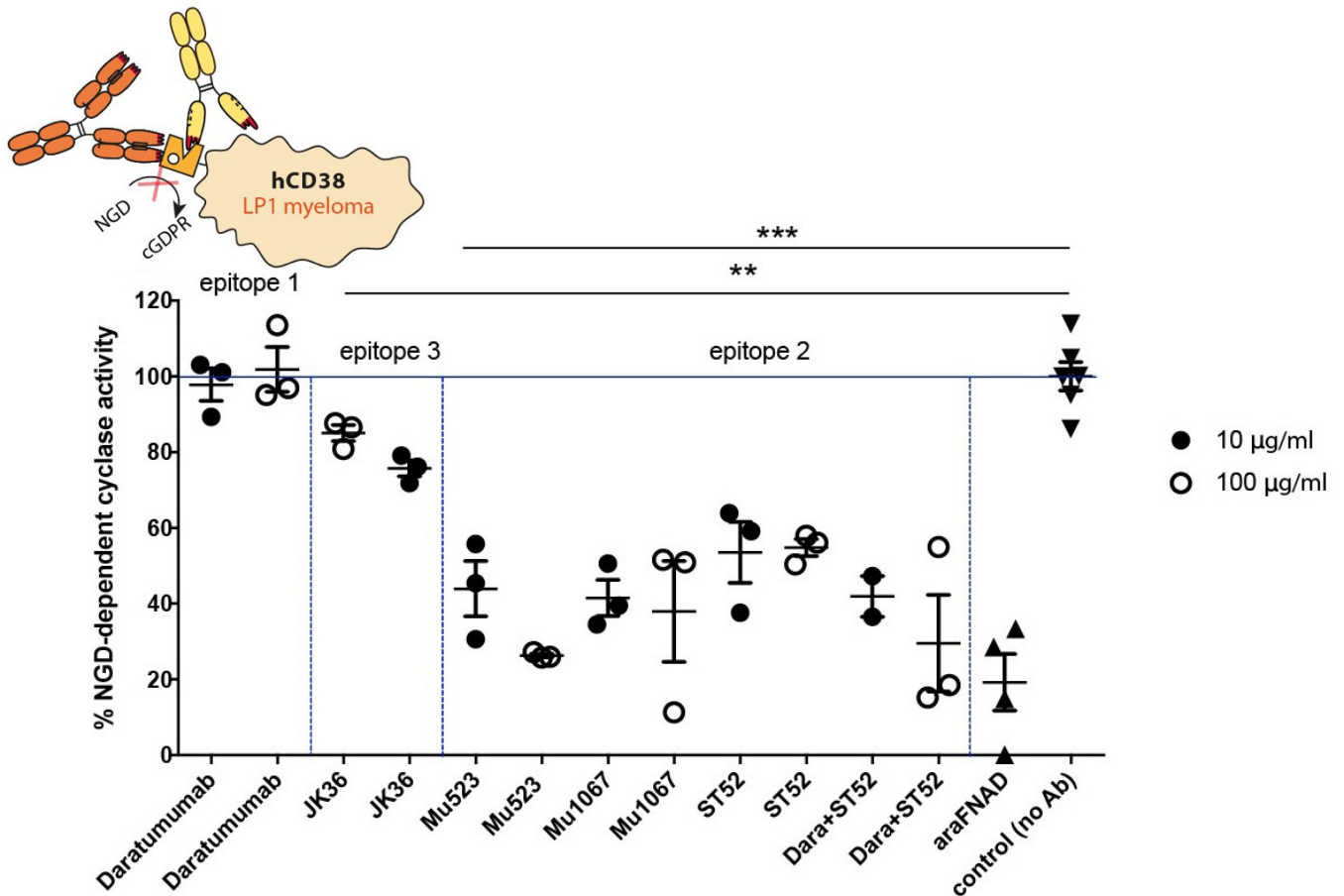


Fig. 5.15: CD38-specific hcAbs of family 2 inhibit the NGD cyclase activity of human LP1 cells.

The NGD cyclase activity of human CD38 expressing LP1 myeloma cells was measured by the colorimetric NGD assay using the Infinite M200 PRO microplate reader (Tecan) as described in Figure 5.7. Names and epitope-assignment of human CD38-specific Nbs are as described in Fumey *et al.*, 2017. ST52 is a variant of Nb JK2 that contains a H>D substitution in the CDR3. LP1 cells (1×10^5 cells/well) were incubated with the indicated hcAbs-hlgG1 (10 µg/ml or 100 µg/ml) or daratumumab (20 µg/ml or 200 µg/ml) or 10 µM ara-F-NAD for 15 minutes at 37°C before measurement was started. After the first 20 cycles, 50 µM NGD⁺ was added and kinetic fluorescence reading (ex/em: 300/410 nm) was continued for 50 minutes. Dots indicate the slope of curves during the linear phase, e.g. from $t = 500$ seconds to $t = 1200$ seconds ($n = 3$). Statistical analysis was calculated using an one-way ANOVA followed by a Tukey post hoc test for multiple comparisons. **, $P < 0.05$; ***, $P < 0.001$.

Next, we adapted the HPLC assay to monitor NAD⁺ catalysis by living human CD38 expressing LP1 cells (see Fig. 5.6 above). Therefore, LP1 cells were incubated with NAD⁺ (500 µM) for 180 minutes (Fig. 5.16A). Analysis of metabolic products was performed using a reversed-phase HPLC on a Multohyp BDS C18 column. Chromatograms in Fig. 5.16A (left panel) show that LP1

cells metabolize NAD^+ mostly to ADPR and to a small extent also to cADPR (inset). Whereas the area under the curve (AUC) declines for NAD^+ with increasing time points, the AUC of ADPR and cADPR is increased. In Fig. 5.16A, right panel, the AUCs were used for quantification of total NAD metabolism. Only ~1% (cADPR) of total product (ADPR) is generated by the ADPR cyclase (notice the 100-fold difference in the scale of the Y-axes). Half of the NAD^+ was hydrolyzed to ADPR within 50 minutes of incubation. We also incubated LP1 cells with cADPR (500 μM) for 24 hours in order to monitor hydrolysis of cADPR to ADPR (Fig. 5.16B). Chromatograms in Fig. 5.16B show a reduced AUC of the substrate cADPR and an increase in AUC of the product ADPR over time. The right panel of Fig. 5.16B shows the quantification of AUCs from the left panel depicting a slower rate of hydrolysis of cADPR to ADPR (~12h for the conversion of half of the ADPR) by LP1 cells compared to hydrolysis of NAD^+ to ADPR. Incubation times of 60 and 180 minutes were chosen as the time point with NAD^+ and cADPR⁺, respectively, for further experiments.

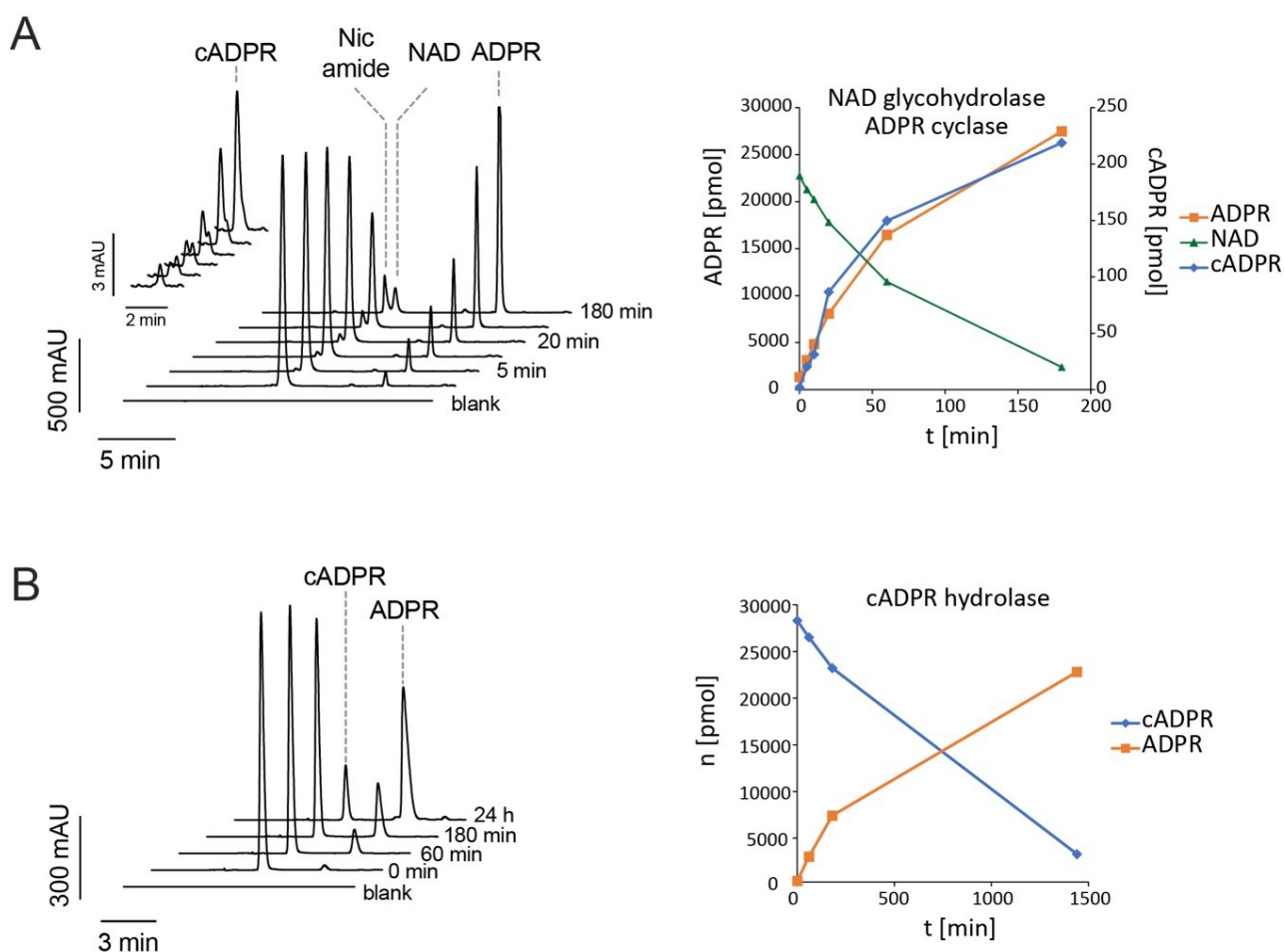


Fig. 5.16: Kinetic analyses of the enzymatic activities of CD38-expressing LP1 cells.

LP1 cells (1×10^5 cells/well) were incubated at 37°C in the presence of 500 μM NAD^+ (A) or cADPR⁺ (B). The reaction was stopped at the indicated time points by centrifugation at 4°C and supernatant was loaded onto a Vivaspin column. The flow through was mixed 1:1 with HPLC buffer and analysis of metabolic products was performed using a reversed-phase HPLC on a Multohyp BDS C18 column as described in Figure 5.6. Detection of nucleotides was performed at $\lambda = 260$ nm.

CD38 has six disulfide bonds, five of them are conserved also with the well characterized structurally related ADPR cyclase of the Californian hermaphrodite sea slug, *Aplysia californica*. The latter catalyzes a much higher production of cADPR vs. ADPR. The extra non-conserved disulfide bond between C119 and C201 of CD38 is located near the surface of the molecule and might be sensitive to reduction in an inflammatory or tumor microenvironment. We therefore wanted to determine whether reduction agents influence the enzymatic activities of human CD38 expressing LP1 cells. Hence, LP1 cells were pre-incubated with dilutional series of the reducing agents DTT, TCEP and GSH for 10 minutes at 37°C followed by addition of NAD⁺ and further incubation for 60 minutes (Fig. 5.17). The results show a dose-dependent inhibition of the NAD⁺ hydrolysis by high concentrations of the chemical reducing agents DTT and TCEP (Fig. 5.17A, B). At intermediate concentrations of DTT and TCEP (0.3 – 1 mM) a slight increase in the relative amounts of cADPR (blue) vs. ADPR (orange) was observed. The physiological reducing agent GSH, a tripeptide composed of the amino acids glutamate, cysteine and glycine with a gamma peptide linkage between the carboxyl group of the glutamate side chain and cysteine, showed little if any effect on NAD⁺ catalysis by LP1 cells at concentrations below 1 mM. Treatment of cells with GSH at concentrations of 1-5 mM, resulted in elevated production of cADPR (Fig. 5.17C).

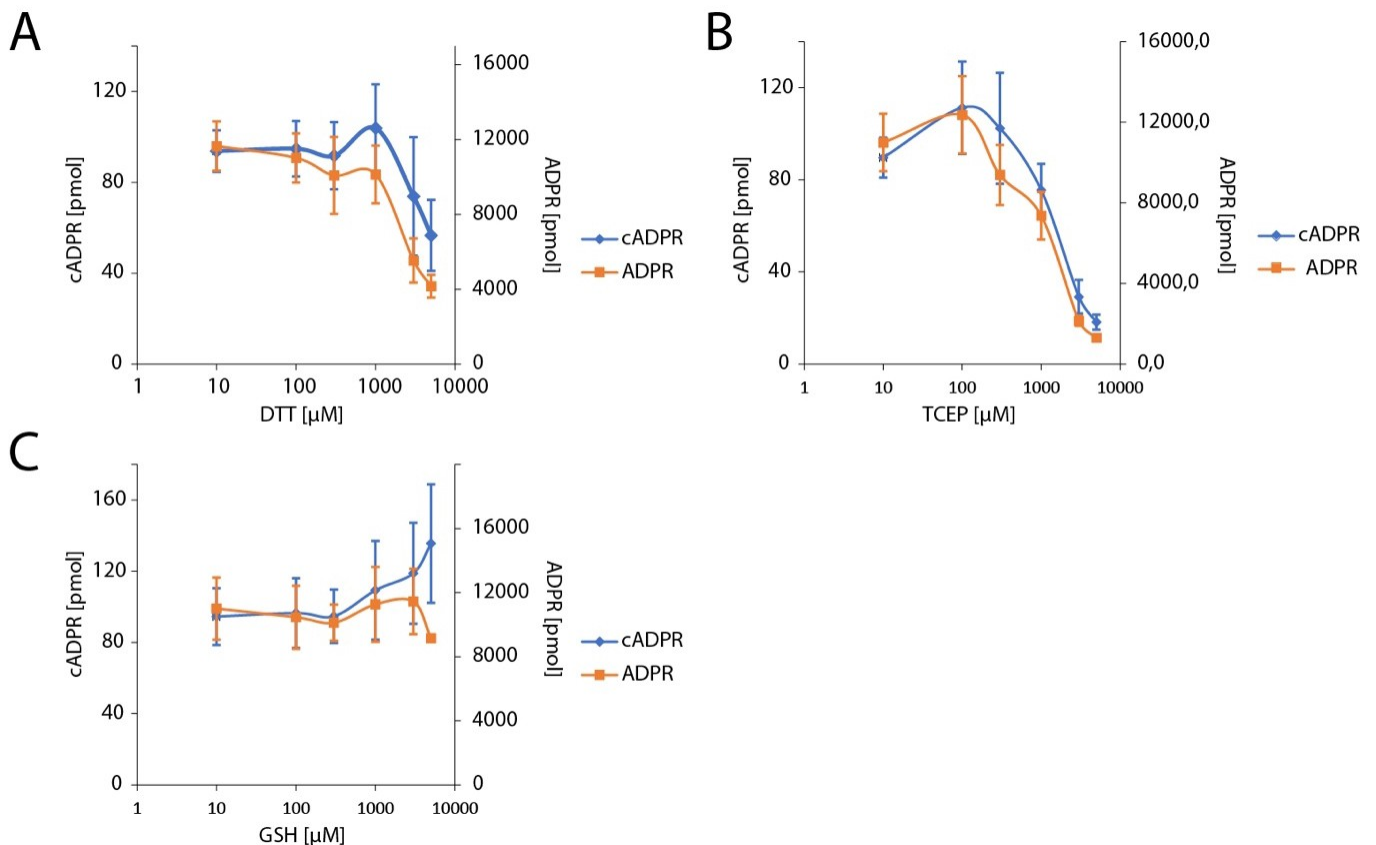


Fig. 5.17: The reducing agents DTT, TCEP and GSH affect the production of cADPR and ADPR by LP1 myeloma cells in a dose-dependent manner.

LP1 cells (1×10^5 cells/well) were incubated for 10 minutes with the indicated concentrations of the reducing agents DTT (A), TCEP (B), or GSH (C), followed by addition of 500 μM NAD⁺ and further incubation for 60 minutes at 37°C. Analysis of cADPR and ADPR was performed using a reversed-phase HPLC on a Multohyp BDS C18 column as in Fig. 5.16. Detection of nucleotides was performed at $\lambda = 260$ nm.

5.2.3. Fc-engineered EGFR- and CD38-specific hcAbs induce CDC and ADCC of human tumor cell lines

In the following section, Fc-mediated effects of hcAbs on EGFR and CD38 expressing tumor cell lines will be examined. In these experiments hcAbs were used in which nanobodies were fused to the hinge, CH2, and CH3 domains of human IgG1. The CDC-enhancing hexabody mutation E345R was introduced into the EGFR-specific hcAb by site directed mutagenesis as described for mouse IgG2a hcAbs (see Fig. 5.2 above), the corresponding mutant was designated 7D12-E. In addition, a triple mutant, designated 7D12-T was generated (G236A, S239D and I332E) that reportedly enhances antibody-dependent cellular cytotoxicity.

The capacity of EGFR-specific 7D12-hcAb to induce CDC in head and neck squamous cell carcinoma (HNSCC) expressing EGFR WT (UTSCC14) or the SNP EGFR R521K (SAT) was analyzed by flow cytometry using uptake of propidium iodide as an indicator of cell lysis (Fig. 5.18). UTSCC14 and SAT cells were pre-incubated for 15 minutes with hcAbs 7D12-WT or 7D12-E, or with the therapeutic mAbs cetuximab or panitumumab, before human serum was added as a source of complement for 3 hours; heat inactivated serum served as a control. The results show that effective and significant CDC against UTSCC14 cells could only be induced with the hexabody mutant hcAb 7D12-E, but not with any of the other hcAbs and mAbs. hcAb 7D12-E induced about 70 % lysis of UTSCC14 cells, whereas all other constructs showed similar background compared to control with inactivated serum (20%). hcAb 7D12-E also induced significant lysis of SAT cells compared to control and other constructs, albeit less effectively than in case of UTSCC-14 cells with a maximal killing of 30 % vs. 10 % background lysis with heat-inactivated serum control.

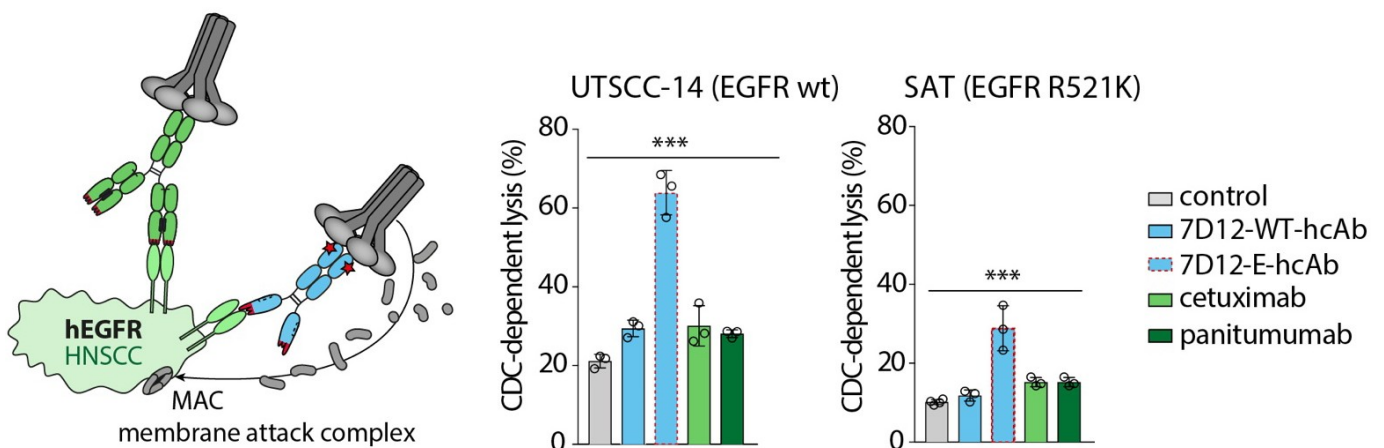


Fig. 5.18: The hexabody (E345R) mutant of 7D12-hcAb induces CDC toward HNSCC cell lines.

The schematic illustrates the experimental set up of the assay. HNSCC cell lines UTSCC14 and SAT (5×10^4 cells/well) were pre-incubated for 15 minutes with 60 μ M of 7D12-hcAb or the E345R mutant (7D12-E-hcAb) or 32.8 μ M of cetuximab or 17 μ M of panitumumab. Human serum was added as a source for complement (25 % of total volume); heat inactivated serum served as a control. Cells were incubated for 3 hours at 37°C. Cells were washed and resuspended in propidium iodide for 15 minutes at RT (PI) before analysis by flow cytometry. Statistical analysis was calculated using an one-way ANOVA followed by a Tukey post hoc test for multiple comparisons. ***, $P < 0.001$.

The capacity of 7D12-hcAb to induce ADCC of head and neck squamous cell carcinoma (HNSCC) expressing EGFR WT (UTSCC14) or EGFR R521K (SAT cells) was analyzed using a ^{51}Cr release assay. As effector cells, human PBMCs were isolated via Percoll density gradient. UTSCC14 and SAT target cells were loaded with ^{51}Cr and pre-incubated with hcAbs 7D12-WT or 7D12-T-hcAb with the therapeutic mAbs cetuximab or panitumumab. Then, effector cells were added at a 40:1 ratio and incubation was continued for 3 hours. Cell lysis was quantified by ^{51}Cr release in a scintillation counter (Fig. 5.19). The results show that hcAb 7D12 and cetuximab induce cell lysis in a concentration dependent manner of both UTSCC14 and SAT cells, with the triple mutant of hcAb 7D12 showing significantly higher effectivity than the other Abs. Panitumumab mediated only residual ADCC-dependent lysis of < 10 %.

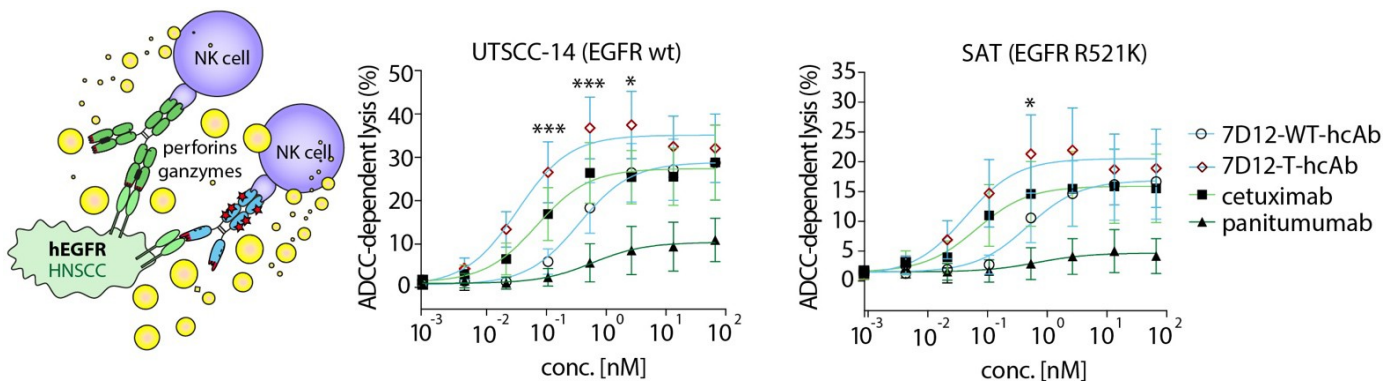


Fig. 5.19: Fc engineering of hcAb 7D12-hlgG1 enhances ADCC of HNSCC cell lines.

The schematic illustrates the experimental set up of the assay. UTSCC14 and SAT cells were loaded with ^{51}Cr for 2 hours at 37°C before addition of antibody constructs. ^{51}Cr -tagged UTSCC14 and SAT were incubated for 15 minutes on ice with dilution series (0.001 – 100 nM) of 7D12-hcAb, its triple mutant ADE (7D12-T-hcAb), cetuximab, or panitumumab. Then, human PBMCs were added as effector cells at a 40:1 effector to target ratio and incubation continued for 3 hours at 37°C. Dead cells were quantified by ^{51}Cr release in a scintillation counter. Statistical analysis was calculated performing an one-way ANOVA followed by a Tukey post hoc test for multiple comparisons. *, P<0.05; ***, P<0.001

5.2.4. Cultivation of primary multiple myeloma cells from patient bone marrow samples may alter their sensitivity toward CDC

Primary multiple myeloma cells from patient bone marrow aspirates often express high levels of CD38. Our aim was to better understand the problems of cultivating primary MM cells and to find optimal cultivation conditions to allow further analysis of patient samples at different days. Therefore, fresh bone marrow mononuclear cells (BMMCs) from a MM patient bone marrow aspirate were isolated using Ficoll density gradient and seeded in complete α Mem medium with different growth factors or cytokines, or without as a control. Cell growth was monitored by microscopy and multiple myeloma cells were identified by flow cytometry as cells co-expressing CD38 and CD138 (Fig. 5.20). Dead cells were excluded on the basis of their low forward scatter (FSC-A). On the day of isolation (day 0) the BMMC preparation contained 58% live cells, of which 10% were identified as MM cells. At day 6 of cultivation in the presence of IL2 only, the percentage of living cells had increased to 80%, and the relative proportion of MM cells to 13.7 %. The relative fraction of MM cells was slightly higher in cells cultivated in

the presence of the growth factors EGF (16.3%), IL6 (15%) and VEGF (15%). In contrast, cultivation in the presence of the pro-inflammatory cytokine IL1 β resulted in a reduction in both, the proportion of living cells (65%) and in the proportion of CD38/CD138 double positive MM cells (8%). Additional application of EGF to each of the growth factors and cytokines did not have any further stimulatory effects. Microscopic analysis revealed an adherent cell layer, possibly constituted of dendritic cells, fibroblasts and other stromal cells. The depicted picture in Fig. 5.20 was taken at day 6; Myeloma cells appeared to have formed little islets on adherent cells.

Patient 1, day 0

Patient 1, day 6

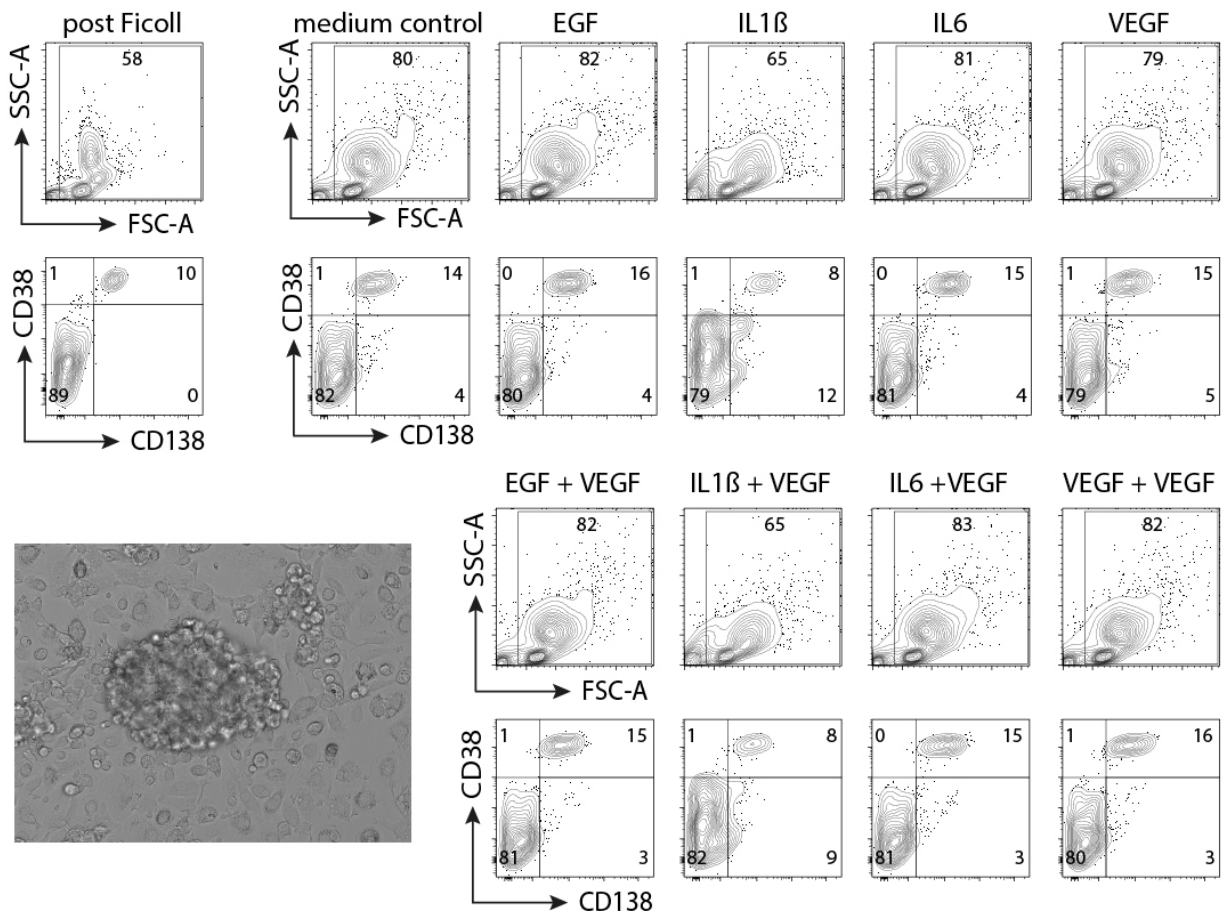


Fig. 5.20: Primary MM cells from a patient bone marrow samples survive in culture for 6 days.

Fresh bone marrow mononuclear cells (BMMCs) were isolated from a MM patient bone marrow aspirate using Ficoll density gradient centrifugations. Cells were seeded at a concentration of 1×10^6 cells/ml in α Mem medium with 10% FCS, 10% horse serum, IL2 (5 ng/ml), glutamine and sodium pyruvate with or without the indicated additional growth factors or cytokines. One third of medium was exchanged with fresh medium on day 3. Cells were stained on day 0 (left panel) and day 6 (right panel) for with fluorochrome-conjugated antibodies against CD38 and CD138 and analyzed by flow cytometry. Cellular debris (low FSC) was excluded by gating. The inset shows a light microscopy image captured before cell harvest at day 6 at 10x magnification.

Next, we wanted to determine the potential cytotoxic effects of CD38-specific hcAbs and the therapeutic mAb daratumumab on primary CD38/CD138 double positive MM cells. Therefore, CDC assays were performed with the patient described above on day 0 and day 6. BMMC cells were pre-incubated with CD38-specific heavy chain antibodies, daratumumab, or isotype control (L-15-WT-hcAb), followed by addition of 12.5% pooled human serum for 1.5 hours. MM cells were identified by staining with α CD138 and α CD38. Apoptotic cells were identified by staining with Pacific Orange (PacO) (Fig. 5.21). Since shrinkage of cells upon dying results in a decrease in FSC-A, some dead cells were lost from analysis due to the gating procedure. Color coding for increasing PacO reflects cell viability from blue with the highest viability to red with the lowest viability. Living CD38/CD138 double positive MM cells were quantified using flow cytometry at day 0 and day 6. At day 0, the sample contained 70% living cells, of which 13 % showed high cell surface levels of both CD38 and CD138. Whereas addition of JK36-WT-hcAb had little if any cytotoxic effect compared with the isotype control L-15-WT-hcAb, applying daratumumab or a combination of JK36-WT-hcAb and MU1067-WT-hcAb resulted in almost complete loss of CD38^{hi}/CD138^{hi} MM cells. Concurrently PacO staining cells appear in a new population of cells with intermediate levels of cell surface CD38 and CD138. At day 6, the proportion of living cells had increased (from 70 to 80%) as the proportion of CD38/CD138 double positive MM (from 13% to 17 %). While application of hcAb JK36 alone again showed little cytotoxicity compared to the isotype control L-15-WT-hcAb, addition of daratumumab or a combination of JK36-WT-hcAb and MU1067-WT-hcAb resulted in a loss of CD38^{hi}/CD138^{hi} cells (1 %, 2% residual MM cells, respectively), and the appearance of apoptotic CD38^{int}/CD138^{int} cells.

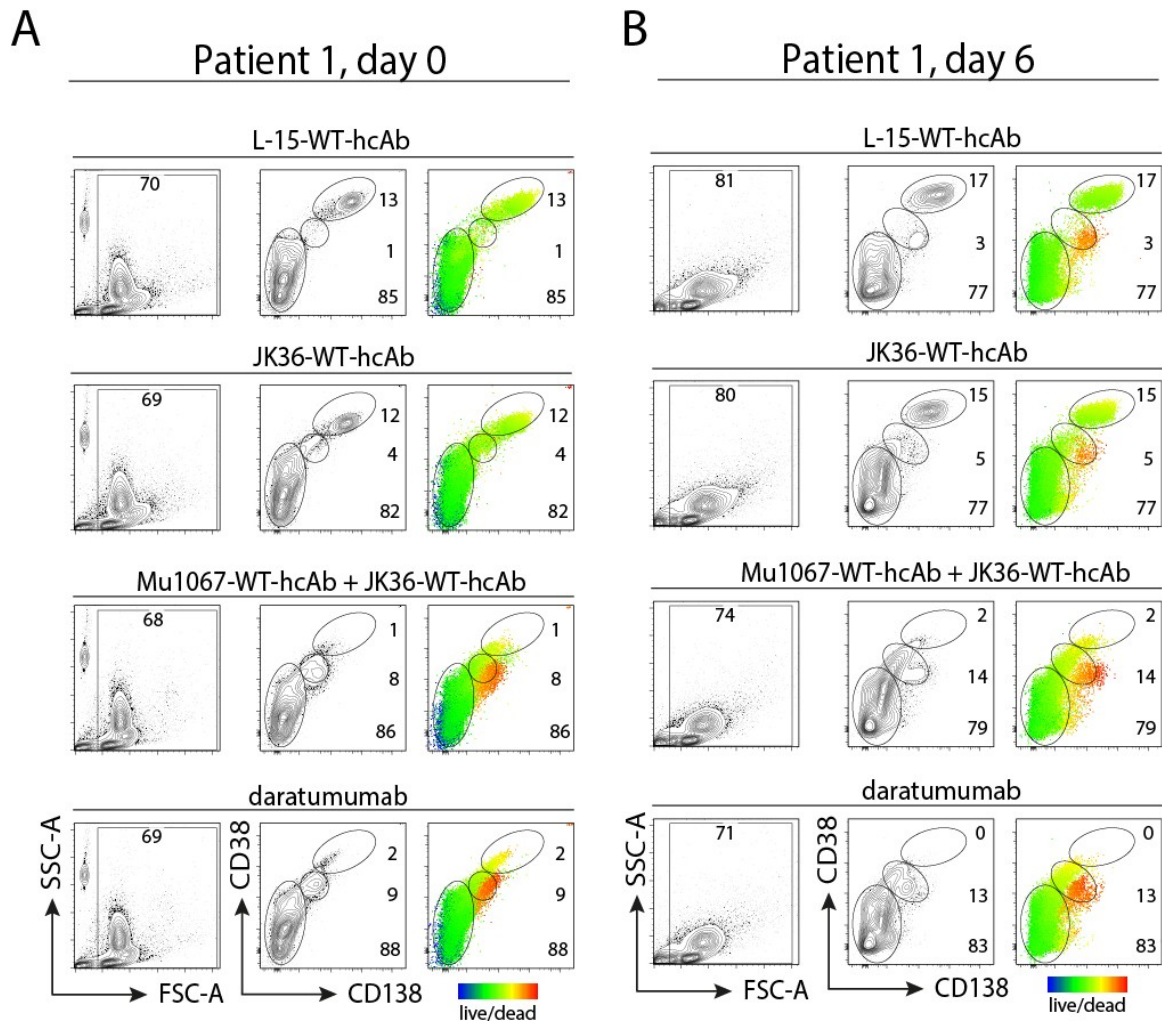


Fig. 5.21: Daratumumab and combinations of two hcAbs mediate effective CDC of multiple myeloma cells in a patient bone marrow sample at d0 and d6.

BMMCs from a MM patient bone marrow aspirate were analyzed either on the day of preparation or after 6 days of cultivation in the presence of IL2 as described in Fig. 5.19. Cells were incubated for 15 minutes at 4°C with 100 nM of the indicated hcAbs or daratumumab, before addition of 12.5% pooled human serum as source of complement and further incubation for 1.5 hours at 37°C. Cells were washed and stained for 30 minutes at 4°C with fluorochrome-conjugated Abs against CD138 and CD38 and with PacO before analysis by flow cytometry. Decreasing cell vitality is indicated by stronger staining with PacO (live/dead) and decreased staining for CD38 and CD138. Numbers indicate the percentage of cells contained within the indicated gates, i.e. live MM cells CD38+/CD138+/green, apoptotic MM cells CD38int/CD138int red, and non MM cells (CD38-/CD138- green).

The CDC assay was repeated with primary MM cells from another patient. Fresh BMMCs from a bone marrow aspirate were isolated using Ficoll density gradient. BMMCs were pre-incubated with CD38-specific hcAbs or daratumumab, followed by further incubation for 1.5 hours in the presence of 12.5% pooled human serum (Fig. 5.22). Cells were stained with PacO, α CD138, and α CD38 to quantify the number of living CD38/CD138 double positive MM cells at day 1 (A) and day 6 (B). Color coding again reflects live/dead staining by PacO ranging from blue with the highest viability to red with the lowest viability. Results reveal that at day 1, patient 2 showed a high proportion of CD38+/CD138+ cells (77 %). At day 6 of cultivation, cell vitality had decreased to 43% and the proportion of MM cells to 65%. Interestingly, neither

daratumumab nor the combination of hcAbs JK36 and JK2 had any detectable cytotoxic effect at day 1. At day 6, in contrast, addition of daratumumab or a combination of hcAbs JK36 and JK2 resulted in a partial loss of CD38^{hi}/CD138^{hi} cells, with a concomitant appearance of CD38^{int}/CD138^{int} cells, many of which were strongly stained by PacO.

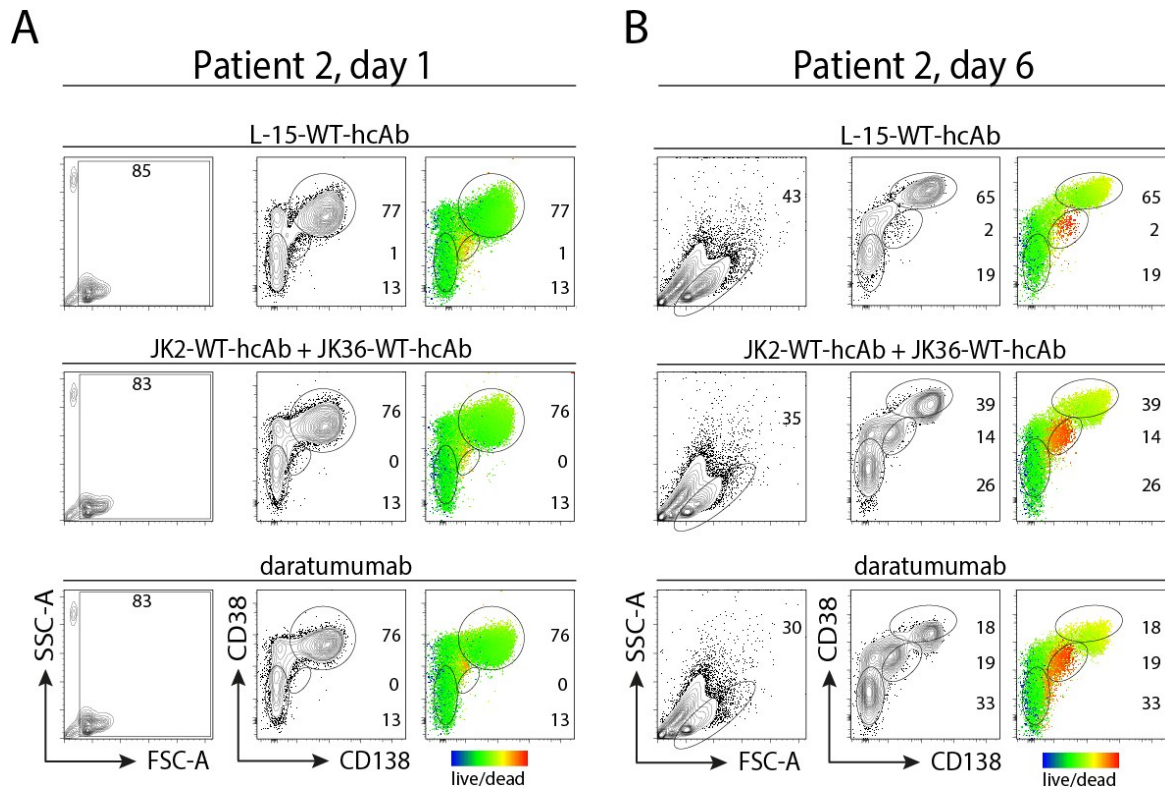


Fig. 5.22: Daratumumab and combinations of two hcAbs mediate effective CDC of multiple myeloma cells in a patient bone marrow sample at day 6, but not at day 1.

BMMCs from a MM patient bone marrow aspirate were analyzed either on day 1 or day 6 of cultivation in the presence of IL2 as described in Fig. 5.20. Cells were incubated for 15 minutes at 4°C with 100 nM of the indicated hcAbs or daratumumab before addition of 12.5% pooled human serum as source of complement and further incubation for 1.5 hours at 37°C. Cells were stained and analyzed as described in Fig. 5.21.

5.3. Using nanobodies to improve the targeting of tumor cells by AAV

In the last part of this PhD thesis, a third strategy to target tumor cells with nanobodies is employed – nanobody-displaying AAV and bi-specific adaptors. A limiting factor for successful gene delivery with AAV vectors is the broad tropism of most AAV serotypes. Nanobodies as ligands are promising tools to target AAVs specifically to cells. The goal was to use nanobodies directed against the cell surface protein CD38, which is overexpressed in multiple myeloma – to specifically target AAVs to MM cells. Nanobody-displaying AAV and bispecific adaptors composed of a CD38-specific nanobody genetically fused to an AAV-specific nanobody were previously generated in the Nolte lab (Eichhoff A, dissertation MIN faculty, Hamburg, 2018, (61)). In this thesis, we aimed to test the potential of nanobody-displaying AAV and bi-specific adaptors to specifically mediate transduction of primary myeloma cells from a patient bone marrow.

5.3.1. Display of CD38-specific nanobody on the AAV-capsid specifically enhances the transduction of primary MM cells from a patient bone marrow

AAV1 capsids displaying a CD38-specific nanobody fused to a surface loop of the VP1 capsid protein were tested for their potential to specifically transduce MM cells from a patient bone marrow. Therefore, BMMCs were isolated via Ficoll density gradient at day 0 and cultivated for 7 days. At day 7, cells were incubated with α CD38-displaying AAV1 and α P2x7-displaying AAV as a control for 48 hours at 37°C. These AAV carried a YFP encoding sequence that allowed a later determination of transduction efficacy. At day 9, BMMCs were stained for CD38 (epitope 3), CD56 and CD45 to allow differentiation between MM cells, cellular debris and other stromal cells by flow cytometry (Fig. 5.23). The results show that ~ 16 % of living cells were CD45 negative/CD38 positive, and CD56 positive/CD38 positive. Transduction efficiency was assessed by the level of YFP fluorescence encoded by the AAV. The results show a strong YFP signal for almost all MM cells treated with 2.000 viral genomes (vg) per cell of the CD38-nanobody displaying AAV. There was little if any transduction of other cells. In contrast, treatment of cells with control P2X7-specific nanobody displaying AAV resulted in little if any YFP expression.

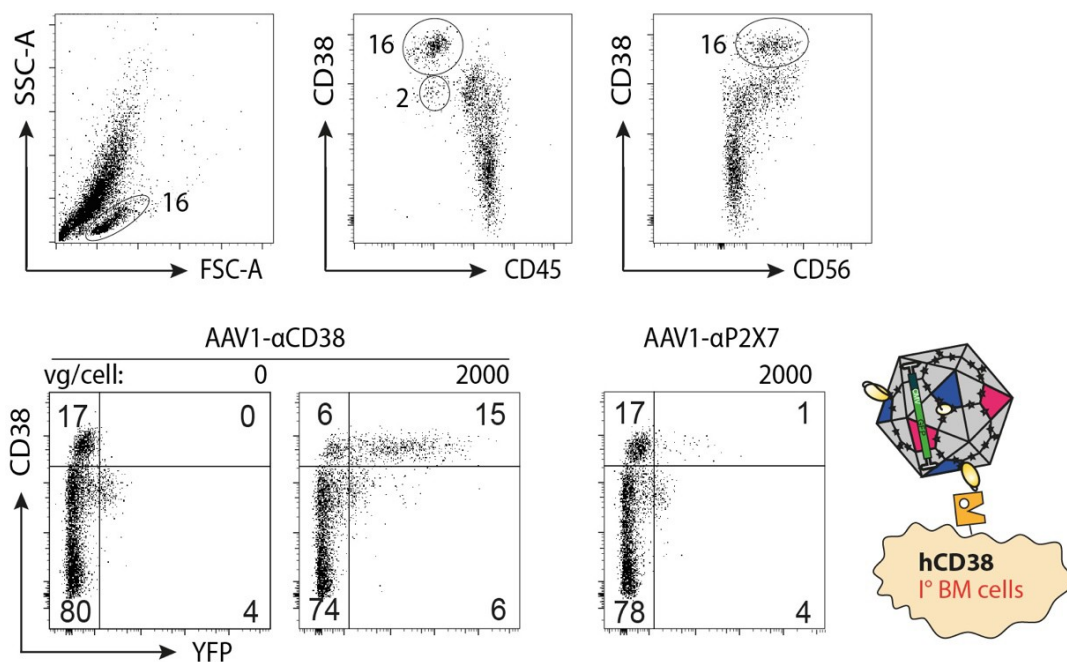


Fig. 5.23: Insertion of CD38-specific Nb 1067 into the VP1 capsid protein of AAV2RA enhances transduction of primary MM cells by AAV2RA.

The schematic illustrates the experimental set up. Nb-displaying AAV were produced as described in Eichhoff et al., 2019. BMMCs were isolated via Ficoll density gradient and cultivated for 7 days in medium containing IL2 as described in Fig. 5.21. Cells were transferred to a 96 well plate (1.5×10^5 cells/well) and incubated further in the absence or presence of the indicated amounts (vg = viral genomes) of AAV1 displaying either the CD38-specific Nb Mu1067 or mouse P2X7-specific Nb (1c81) as control. AAV1 carried a YFP reported gene that allowed evaluation of transduction efficacy. At day 9, cells were stained for 30 minutes at 4°C with fluorochrome-conjugated antibodies against CD38, CD56, and CD45 to allow differentiation of MM cells before analysis by flow cytometry.

5.3.2. Bispecific adaptors enhance specific transduction of primary MM cells by AAV

As a second approach, we wanted to determine whether bispecific α CD38- α AAV adaptors mediate specific transduction of primary MM cells from the same patient bone marrow aspirate that was used in the previous experiment (Fig. 5.24). Therefore, bispecific nanobody-AAV adaptors were tested for their potential to promote the transduction of AAVs into patient MM cells. To examine this, 7-day old primary BMMCs were incubated with α CD38 (MU1067)- α AAV adaptors or α CD296- α AAV control-adaptors for 30 minutes, before AAV6 was added, again using a YFP encoding reporter gene that allow the determination of transduction efficacy. 48 hours later, BMMCs were stained with the same marker panel used above (α CD38 (E3), α CD56, α CD45) and analyzed by flow cytometry. Results show that MM cells treated with the CD38-specific adaptor have a strong YFP positive signal. Other cell population showed little if any YFP expression. Similarly, MM cells treated with the control α CD296- α AAV adaptor also showed only weak expression of YFP.

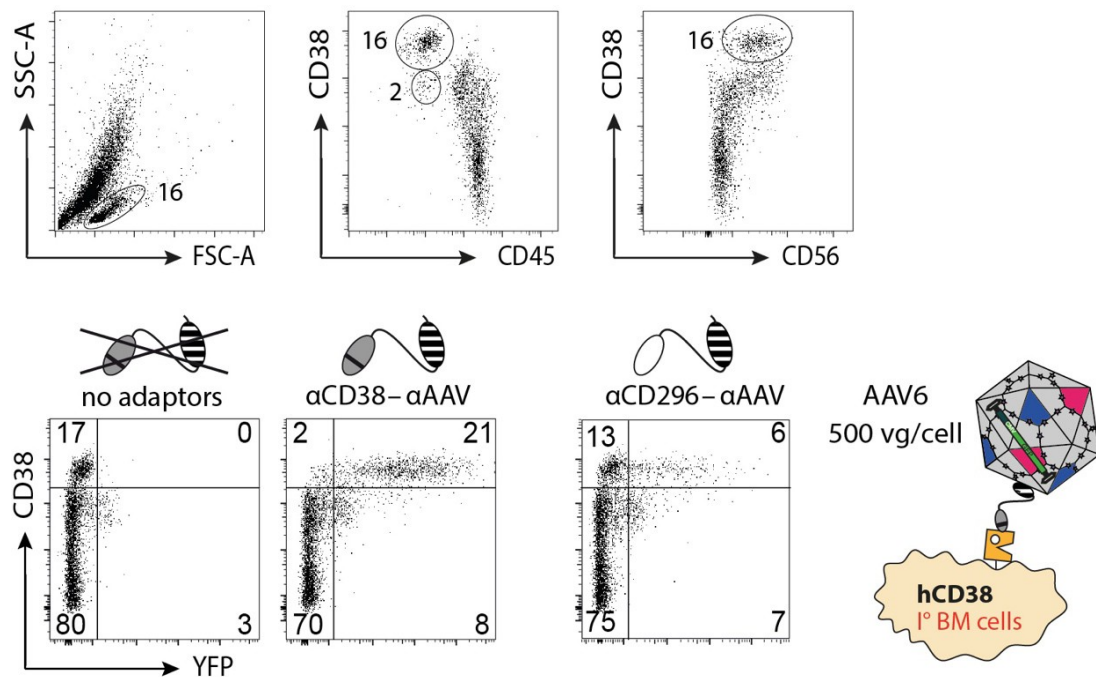


Fig. 5.24: Bispecific nanobody adaptors mediate transduction of AAV6 into primary human MM cells.

Bi-specific nanobody adaptors consisting of a membrane-protein specific nanobody fused via a peptide linker to an AAV-specific nanobody were cloned and produced as described in Eichhoff A, dissertation MIN faculty, Hamburg, 2018. The schematic illustrates the experimental set up. For this assay, the same 7-day old primary BMMCs as described in the Fig. 5.23 were used. Cells were incubated with α CD38 (MU1067)- α AAV adaptors or α P2x7- α AAV control-adaptors for 30 minutes at RT. Cells were washed and transferred to a 96 well plate. YFP-encoding AAV6 were added (500 viral genomes/cell). 48 hours later, MM cells were stained for 30 minutes at 4°C with fluorochrome-conjugated Abs before analysis by flow cytometry as in Fig. 5.23.

6. Discussion

The aim of this work was to generate CD38- and EGFR-specific hcAbs and to investigate their potential use for targeting CD38 or EGFR-overexpressing tumor cells. The following discussions follows the order in which the results were presented in the previous section.

6.1. Mouse CD38 nanobody discovery and generation of heavy chain antibodies

Phage display technology was used to select 5 families of mouse CD38-specific nanobodies from two immunized llamas. The nanobodies were selected by panning on the mouse CD38-expressing EL4 cell line and splenocytes from WT mice. Specificity was increased by a pre-absorption of phage on splenocytes from CD38-deficient mice. Sequencing revealed a small family 1 consisting of JK3 and NB11 with a QREL framework and a CDR3 of 13 amino acids (aa), two single clone families JK5 (family 2) with an EREF framework and a 13aa CDR3, and NB32 (family 3) with a QREV framework and a short 3 aa CDR3. Family 4 was the largest family with 6 distinct clones (JK13, JK16, NB3, NB7, NB22, NB24) containing a QREL framework and a 13 aa CDR3. Notably, this family contained a tryptophan (W) residue in the CDR3. Family 5 consists of three clones NB38, NB40 and NB42, with a QREL framework and a 13 aa CDR3.

In order to generate heavy chain antibodies with the capacity to mediate Fc-effector functions, nanobodies were fused to the hinge, CH2 and CH3 domains of mouse IgG2a. Moreover, mutations that had previously been reported to enhance CDC (E430S) or to abrogate CDC and ADCC (L234A, L235A, P329G) effector functions of human IgG1, were introduced into the corresponding positions of mouse IgG2a (28) (66). IgG2a was chosen because this isotype reportedly exhibits relatively high affinity to various FcγR subtypes and a good capacity to activate the complement cascade (67).

Ultimately, elucidation of the 3D-structure of a protein in complex with an antibody by X-ray crystallography is the most informative means to map an antibody binding epitope. In the absence of such a structural model, cross blockade analyses can provide information on the relative binning epitopes of different antibodies. The results of such cross blockade analyses revealed three non- or only partially overlapping independent epitopes on mouse CD38. Family 1 binds to epitope 1; the single clone family 2, as well as the other single clone family 3, bind to epitope 2. The larger families 4 and family 5 bind to an overlapping epitope, which was assigned to epitope 3. Independent, non-overlapping epitopes allow monitoring the targeting of CD38-expressing lymphocytes and tumor cells that had been pre-treated with another hcAb.

We next aimed to evaluate the relative binding strengths of the selected hcAbs to mouse CD38 on the cell surface. To this end, we monitored the rate of dissociation of hcAbs from EL4 cells as a correlate of binding strength. The results indicate that family 4 hcAb bind with highest avidity to cell surface CD38, followed by families 2, 3, and 1. Whereas in single application of hcAbs a high affinity to the target protein is desirable, low binding affinities of hcAbs may be of advantage for the construction of bispecific hcAbs. Bispecific hcAbs preferentially target

cells that co-express two different antigens on the same cell surface over cells that express only one of these antigens and hence, require low binding affinities. Bispecific hcAbs directed against two different tumor antigens might increase specificity for the tumor and decrease off-target effects and hence, are seen to be promising tools for future cancer therapies.

Furthermore, we aimed to analyze the capacity of the selected hcAbs to modulate CD38 enzyme activity using EL4 mouse thymoma cells that express high levels of CD38. Chromatograms of a reversed-phase HPLC on a Multohyp BDS C18 column of NAD metabolites revealed that EL4 cells specifically metabolized NAD⁺ to ADPR. Hence, the next step was to analyze the effect of mCD38-specific hcAbs on mCD38 cyclase. The results show that family 4 and 5 hcAbs, i.e. all epitope 3 nanobodies, inhibited the CD38-catalyzed conversion of NGD⁺ to cyclic GDPR in a dose dependent fashion. Family 1, 2 and 3 directed against epitope 1 and 2, respectively, had no detectable effects on CD38 cyclase activity. Titrating the two strongest inhibiting hcAbs NB38 and NB42 revealed a low IC₅₀ of ~ 10 nM. Combined application of family 4 and family 5 hcAbs did not show any additive effects. It has been proposed that the tumor microenvironment (TME) in MM might be shaped *inter alia* by CD38 (14), leading to tumor growth and immunosuppression (68). Thus, blocking the enzymatic activity of CD38 may be of therapeutic benefit in multiple myeloma. Although CD38 cyclase might play only a minor role in the production of anti-inflammatory metabolites during purinergic signaling, it generates the second messenger cADPR. cADPR mobilizes intracellular calcium stores and hence, is involved in many diverse cell functions, such as cell proliferation and differentiation (25).

Finally, we tested the capacity of mCD38-hcAbs to activate Fc-mediated immune effector functions, i.e. complement-dependent cytotoxicity (CDC) and antibody-dependent cellular cytotoxicity (ADCC). Monitoring CDC-mediated killing of mouse target cells proved difficult since enzymatic complement components are not stable in mouse serum. Using human serum as a source of complement resulted in a high level of background killing (i.e. in the absence of any added hcAbs) of mouse EL4 cells. An explanation might be that human serum contains IgM antibodies that cross-react with antigens on mouse cells and hence, mediate effective CDC even in the absence of added CD38-specific Abs. However, a different approach, i.e. the transient transfection of human target cells with mouse CD38 and use of human serum as a source of complement at last was successful. We transiently co-transfected HEK cells with expression vectors for mouse CD38 and GFP and monitored complement-mediated permeabilization of the plasma membrane to GFP and propidium iodide by flow cytometry as indicators of antibody-mediated, complement dependent cytotoxic effects of mCD38 hcAbs. Individual mouse IgG2a hcAbs induced CDC against mCD38-transfected HEK cells with varying efficiencies. hcAbs directed against epitope 3 appeared more effective than hcAbs directed against epitope 1 and epitope 2. Previous studies reported a similar higher capacity to induce CDC of daratumumab compared to mAbs targeting other epitopes of human CD38 (69). In contrast, individual human IgG1 hcAbs against human CD38 were rather ineffective at inducing CDC (70). Introduction of the E435R hexabody mutation markedly increased the CDC potencies of both, human CD38-specific mAbs and hcAbs (71), (70). Introduction of the

hexabody mutation E430S moderately increased, introduction of the triple mutant (L234A, L235A, P329G) abrogated the capacity of mIgG2a hcAbs to induce CDC.

To analyze antibody dependent cytotoxic effects of mCD38-specific hcAbs, mCD16-transfected NK92 effector cells were added to CD38-expressing EL4 cells in a ratio of 3:1. All analyzed hcAbs (JK3, JK5 and JK13) mediated effective ADCC of EL4 cells. The capacity to induce ADCC was abrogated by introduction of the (L234A, L235A, P329G) LALAPG triple mutation.

In conclusion, five nanobody families were identified and converted into heavy chain antibodies with different affinities directed against three independent epitopes on mouse CD38. Antibodies that bind an independent epitope allow their use for detecting tumor cells during treatment with a therapeutic Ab. Furthermore, our results emphasize the potential of mCD38-hcAbs for modulating the enzymatic activity of CD38 cyclase, which might be of therapeutic value for reducing the proliferation of myeloma cells in the tumor microenvironment. Our CDC and ADCC assays are of value for monitoring the cytotoxic efficacy of hcAbs vs. tumor cells that overexpress the targeted antigen. The hcAbs reported here thus hold promise as potential diagnostic and therapeutic tools in myeloma and other CD38-expressing malignancies in mouse models with a fully immune-competent background.

6.2. Targeting EGFR-variants and CD38 with heavy chain antibodies

Monoclonal antibodies (mAbs) targeting the EGF-receptor (cetuximab, panitumumab) or CD38 (daratumumab) show therapeutic efficacy in solid and hematological malignancies, respectively. However, many patients do not respond to targeted therapy due to acquired and primary resistance. Because of the increasing necessity of new therapeutics, the goal of this work was to develop and analyze two different nanobody-based therapeutic strategies. First, heavy chain antibodies were tested on their direct (downstream signaling, enzymatic activity) and indirect (immune effector functions) effects on tumor cells. Second, nanobodies were used to increase the specificity of AAVs targeting CD38-overexpressing myeloma cells from a patient bone marrow.

6.2.1. Direct effects of EGFR- and CD38-specific hcAbs

The EGFR is overexpressed in metastatic colorectal cancer (mCRC) and head and neck squamous cell carcinoma (HNSCC) patients. Downstream EGFR signaling results in proliferation, survival and invasion of tumor cells, thereby allowing tumor cells growth advantages over benign cells. mCRC patients develop EGFR ectodomain mutations under therapy at positions V441, S442, R451, I462, S464, G465, K467, K489, I491, and S492. When located in the epitope of the corresponding mAbs these mutations may abrogate binding of cetuximab and/or panitumumab (38). We addressed the question whether nanobody 7D12 which had been isolated by others from immunized Llamas (72), (73), (74) could bind to the

EGFR escape mutants S492R, G465R, S464L, and R451C. 7D12 competes with cetuximab for EGFR binding and hence, is called a “cetuximab like nanobody” (75). All work addressing the retargeting of EGFR variants were performed in the lab of Prof. Dr. Mascha Binder. We tested the binding of 7D12-hcAb in comparison with cetuximab on Ba/F3 cell lines stably transfected with either the EGFR WT or S492R, G465R, S464L, and R451C. FACS-binding results confirmed the loss of binding for cetuximab and panitumumab to the EGFR escape variants G465R and S464L, whereas binding of 7D12-hcAb was maintained. It is noteworthy that there is a complete binding abrogation of cetuximab to the S492R mutant, although panitumumab and 7D12-hcAb binding are both fully conserved. Our results are in line with previous findings of Montagut et al. who showed that the acquired mutation S492R only mediates resistance against cetuximab, but not against panitumumab *in vivo* (40). One reason for maintained binding of 7D12-hcAb to these EGFR variants might be that the epitope of 7D12-hcAb almost fully overlaps with the EGF binding site after conformational change of the EGFR (13, 75). Since EGF binding to the EGFR enables tumor cells growth advantages over benign cells, there would be no acquired mutations located in the EGF binding site. The S492R and G465R mutations appear in 20 % of all mCRC patients (38), (39, 76). Hence, we wanted to test the effect of 7D12-hcAb on proliferation of EGFR variant cells with G465R in comparison to EGFR WT cells. Results showed that proliferation was significantly reduced with 7D12-hcAb, but not cetuximab. A possible explanation for this might be that the G465R mutation, just like R451C, S464L, S492R (Fig. 6.1, red dots), is outside the 7D12 epitope and hence, an inhibition of intracellular downstream signaling pathways such as RAS-RAF-MEK-ERK-MAPK-, PI3K-AKT-mTOR- and PLC- γ 1-PKC was preserved.

In addition to acquired resistance within the EGFR in mCRC, primary resistance in one third of all HNSCC patients was described by Braig et. al. Primary resistance is mediated by the EGFR single-nucleotide polymorphism (SNP) at position 521 (R521K). R521K (Fig. 6.1, green dot) is not located within the cetuximab epitope, hence resistance is most likely not due to any escape mechanisms (29), (77), (78), (79). Primary resistance might be due to an increased N-glycosylation pattern of the EGFR ectodomain III, leading to a decreased affinity of cetuximab. In turn, EGFR downstream signaling pathways are no longer inhibited, which is most likely the cause for poor prognosis of patients with a high K-allele frequency (29). Hence, we next wanted to test the effects of 7D12-hcAb on R521K expressing cells in a 3D HNSCC spheroid model. HNSCC spheroids with EGFR R521K (SAT) and EGFR WT (UTSCC14) were treated with 7D12-hcAb, cetuximab and panitumumab starting at day 7 at every second day. Results show that growth of EGFR WT spheroids was fully stopped upon start of treatment with cetuximab, panitumumab and 7D12-WT-hcAb as expected. However, spheroid size was not decreased overtime. One reason might be that the constructs could not penetrate the 3D spheroid, due to high interstitial fluid pressure. Growth of EGFR R521K spheroids was significantly slower upon treatment independent of the constructs compared to untreated control spheroids; however, growth was not stopped over time with either cetuximab, panitumumab or 7D12-WT-hcAb.

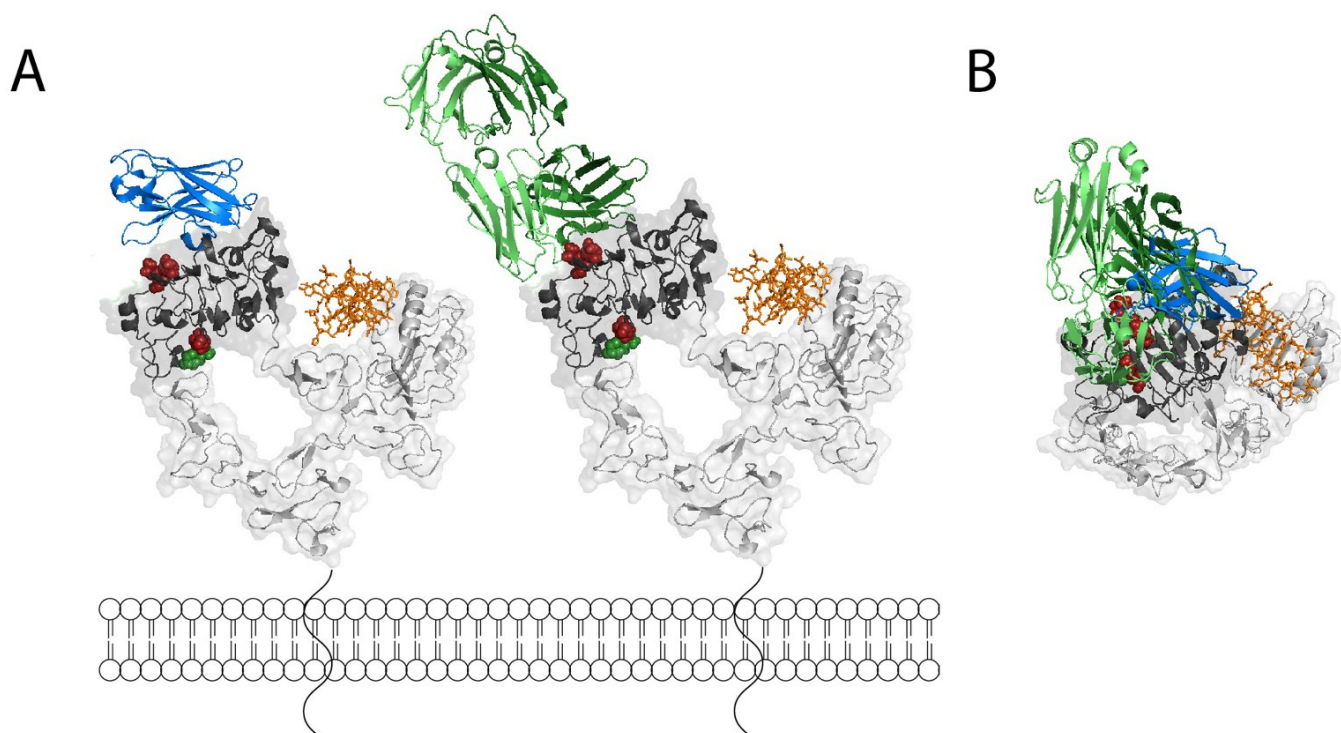


Fig. 6.1: Binding of the mAb cetuximab and hcAb 7D12 to the EGFR.

The 3D structure of the tethered EGFR was depicted using PDB and PyMOL. Domain I, II and IV are shown in light grey with EGF (orange sticks) binding to domain I, and domain III is depicted in dark grey. (A) 7D12 (blue, on the left EGFR) and cetuximab (heavy chain in dark green, light chain in light green, on the right EGFR) both bind to domain III of the EGFR. The acquired mutations S464L, G465R, K467T, S492R (red dots) in domain III are located within the cetuximab epitope but are outside the 7D12 epitope. The acquired mutation R451C (red dot) and the primary SNP R521K (green dot) are close to each other outside of the cetuximab and 7D12 epitope. In (B), the EGFR is depicted from top view showing 7D12 and cetuximab binding to an overlapping epitope.

Acquired resistance of multiple myeloma patients to treatment with the CD38-specific mAb daratumumab is thought to be the result of reduced cell surface expression of CD38 rather than due to mutations as described for the EGFR in mCRC and HNSCC (42), (57). Hence, we aimed to develop CD38-specific hcAbs directed against independent epitopes of daratumumab. We hypothesized that some nanobodies could bind to cavities on CD38 and inhibit its enzymatic activities. Furthermore, we hypothesized that CD38-specific hcAbs targeting different epitopes compared to daratumumab might show improved ADCC- and CDC-mediated killing of myeloma cells (addressed in 6.2.2.).

Prior to this thesis, CD38 nanobodies had been isolated by our group from immunized llamas and shown to recognize three epitopes of CD38 (65). To generate CD38-specific hcAbs, nanobodies were fused to a Fc-portion to allow later effector function (80) and the effect of these hcAbs on CD38 enzymatic activity was analyzed. CD38 catalyzes three distinct enzymatic reactions. NAD^+ is metabolized to ADPR and cADPR by NAD glycohydrolase and ADPR cyclase, respectively. Under physiological conditions, CD38 displays much stronger hydrolase (99%) than cyclase (1%) activity. The third reaction mediated by cADPR hydrolase metabolizes cADPR to ADPR. First, the effect of our CD38-specific hcAbs on NGD cyclase naturally expressed on the LP1 multiple myeloma cell line was tested. Results show that CD38-specific hcAbs against epitope 2 (MU523, MU1067, ST52) inhibited the CD38-catalyzed conversion of NGD^+ to cyclic

GDPR by 50-70%, whereas JK36 against epitope 3 only showed a slight inhibition (10-20%). Daratumumab against epitope 1 had little to no effect on cyclase. This data is in line with previous results from our group (65).

We aimed to monitor NAD glycohydrolase, cADPR cyclase and cADPR hydrolase activities by LP1 myeloma cells using HPLC. Results show that conversion of NAD⁺ to ADPR and cADPR followed similar kinetics, but only 0.8% of the product was cADPR. Hydrolysis of ADPR to cADPR reflecting cADPR hydrolase activity was significantly slower compared to the conversion of NAD⁺ to ADPR by the NAD glycohydrolase. One reason for the slow metabolism of cADPR to ADPR might be the low K_m of cADPR hydrolase compared to glycohydrolase.

CD38 contains a non-conserved surface exposed disulfide bond connecting C119 and C201 and hence, enzymatic activity might be prone to redox-mediated reduction by the tumor microenvironment (TME). Glutathione (GSH) is one of the key redox regulators to compensate tumor-associated oxidative stress, hypoxia and acidosis and hence, GSH is increased among different tumors. Elevated levels of GSH in tumors were associated with enhanced cell proliferation (81), decreased levels of apoptosis (82), increased resistance to chemotherapeutic drugs (83), (84), and radiation therapy (85). Glutathione disulfide–glutathione couple (GSSG/2GSH) allows cancers to compensate severe oxidative damage and to maintain balanced intracellular ROS levels leading to an increased tumor cell proliferation through activation of redox signaling pathways. Although GSSG/2GSH measures highest concentrations intracellularly (86), GSH is also present in the extracellular room (ECR). Next to the liver being the main supplier for extracellular GSH (87), GSH is also exported from the ICR to the ECR by GSH complex export transporters (GS-X pumps) and multidrug resistance proteins (MRP1) that are both upregulated in cancer cells (88, 89). Therefore, extracellular glutathione in multiple myeloma might play a role in reducing disulfide bridges of CD38, thus leading to an altered 3D tertiary structure and enzymatic activity. Hence, we tested different reducing agents – the chemical compounds DTT and TCEP, and the naturally occurring GSH - for their capacity to influence NAD glycohydrolase and ADPR cyclase activities of LP1 myeloma cells. The results show a concentration dependent inhibition of both enzymatic activities by high concentrations of DTT and TCEP, while intermediate concentrations had a slight stimulatory effect. Interestingly, the naturally occurring GSH stimulated cyclase activity in a dose dependent manner, and slightly inhibited glycohydrolase activity at the highest concentration of 5 mM. C119 and C201 distinguish human CD38 from Aplysia ADPR cyclase that elsewhere show homology in 10 of the 12 cysteine residues. The two non-conserved cysteines at position 119 and 201 in human CD38 are replaced by lysine and glutamic acid, respectively, and this enzyme displays a much stronger cADPR-cyclase than NAD-hydrolase activity (26). This emphasizes the potential role of C119 C201 in CD38 enzymatic activity. C119 and C201 are located outside the MU523 epitope (Fig. 6.2A, left CD38), but within the epitope of isatuximab, which is on the opposite site of the catalytic center of CD38 (Fig. 6.2A, right CD38). Hence, it is most interestingly that isatuximab was described to strongly inhibit CD38 cyclase activity, suggesting isatuximab to be an allosteric inhibitor (43). The finding of an allosteric inhibition is supported by our results showing that cyclase activity is also significantly

reduced upon application of MU523 that binds to a non-overlapping epitope compared to isatuximab far apart from the catalytic site (Fig. 6.2B).

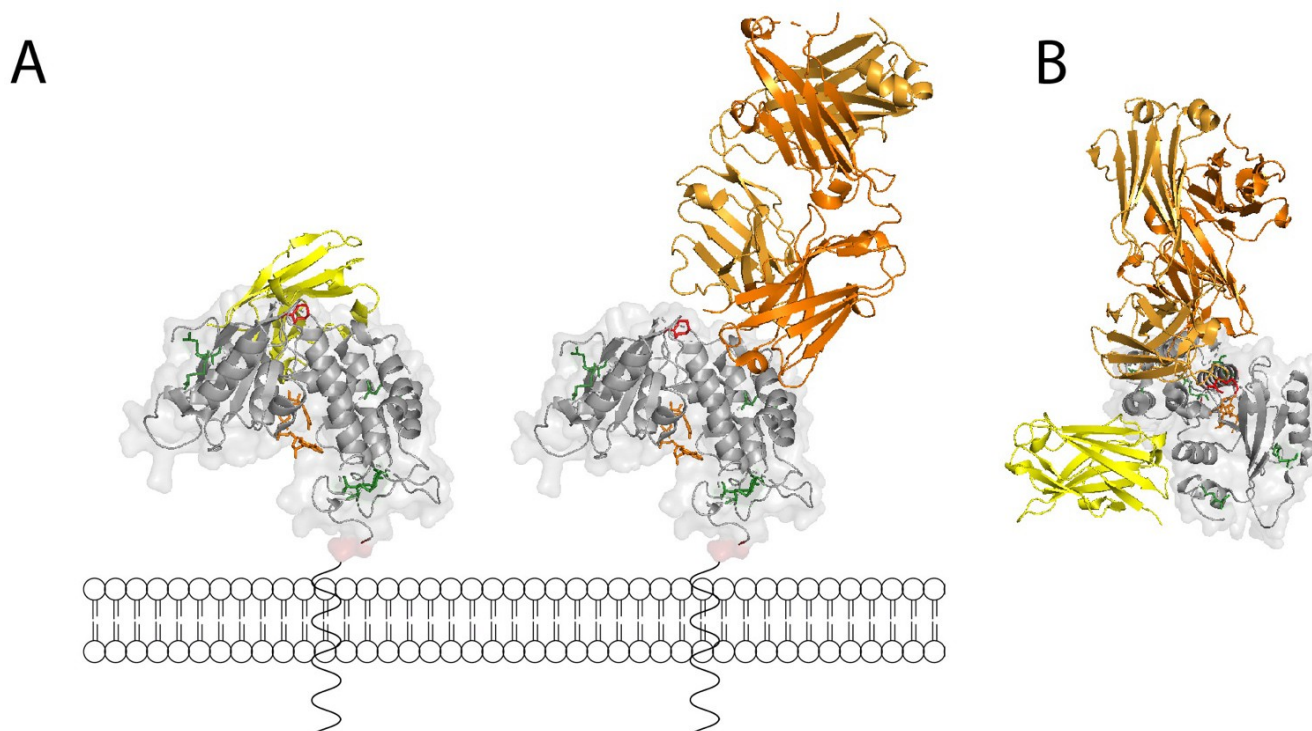


Fig. 6.2: Binding of hcAbs MU375 and MU523, and mAb isatuximab to CD38.

The 3D structure of CD38 was generated using PDB and PyMOL. CD38 is depicted in light grey with NAD⁺ (orange sticks) binding to the active center. The 5 conserved disulfide bridges within the CD38 molecule are shown in green, the non-conserved disulfide bond at C119/C201 in red. (A) The N-terminus is depicted in red and is connected to a schematic illustration of the transmembrane domain. MU523 against epitope 2 (yellow, on the left CD38) binds more to the backside of CD38 and isatuximab against epitope 3 (heavy chain in dark orange, light chain in lighter orange, on the right CD38) binds onto the C119/C201 disulfide bridge. In (B), CD38 is depicted from top view showing MU523 and isatuximab binding to non-overlapping epitopes.

6.2.2. Indirect effects of EGFR- and CD38 specific hcAbs

To allow effector functions in terms of immune cell recruitment and complement activation, selected α EGFR- and α CD38 nanobodies were fused to the hinge, CH2, and CH3 domains of human IgG1. Newly generated chimeric llama/human heavy chain antibodies (hcAb) are about half the size of conventional mAbs (75 kDa vs. 150 kDa), which might facilitate tumor penetration and thereby we suggest an improved efficacy for cancer treatment (65). Furthermore, Fc-engineering was employed (5), to enhance ADCC and/or CDC of tumor cells. This idea was initiated in 2016 by the randomized, controlled, open label, multicenter phase II study RESGEX, in which the efficacy and safety of cetuGEX plus chemotherapy (CT) in comparison to cetuximab plus CT in patients with stage III/IV recurrent and/or metastatic HNSCC was tested. CetuGEX – an ADCC optimized mAb - against HNSCC back then was shown to increase anti-tumor activity by sensitizing SNP R521K HNSCC cells again (ClinicalTrials.gov Identifier NCT02052960). Hence, we inserted either ADCC (G236A, S239D and I332E = T for

triple mutation)- or CDC (E345R or E430S = E)- or both enhancing mutations into the Fc-portion of EGFR- and CD38-specific hcAbs to overcome resistance and allow better killing of mCRC, HNSCC and MM cell lines and primary cells.

Cetuximab and panitumumab have been shown to induce effective ADCC in HNSCC- and mCRC patients, respectively. However, there is a lack of therapeutic response in patients showing primary and acquired resistance. Hence, we aimed to develop a CDC (E345R, E)- and ADCC (G236A, S239D and I332E = T)-enhancing 7D12-hcAb binding to an epitope not involved in resistance. 7D12-hcAbs with different Fc-portions were tested on EGFR WT and EGFR variant mCRC and HNSCC cells. On the contrary to 7D12-WT-hcAb, cetuximab and panitumumab that did not induce CDC-mediated killing, 7D12-E-hcAb induced a 2.2-fold stronger killing of EGFR WT expressing HNSCC cells. That none of the mentioned constructs, except 7D12-E-hcAb, induced killing goes in line with previous published data of cetuximab or panitumumab in single application being unable to induce CDC, since they bind to an overlapping epitope. Combinations of two different mAbs targeting two non-overlapping epitopes on the same surface antigen can mediate cross-connection of cell surface antigens, leading to enhanced binding of the hexameric C1q molecule. This in turn activates the complement cascade and membrane attack complex (MAC) induced osmotic cell death (90). CDC-mediated killing of EGFR R521K expressing HNSCC cells showed similar results compared to EGFR WT HNSCC cells, in that the overall killing by 7D12-E-hcAb was half as strong in SNP cells. This suggests that primary resistance in HNSCC cells could only partially be overcome by 7D12-E-hcAb.

The main anti-tumor effect of cetuximab is antibody-dependent cell cytotoxicity. Therefore, the effect of 7D12-WT-hcAb, 7D12-T-hcAb, cetuximab and panitumumab on mediating ADCC was also tested on EGFR WT and EGFR R521K HNSCC cell lines. The results show a significantly greater killing of EGFR WT HNSCC cells with the ADCC-optimized 7D12-T-hcAb compared to 7D12-WT-hcAb and cetuximab in single application. Interestingly, panitumumab hardly mediated any ADCC. This is contrary to literature describing that the IgG2-Fc part of panitumumab primarily connects with FcγRIIIa expressed on myeloid cells like neutrophils and monocytes, thereby mediating ADCC (31). The assay here was performed with peripheral blood mononuclear cells containing lymphocytes and monocytes. The lack of response to panitumumab therefore remains to be elucidated. One explanation might be that the hIgG1-Fc part of 7D12-T-hcAb, 7D12-WT-hcAb and cetuximab connecting with NK cells might be more potent in killing compared to myeloid cells. The killing rate of EGFR R521K expressing HNSCC cells by 7D12-T-hcAb was not significantly greater compared to 7D12-WT-hcAb, and cetuximab. Overall killing mediated by 7D12-E-hcAb in the CDC assay was similar to 7D12-T-hcAb in the ADCC assay. At first glance, this finding was also rather surprising, since post start of the RESGEX study, the ADCC-optimized cetuximab (cetugEX) was seen as a promising tool to overcome primary resistance in HNSCC. Although cetuximab did not inhibit the downstream EGFR pathway in cells expressing the EGFR R521K variant, its binding affinity was sufficient to mediate ADCC when applied with an ADCC-optimized Fc-portion. However, the post study evaluation showed that cetugEX has no superior effects over cetuximab. Hence, both mAbs seem to have similar efficacies (Keilholz U., *Journal of Clinical Oncology*, 2018).

To conclude, CDC- and ADCC-optimized 7D12-hcAb mediated better HNSCC cell lysis compared to their WT-Fc counterpart, at least in the EGFR WT expressing cells. Targeting primary resistance of HNSCC cells was partially successful; however, overcoming resistance is still a major challenge.

In contrast to the growth factor blocking effects of cetuximab and panitumumab, daratumumab has no direct anti-tumorigenic downstream signaling effects. The main therapeutic mode of action for daratumumab is thought to be ADCC and CDC of multiple myeloma cells and regulatory immune cells (91).

In the following part, CDC- and ADCC data of two different patients with diagnosed multiple myeloma is shown, the sample of patient 1, which was sensitive to CDC and sample of patient 2, which was resistant to CDC-mediated killing, but sensitive to ADCC at day 0 and 1 (data not shown), respectively. After Ficoll-gradient isolation of bone marrow mononuclear cells (BMMCs) from bone marrow aspirates of myeloma patients, CDC- and ADCC assays were performed. CDC assay of patient 1 at day 0 shows that the CD38+/CD138+ myeloma population (13%) was killed upon administration by the combination of daratumumab+JK36-WT-hcAb and MU1067-WT-hcAb+JK36-WT-hcAb and WF211-E345R-hcAb, which was absent with the isotype control L-15-WT-hcAb. These results were expected, since hexameric clustering with subsequent CDC induction is only mediated upon administering a combination of mAbs binding to two independent epitopes or E345R-optimized constructs (33). Therefore, it is not surprising that the single application of JK36-WT-hcAb did not cause killing of the myeloma population. Unlike Dechant's hypothesis, daratumumab alone did mediate CDC-dependent lysis of myeloma cells to the same extent as the combination of daratumumab with JK36-WT-hcAb. This goes in line with literature describing that daratumumab, unlike cetuximab or panitumumab, can induce CDC in single application (91). Analysis of bone marrow aspirate of patient 2 showed an enormously high infiltration with 77% CD38+/CD138+ myeloma cells. At day 1, no killing of CD38+/CD138+ myeloma cells could be induced with either of the tested constructs. Patient 2 represents classic resistance to CD38-targeting of unknown reasons. However, patient 2 when tested in an ADCC assay at day 1, was shown to be sensitive to all of the tested constructs (daratumumab, JK36-WT-hcAb, WF211-T-hcAb, daratumumab + JK36-WT-hcAb). Up to now, we cannot explain the resistance in CDC assay, but sensitivity in the ADCC assay of patient 2.

Hence, to better understand resistance mechanisms and to analyze changes in the sensitivity to mAb- and hcAb targeting, a system for cultivating primary BMMCs was established. Results show that myeloma cells survive in α Mem medium with horse serum, fetal calve serum, glutamine, sodium pyruvate and IL2. Microscopic pictures showed that 8 out of 10 patients (data only shown for one representative patient) formed an adherent stroma cell layer and MM cells were attached to cell arms and formed little 3D islets on the adherent cell layer. Cytokines that are naturally produced by malignant B cells, stromal cells, and activated T lymphocytes, such as IL1 β and IL6, were added to the cell culture (92). Furthermore, different growth factors, such as EGF and VEGF (vascular endothelial growth factor) have been described to drive carcinogenesis in myeloma (93), (94). The addition of IL6, EGF, and VEGF resulted in slightly higher proportions of living cells and of the relative proportion of MM cells.

Addition of IL1 β , in contrast, resulted in decreased cell vitality and a strong decrease in the proportion of MM cells.

The successfully established culture method of primary BMMCs enabled us to perform assays at different time points. BMMCs of patient 1 showed similar CDC-sensitivity at day 0 and day 6. The CD38+/CD138+ myeloma population showed an increase over 6 days in culture of about 30% (13% vs. 17%). Daratumumab and the combination of two hcAbs JK36-WT-hcAb and MU1067-WT-hcAb showed specific cytotoxicity toward MM cells, whereas the single JK36-WT-hcAb in a single application did not mediate CDC.

A second patient 2 appeared completely resistant to CDC on day 1. BMMC cells of this patient were again analyzed on day 6. Of note, overall cell viability was decreased at day 6 (85% day 1, to 43% day 6). In the viable population, a decrease of CD38+/CD138+ MM cells (77% day 1, 65% day 6) was observed. Although patient 2 showed CDC-mediated resistance at day 1, the MM cells were at least partially sensitive to CDC at day 6. Treatment with daratumumab or a combination of two hcAbs JK36-WT-hcAb and JK2-WT-hcAb showed a loss of CD38^{hi}/CD138^{hi} cells and a concomitant appearance of CD38^{int}/CD138^{int} cells that were highly stained by PacO. A possible explanation is that apoptotic cells excrete and/or internalize portions of their cell membranes. A decrease in cell size and thereby FSC as a consequence of cell lysis could also account for the reduction in the proportion of cells in the live gate (from 43% to 30%).

6.3. Using α CD38 nanobodies to enhance cell-specific targeting of AAV gene therapy vectors

AAVs are being used with increasing success for gene therapy (58), (59), (60). More than 100 clinical studies are currently focusing on the use of AAVs to correct rare hereditary diseases. After transduction of target cells, the AAV genome is multiplied and expressed episomally, i.e. without integration into the genome of the target cell. A limiting factor for the use of AAV vectors in gene therapy is the broad tropism of AAV serotypes, i.e. the parallel infection of several cell types (61) and hence, production costs are extremely high.

Reducing production costs is possible when specificity of AAVs is increased. One strategy to increase specificity is to equip replication defective AAV vectors with a tumor targeting ligand that can be used for the delivery of (suicide) genes to tumor cells. Prior to this thesis, Dr. Anna Marei Eichhoff developed two nanobody-based approaches to enhance target cell specificity and efficiency of AAVs in the Nolte lab. First, the direct incorporation of Nbs in the viral capsid (61); and second, the use of nanobody-based bispecific adapter proteins, which can increase the transduction of target cells with AAV2RA (Eichhoff A, dissertation MIN faculty, Hamburg, 2018). For the first approach, nanobodies were inserted into a surface loop of the VP1 capsid protein at position 453-459 (GTTTQSR) that had been previously published as a successful insertion position of the fluorescent protein mCherry (95). The CD38 nanobody was provided with a 25 AS long GS-linker so that the N-terminal antigen-binding side of the nanobody can protrude from the capsid. For the second strategy, a CD38-specific nanobody was genetically

fused via a linker peptide to AAV-specific nanobodies. Bispecific adapters thereby link AAVs and the cell surface protein CD38.

An aim of the thesis presented here was to determine whether α CD38 nanobodies can be used to enhance the transduction by recombinant AAV of primary multiple myeloma cells from a patient bone marrow. Transduction efficacy was evaluated by the AAV-containing YFP cassette, which gave a positive signal upon successful transduction. Nanobody-displaying AAV were incubated with primary cells from the patient 2 bone marrow and transduction rate was subsequently analyzed. Display of CD38-specific nanobodies on the AAV capsid resulted in a 20- to 100-fold enhanced transduction of patient 2 myeloma cells. Furthermore, results show that CD38 Nb-AAV-fusion-proteins specifically transduced only CD38/CD138 high expressing MM patient cells and no other CD45+/CD56- patient stroma- and bone marrow cells. This might be most likely due to the selectively high expression of CD38 on myeloma cells, suggesting that this approach might reduce off-target effects. To prove this, an *in vivo* mouse model is needed. Similar results were obtained with the adapter strategy. A successful and specific transduction of CD38/CD138 high expressing MM patient cells was observed, whereas other CD45+/CD56- patient stroma- and bone marrow cells were not transduced. Again, the reason for the high specificity of this method is most likely mediated by the overexpression of CD38 on myeloma cells.

When comparing Nb-AAV-fusion-proteins with the bispecific adaptor approach it can be said that there are certain advantages of adapters over Nb-AAV-fusion-proteins. Bispecific adapters are easy reformattable in terms of exchanging both the receptor-specific Nbs and the AAV-specific Nbs (96). This enables also two identical or different nanobodies that could be linked on the side of the membrane protein as well as on the side of the AAV; avidity of the adapters for the AAVs or for the target cells might be thereby improved. By coating the viral capsid with adapter proteins, immunogenic epitopes of the capsid might be masked or the binding of neutralizing antibodies upon administration could be sterically prevented. Thus, in addition to improving the transduction of patient myeloma cells, the viral capsids could also escape the recognition by the immune system.

However, there are also certain advantages of the fixed incorporation of Nbs into the AAV capsid over bispecific adapters. When it comes to clinical trials with Nb-AAV-fusion-proteins, there is only the safety of one reagent as a therapeutic agent in tumor therapy that would have to be evaluated; for bispecific adapter proteins, the safety of two combined reagents would be necessary to be evaluated in each case. *In vivo* experiments with adapters are also a lot more complex since it needs to be determined whether simultaneous or sequential administration of adapter proteins and AAVs would achieve better effects. As a prerequisite for clinical applications, it will be essential to test both strategies *in vivo* in mouse models. First, it is necessary to evaluate, if the tropism of the AAVs is altered by the incorporation of Nbs or the use of bispecific adapter proteins; And second, the limiting point is whether target cells are also transduced *in vivo*. To test this, GFP- or luciferase-encoding AAVs could be injected into WT mice and target receptor knock-out (KO) mice.

7. Conclusion and Outlook

Acquired and primary resistance to α EGFR- and α CD38 monoclonal antibodies in cancer patients is still a major challenge. The results of this thesis show improved anti-tumor activity of EGFR- and CD38-specific hcAbs carrying CDC- and ADCC-enhancing mutations. The engineered 7D12-hcAbs constructs thus hold promise for closing the therapeutic gap for patients with EGFR ECD variants not responding to cetuximab or panitumumab. Similarly, the Fc engineered WF211 hcAb may have the potential to improve already existing therapy regimes for patients diagnosed with multiple myeloma. Moreover, in primary bone marrow samples from MM patients, the combination of daratumumab with CD38-specific hcAbs that recognize a distinct epitope enhanced CDC- mediated tumor cell lysis compared to daratumumab alone. It is tempting to speculate that small hcAbs might improve the therapeutic efficacy of approved FDA mAbs by binding to distinct epitopes, inhibiting the enzymatic activity of the target protein, inhibit downstream signaling, and/or enhance immune effector functions, such as NK-cell- and complement mediated lysis of tumor cells. Finally, AAV vectors displaying a CD38-specific nanobody were shown to mediate specific transduction of primary multiple myeloma cells from a patient bone marrow with a GFP reporter gene. Similar effects were achieved with bispecific Nb-Nb adaptors. Further studies will show whether this strategy can be used to produce checkpoint inhibitors, pro-inflammatory cytokines or other therapeutic proteins in the tumor microenvironment *in vivo*.

8. Lists

8.1. List of abbreviations

AA	amino acid
AAV	adeno-associated virus
ADCC	antibody-dependent cell-mediated cytotoxicity
ADP	Adenosine diphosphate
ADPR	adenosine diphosphate ribose
cADPR	cyclic adenosine diphosphate ribose
AF647	Alexa fluor 647
AKT	protein kinase
AMP	adenosine monophosphate
ATP	adenosine triphosphate
BSA	bovine serum albumin
bp	base pairs
CDC	complement-dependent cytotoxicity
CD	cluster of differentiation
CDKN2A/C	cyclin dependent kinase inhibitor 2A/C
cDNA	complementary DNA
CDR	complementarity determining region
CH	constant domain of the heavy chain of an antibody
DMEM	cell culture medium (Dulbecco' s modified Eagle medium)
DMSO	dimethylsulfoxid
DNA	deoxyribonucleic acid
dNTPs	2'-desoxyribonucleotide-5'-triphosphate
DTT	cithiothreitol
E. coli	Escherichia coli
EGF	epidermal growth factor
EGFR	epidermal growth factor receptor
ELISA	enzyme-linked Immunosorbent Assay
ERK	extracellular signal-regulated kinase
Fab	antigen-binding fragment of an antibody (fragment antigen binding)
FACS	fluorescent activated cell sorting
Fc	constant CH2 and CH3 domain of an antibody (fragment crystallizable)
FCS	fetal calf serum
FDA	food and drug administration
FGFR3	fibroblast growth factor receptor 3
Fig.	figure
FITC	fluoresceinisothiocyanate
GDP	guanosine diphosphate
cGDPR	cyclic guanosine diphosphate ribose

GFP	green fluorescent protein
GSH	glutathione
GS-X pump	glutathione S-conjugate pump
H	hour
hcAb	heavy chain antibody
HEK	human embryonic kidney
Her	human epidermal growth factor receptor
HNSCC	head and neck squamous cell carcinoma
hIgG1	human IgG1
Ig	immune globulins
IL	interleukin
JAK	janus kinase
kD	kilo Dalton
ko	knockout
KRAS	Kirsten rat sarcoma viral oncogene
mAb	monoclonal antibody
MAPK	mitogen activated protein kinase
mCRC	metastatic colorectal cancer
MEK	mitogen-activated protein kinase/extracellular signal-regulated kinase
min	minute
mIgG2a	mouse IgG2a
MFI	mean fluorescence intensity
mTOR	mechanistic target of rapamycin
MRP1	multidrug resistance protein 1
NaCl	sodium chloride
NAD ⁺	nicotinamide adenine dinucleotide
Nb	nanobody
NCBI	National Center for Biotechnology Information
NGD	nicotinamide guanine dinucleotide
NGS	next generation sequencing
NK cell	natural killer cell
NRAS	neuroblastoma rat sarcoma viral oncogene
OD	optical density
OS	overall survival
PAGE	polyacrylamide gel electrophoresis
PBS	phosphate buffered saline
PCR	polymerase chain reaction
PDB	protein data bank for 3D structures
PDPK1	phosphoinositide-dependent protein kinase 1
PE	phycoerythrin

PEI	polyethylenimine
PFS	progression free survival
PI3K	phosphatidylinositol 3-kinase
RAF	rapidly accelerated fibrosarcoma
RAS	rat sarcoma viral oncogene
rbFc	rabbit Fc
rpm	rounds per minute
RPMI	cell culture medium from the Roswell Park Memorial Institute
RT	room temperature
SDS	sodium dodecyl sulfate
SOC	super optimal broth
SOS	son of sevenless homolog
STAT	signal transducers and activators of transcription
TAE	tris-acetate-EDTA
TCEP	tris(2-carboxyethyl)phosphine
TGF- α	transforming growth factor alpha
TKI	tyrosine kinase inhibitor
Tris	Tris(hydroxymethyl)-aminomethane
U	unit (enzyme)
UV	ultraviolet
Vg	viral genome
VH	variable domain of a heavy chain of an antibody
VHH	variable domain of the heavy chain of heavy chain antibodies
VL	variable domain of the light chain of an antibody
VP	viral protein
WT	wildtype

8.2. List of figures

Fig. 1.1: Model of domain architecture and activation of the EGFR.	2
Fig. 1.2: Model of architecture and enzymatic activity of CD38.	3
Fig. 1.3: Nanobodies from heavy-chain antibodies.	4
Fig. 2: Graphical abstract illustrating the goals of this thesis.	8
Fig. 5.1: Alignment of anti-mouse CD38 VHHs revealed five new nanobody families.....	35
Fig. 5.2: Sequence alignment of wildtype mouse IgG2a and two Fc-engineered mutants for enhanced (ADS, G236A S239D) and reduced (LALAPG, L234A L235A) Fc-mediated effector function.	36
Fig. 5.3: SDS PAGE analyses confirms high level expression and secretion of recombinant mCD38-specific hcAbs by HEK-6E cells.	37
Fig. 5.4: Cross blockade analysis reveals binding of hcAbs to three independent epitopes on mouse CD38.	38
Fig. 5.5: Nbs JK13 and JK16 (family 4) show the slowest, Nb NB11 (family1) the fastest dissociation from mCD38 EL4-thymoma cells.	39
Fig. 5.6: mCD38 EL4-thymoma cells metabolize NAD ⁺ to ADPR.	41
Fig. 5.7: Family 4 and 5 hcAbs inhibit NGD cyclase activity of mCD38 EL4-thymoma cells.	42
Fig. 5.8: Family 4 and 5 hcAbs inhibit mouse CD38 cyclase activity.	43
Fig. 5.9: hcAbs NB38 (family 4) and NB42 (family 5) inhibit mouse CD38 cyclase activity with similar IC ₅₀ values of ~10 nM.	44
Fig. 5.10: The inhibitory effects of hcAbs NB38 (family 4) and NB42 (family 5) is not enhanced by combination with hcAbs from the other family.	45
Fig. 5.11: CD38-specific hcAbs mediate complement-dependent cytotoxicity (CDC) of mCD38-transfected HEK-293T cells.	47
Fig. 5.12: CD38-specific hcAbs mediate antibody dependent cellular cytotoxicity (ADCC) of mCD38 EL4-thymoma.	48
Fig. 5.13: EGFR-specific hcAb 7D12 binds to and reduces the proliferation of cells carrying acquired EGFR escape variants.	50
Fig. 5.14: EGFR-specific hcAb 7D12 inhibits the growth of 3D spheroids of UTSCC14 and SAT human head and neck cancer cell lines.	51
Fig. 5.15: CD38-specific hcAbs of family 2 inhibit the NGD cyclase activity of human LP1 cells.	52
Fig. 5.16: Kinetic analyses of the enzymatic activities of CD38-expressing LP1 cells.	53
Fig. 5.17: The reducing agents DTT, TCEP and GSH affect the production of cADPR and ADPR by LP1 myeloma cells in a dose-dependent manner.	54
Fig. 5.18: The hexabody (E345R) mutant of 7D12-hcAb induces CDC toward HNSCC cell Lines.	55
Fig. 5.19: Fc engineering of hcAb 7D12-hIgG1 enhances ADCC of HNSCC cell lines.	56
Fig. 5.20: Primary MM cells from a patient bone marrow samples survive in culture for 6 days.	57

Fig. 5.21: Daratumumab and combinations of two hcAbs mediate effective CDC of multiple myeloma cells in a patient bone marrow sample at d0 and d6.	59
Fig. 5.22: Daratumumab and combinations of two hcAbs mediate effective CDC of multiple myeloma cells in a patient bone marrow sample at day 6, but not at day 1.	60
Fig. 5.23: Insertion of CD38-specific Nb 1067 into the VP1 capsid protein of AAV2RA enhances transduction of primary MM cells by AAV2RA.	61
Fig. 5.24: Bispecific nanobody adaptors mediate transduction of AAV6 into primary human MM cells.....	62
Fig. 6.1: Binding of the mAb cetuximab and hcAb 7D12 to the EGFR.	67
Fig. 6.2: Binding of hcAbs MU537 and MU523, and mAb isatuximab to CD38.....	69

8.3. List of tables

Table 3.1: Used laboratory devices and the corresponding manufacturer	9
Table 3.2: Used chemicals and the corresponding manufacturer	10
Table 3.3: Composition of used solutions and buffers	11
Table 3.4: Composition of the used media	12
Table 3.5: Antibodies with corresponding characteristics and manufacturer	13
Table 3.6: Plasmids, origin and reference.....	14
Table 3.7: Size standards used for proteins and double-stranded DNA.....	14
Table 3.8: Enzymes for cloning and PCR	15
Table 3.9: Prokaryotic and eukaryotic cell lines	15
Table 4.1: Reagents used for endonuclease mediated digestion of pCSE2.5 vectors.....	20
Table 4.2: Reagents used for endonuclease mediated digestion of pCSE2.5 vectors.....	21
Table 4.3: Reagents used for PCR	24

9. References

1. Hanahan D, Weinberg RA. Hallmarks of cancer: the next generation. *Cell*. 2011;144(5):646-74.
2. Schreiber RD, Old LJ, Smyth MJ. Cancer immunoediting: integrating immunity's roles in cancer suppression and promotion. *Science*. 2011;331(6024):1565-70.
3. Gabrilovich DI, Ostrand-Rosenberg S, Bronte V. Coordinated regulation of myeloid cells by tumours. *Nat Rev Immunol*. 2012;12(4):253-68.
4. Weigert A, Sekar D, Brune B. Tumor-associated macrophages as targets for tumor immunotherapy. *Immunotherapy*. 2009;1(1):83-95.
5. Weiner LM, Surana R, Wang S. Monoclonal antibodies: versatile platforms for cancer immunotherapy. *Nat Rev Immunol*. 2010;10(5):317-27.
6. Scott AM, Wolchok JD, Old LJ. Antibody therapy of cancer. *Nat Rev Cancer*. 2012;12(4):278-87.
7. Chen M, Chen LM, Lin CY, Chai KX. The epidermal growth factor receptor (EGFR) is proteolytically modified by the Matriptase-Prostasin serine protease cascade in cultured epithelial cells. *Biochim Biophys Acta*. 2008;1783(5):896-903.
8. Roepstorff K, Grandal MV, Henriksen L, Knudsen SL, Lerdrup M, Grovdal L, et al. Differential effects of EGFR ligands on endocytic sorting of the receptor. *Traffic*. 2009;10(8):1115-27.
9. Burgess AW, Cho HS, Eigenbrot C, Ferguson KM, Garrett TP, Leahy DJ, et al. An open-and-shut case? Recent insights into the activation of EGF/ErbB receptors. *Mol Cell*. 2003;12(3):541-52.
10. Ferguson KM, Berger MB, Mendrola JM, Cho HS, Leahy DJ, Lemmon MA. EGF activates its receptor by removing interactions that autoinhibit ectodomain dimerization. *Mol Cell*. 2003;11(2):507-17.
11. Yarden Y, Schlessinger J. Epidermal growth factor induces rapid, reversible aggregation of the purified epidermal growth factor receptor. *Biochemistry*. 1987;26(5):1443-51.
12. Zhang X, Gureasko J, Shen K, Cole PA, Kuriyan J. An allosteric mechanism for activation of the kinase domain of epidermal growth factor receptor. *Cell*. 2006;125(6):1137-49.
13. Schmitz KR, Bagchi A, Roovers RC, van Bergen en Henegouwen PM, Ferguson KM. Structural evaluation of EGFR inhibition mechanisms for nanobodies/VHH domains. *Structure*. 2013;21(7):1214-24.
14. Funaro A, Spagnoli GC, Ausiello CM, Alessio M, Roggero S, Delia D, et al. Involvement of the multilineage CD38 molecule in a unique pathway of cell activation and proliferation. *J Immunol*. 1990;145(8):2390-6.
15. Howard M, Grimaldi JC, Bazan JF, Lund FE, Santos-Argumedo L, Parkhouse RM, et al. Formation and hydrolysis of cyclic ADP-ribose catalyzed by lymphocyte antigen CD38. *Science*. 1993;262(5136):1056-9.
16. Deaglio S, Morra M, Mallone R, Ausiello CM, Prager E, Garbarino G, et al. Human CD38 (ADP-ribosyl cyclase) is a counter-receptor of CD31, an Ig superfamily member. *J Immunol*. 1998;160(1):395-402.

17. Albeniz I, Demir O, Turker-Sener L, Yalcintepe L, Nurten R, Bermek E. Erythrocyte CD38 as a prognostic marker in cancer. *Hematology*. 2007;12(5):409-14.
18. Varol B, Coskun O, Karabulut S, Serin KR, Asoglu O, Albeniz I, et al. Clinical significance of serum ADP-ribosylation and NAD glycohydrolase activity in patients with colorectal cancer. *Tumour Biol*. 2014;35(6):5575-82.
19. Malavasi F, Funaro A, Roggero S, Horenstein A, Calosso L, Mehta K. Human CD38: a glycoprotein in search of a function. *Immunol Today*. 1994;15(3):95-7.
20. Morandi F, Morandi B, Horenstein AL, Chillemi A, Quarona V, Zaccarello G, et al. A non-canonical adenosinergic pathway led by CD38 in human melanoma cells induces suppression of T cell proliferation. *Oncotarget*. 2015;6(28):25602-18.
21. Balkwill FR, Capasso M, Hagemann T. The tumor microenvironment at a glance. *J Cell Sci*. 2012;125(Pt 23):5591-6.
22. Cascone T, McKenzie JA, Mbofung RM, Punt S, Wang Z, Xu C, et al. Increased Tumor Glycolysis Characterizes Immune Resistance to Adoptive T Cell Therapy. *Cell Metab*. 2018;27(5):977-87 e4.
23. Roodman GD. Pathogenesis of myeloma bone disease. *Leukemia*. 2009;23(3):435-41.
24. Malavasi F, Deaglio S, Funaro A, Ferrero E, Horenstein AL, Ortolan E, et al. Evolution and function of the ADP ribosyl cyclase/CD38 gene family in physiology and pathology. *Physiol Rev*. 2008;88(3):841-86.
25. Wei W, Graeff R, Yue J. Roles and mechanisms of the CD38/cyclic adenosine diphosphate ribose/Ca(2+) signaling pathway. *World J Biol Chem*. 2014;5(1):58-67.
26. Tohgo A, Takasawa S, Noguchi N, Koguma T, Nata K, Sugimoto T, et al. Essential cysteine residues for cyclic ADP-ribose synthesis and hydrolysis by CD38. *J Biol Chem*. 1994;269(46):28555-7.
27. Rutkowski MJ, Sughrue ME, Kane AJ, Mills SA, Parsa AT. Cancer and the complement cascade. *Mol Cancer Res*. 2010;8(11):1453-65.
28. Wang X, Mathieu M, Brezski RJ. IgG Fc engineering to modulate antibody effector functions. *Protein Cell*. 2018;9(1):63-73.
29. Braig F, Kriegs M, Voigtlaender M, Habel B, Grob T, Biskup K, et al. Cetuximab Resistance in Head and Neck Cancer Is Mediated by EGFR-K521 Polymorphism. *Cancer Res*. 2017;77(5):1188-99.
30. Ciardiello F, Tortora G. EGFR antagonists in cancer treatment. *N Engl J Med*. 2008;358(11):1160-74.
31. Schneider-Merck T, Lammerts van Bueren JJ, Berger S, Rossen K, van Berkel PH, Derer S, et al. Human IgG2 antibodies against epidermal growth factor receptor effectively trigger antibody-dependent cellular cytotoxicity but, in contrast to IgG1, only by cells of myeloid lineage. *J Immunol*. 2010;184(1):512-20.
32. Veluchamy JP, Spanholtz J, Tordoir M, Thijssen VL, Heideman DA, Verheul HM, et al. Combination of NK Cells and Cetuximab to Enhance Anti-Tumor Responses in RAS Mutant Metastatic Colorectal Cancer. *PLoS One*. 2016;11(6):e0157830.

33. Dechant M, Weisner W, Berger S, Peipp M, Beyer T, Schneider-Merck T, et al. Complement-dependent tumor cell lysis triggered by combinations of epidermal growth factor receptor antibodies. *Cancer Res.* 2008;68(13):4998-5003.
34. Mathern DR, Heeger PS. Molecules Great and Small: The Complement System. *Clin J Am Soc Nephrol.* 2015;10(9):1636-50.
35. Bardelli A, Siena S. Molecular mechanisms of resistance to cetuximab and panitumumab in colorectal cancer. *J Clin Oncol.* 2010;28(7):1254-61.
36. Wheeler DL, Dunn EF, Harari PM. Understanding resistance to EGFR inhibitors-impact on future treatment strategies. *Nat Rev Clin Oncol.* 2010;7(9):493-507.
37. Giampieri R, Scartozzi M, Del Prete M, Maccaroni E, Bittoni A, Faloppi L, et al. Molecular biomarkers of resistance to anti-EGFR treatment in metastatic colorectal cancer, from classical to innovation. *Crit Rev Oncol Hematol.* 2013;88(2):272-83.
38. Braig F, Marz M, Schieferdecker A, Schulte A, Voigt M, Stein A, et al. Epidermal growth factor receptor mutation mediates cross-resistance to panitumumab and cetuximab in gastrointestinal cancer. *Oncotarget.* 2015;6(14):12035-47.
39. Arena S, Bellosillo B, Siravegna G, Martinez A, Canadas I, Lazzari L, et al. Emergence of Multiple EGFR Extracellular Mutations during Cetuximab Treatment in Colorectal Cancer. *Clin Cancer Res.* 2015;21(9):2157-66.
40. Montagut C, Dalmases A, Bellosillo B, Crespo M, Pairet S, Iglesias M, et al. Identification of a mutation in the extracellular domain of the Epidermal Growth Factor Receptor conferring cetuximab resistance in colorectal cancer. *Nat Med.* 2012;18(2):221-3.
41. Overdijk MB, Jansen JH, Nederend M, Lammerts van Bueren JJ, Groen RW, Parren PW, et al. The Therapeutic CD38 Monoclonal Antibody Daratumumab Induces Programmed Cell Death via Fcγ Receptor-Mediated Cross-Linking. *J Immunol.* 2016;197(3):807-13.
42. van de Donk NW, Janmaat ML, Mutis T, Lammerts van Bueren JJ, Ahmadi T, Sasser AK, et al. Monoclonal antibodies targeting CD38 in hematological malignancies and beyond. *Immunol Rev.* 2016;270(1):95-112.
43. Deckert J, Wetzel MC, Bartle LM, Skaletskaya A, Goldmacher VS, Vallee F, et al. SAR650984, a novel humanized CD38-targeting antibody, demonstrates potent antitumor activity in models of multiple myeloma and other CD38+ hematologic malignancies. *Clin Cancer Res.* 2014;20(17):4574-83.
44. Krejcik J, Casneuf T, Nijhof IS, Verbist B, Bald J, Plesner T, et al. Daratumumab depletes CD38+ immune regulatory cells, promotes T-cell expansion, and skews T-cell repertoire in multiple myeloma. *Blood.* 2016;128(3):384-94.
45. Zhang L, Tai YT, Ho M, Xing L, Chauhan D, Gang A, et al. Regulatory B cell-myeloma cell interaction confers immunosuppression and promotes their survival in the bone marrow milieu. *Blood Cancer J.* 2017;7(3):e547.
46. Costa F, Toscani D, Chillemi A, Quarona V, Bolzoni M, Marchica V, et al. Expression of CD38 in myeloma bone niche: A rational basis for the use of anti-CD38 immunotherapy to inhibit osteoclast formation. *Oncotarget.* 2017;8(34):56598-611.

47. Morandi F, Marimpietri D, Horenstein AL, Bolzoni M, Toscani D, Costa F, et al. Microvesicles released from multiple myeloma cells are equipped with ectoenzymes belonging to canonical and non-canonical adenosinergic pathways and produce adenosine from ATP and NAD(). *Oncoimmunology*. 2018;7(8):e1458809.
48. Russo A, Russo G. Ribosomal Proteins Control or Bypass p53 during Nucleolar Stress. *Int J Mol Sci*. 2017;18(1).
49. Zhan F, Huang Y, Colla S, Stewart JP, Hanamura I, Gupta S, et al. The molecular classification of multiple myeloma. *Blood*. 2006;108(6):2020-8.
50. Avet-Loiseau H, Attal M, Moreau P, Charbonnel C, Garban F, Hulin C, et al. Genetic abnormalities and survival in multiple myeloma: the experience of the Intergroupe Francophone du Myelome. *Blood*. 2007;109(8):3489-95.
51. Hsu PP, Sabatini DM. Cancer cell metabolism: Warburg and beyond. *Cell*. 2008;134(5):703-7.
52. Wang T, Kumru OS, Yi L, Wang YJ, Zhang J, Kim JH, et al. Effect of ionic strength and pH on the physical and chemical stability of a monoclonal antibody antigen-binding fragment. *J Pharm Sci*. 2013;102(8):2520-37.
53. Bronte V. Tumor cells hijack macrophages via lactic acid. *Immunol Cell Biol*. 2014;92(8):647-9.
54. Dosani T, Carlsten M, Maric I, Landgren O. The cellular immune system in myelomagenesis: NK cells and T cells in the development of myeloma [corrected] and their uses in immunotherapies. *Blood Cancer J*. 2015;5:e306.
55. Gottfried E, Kunz-Schughart LA, Ebner S, Mueller-Klieser W, Hoves S, Andreessen R, et al. Tumor-derived lactic acid modulates dendritic cell activation and antigen expression. *Blood*. 2006;107(5):2013-21.
56. Gorgun GT, Whitehill G, Anderson JL, Hideshima T, Maguire C, Laubach J, et al. Tumor-promoting immune-suppressive myeloid-derived suppressor cells in the multiple myeloma microenvironment in humans. *Blood*. 2013;121(15):2975-87.
57. Nijhof IS, Casneuf T, van Velzen J, van Kessel B, Axel AE, Syed K, et al. CD38 expression and complement inhibitors affect response and resistance to daratumumab therapy in myeloma. *Blood*. 2016;128(7):959-70.
58. Wang D, Tai PWL, Gao G. Adeno-associated virus vector as a platform for gene therapy delivery. *Nat Rev Drug Discov*. 2019;18(5):358-78.
59. High KA, Roncarolo MG. Gene Therapy. *N Engl J Med*. 2019;381(5):455-64.
60. Pasi KJ, Rangarajan S, Mitchell N, Lester W, Symington E, Madan B, et al. Multiyear Follow-up of AAV5-hFVIII-SQ Gene Therapy for Hemophilia A. *N Engl J Med*. 2020;382(1):29-40.
61. Eichhoff AM, Borner K, Albrecht B, Schafer W, Baum N, Haag F, et al. Nanobody-Enhanced Targeting of AAV Gene Therapy Vectors. *Mol Ther Methods Clin Dev*. 2019;15:211-20.
62. Koch-Nolte F, Duffy T, Nissen M, Kahl S, Killeen N, Ablamunits V, et al. A new monoclonal antibody detects a developmentally regulated mouse ecto-ADP-

- ribosyltransferase on T cells: subset distribution, inbred strain variation, and modulation upon T cell activation. *J Immunol.* 1999;163(11):6014-22.
63. Lo M, Kim HS, Tong RK, Bainbridge TW, Vernes JM, Zhang Y, et al. Effector-attenuating Substitutions That Maintain Antibody Stability and Reduce Toxicity in Mice. *J Biol Chem.* 2017;292(9):3900-8.
64. de Jong RN, Beurskens FJ, Verploegen S, Strumane K, van Kampen MD, Voorhorst M, et al. A Novel Platform for the Potentiation of Therapeutic Antibodies Based on Antigen-Dependent Formation of IgG Hexamers at the Cell Surface. *PLoS Biol.* 2016;14(1):e1002344.
65. Fumey W, Koenigsdorf J, Kunick V, Menzel S, Schutze K, Unger M, et al. Nanobodies effectively modulate the enzymatic activity of CD38 and allow specific imaging of CD38(+) tumors in mouse models in vivo. *Sci Rep.* 2017;7(1):14289.
66. Schlothauer T, Herter S, Koller CF, Grau-Richards S, Steinhart V, Spick C, et al. Novel human IgG1 and IgG4 Fc-engineered antibodies with completely abolished immune effector functions. *Protein Eng Des Sel.* 2016;29(10):457-66.
67. Nimmerjahn F, Bruhns P, Horiuchi K, Ravetch JV. FcγR4: a novel FcR with distinct IgG subclass specificity. *Immunity.* 2005;23(1):41-51.
68. Chillemi A, Quarona V, Antonioli L, Ferrari D, Horenstein AL, Malavasi F. Roles and Modalities of Ectonucleotidases in Remodeling the Multiple Myeloma Niche. *Front Immunol.* 2017;8:305.
69. de Weers M, Tai YT, van der Veer MS, Bakker JM, Vink T, Jacobs DC, et al. Daratumumab, a novel therapeutic human CD38 monoclonal antibody, induces killing of multiple myeloma and other hematological tumors. *J Immunol.* 2011;186(3):1840-8.
70. Schutze K, Petry K, Hambach J, Schuster N, Fumey W, Schriewer L, et al. CD38-Specific Biparatopic Heavy Chain Antibodies Display Potent Complement-Dependent Cytotoxicity Against Multiple Myeloma Cells. *Front Immunol.* 2018;9:2553.
71. Diebolder CA, Beurskens FJ, de Jong RN, Koning RI, Strumane K, Lindorfer MA, et al. Complement is activated by IgG hexamers assembled at the cell surface. *Science.* 2014;343(6176):1260-3.
72. Gainkam LO, Huang L, Caveliers V, Keyaerts M, Hernot S, Vaneycken I, et al. Comparison of the biodistribution and tumor targeting of two ^{99m}Tc-labeled anti-EGFR nanobodies in mice, using pinhole SPECT/micro-CT. *J Nucl Med.* 2008;49(5):788-95.
73. Huang L, Gainkam LO, Caveliers V, Vanhove C, Keyaerts M, De Baetselier P, et al. SPECT imaging with ^{99m}Tc-labeled EGFR-specific nanobody for in vivo monitoring of EGFR expression. *Mol Imaging Biol.* 2008;10(3):167-75.
74. Roovers RC, Laeremans T, Huang L, De Taeye S, Verkleij AJ, Revets H, et al. Efficient inhibition of EGFR signaling and of tumour growth by antagonistic anti-EGFR Nanobodies. *Cancer Immunol Immunother.* 2007;56(3):303-17.

75. Roovers RC, Vosjan MJ, Laeremans T, el Khoulati R, de Bruin RC, Ferguson KM, et al. A biparatopic anti-EGFR nanobody efficiently inhibits solid tumour growth. *Int J Cancer*. 2011;129(8):2013-24.
76. Strickler JH, Loree JM, Ahronian LG, Parikh AR, Niedzwiecki D, Pereira AAL, et al. Genomic Landscape of Cell-Free DNA in Patients with Colorectal Cancer. *Cancer Discov*. 2018;8(2):164-73.
77. Wang Y, Zha L, Liao D, Li X. A Meta-Analysis on the Relations between EGFR R521K Polymorphism and Risk of Cancer. *Int J Genomics*. 2014;2014:312102.
78. Stoecklacher-Williams J, Obermann L, Ehninger G, Goekkurt E. Polymorphisms of the epidermal growth factor receptor (EGFR) and survival in patients with advanced cancer of the head and neck (HNSCC). *Anticancer Res*. 2012;32(2):421-5.
79. Klinghammer K, Knodler M, Schmitt A, Budach V, Keilholz U, Tinhofer I. Association of epidermal growth factor receptor polymorphism, skin toxicity, and outcome in patients with squamous cell carcinoma of the head and neck receiving cetuximab-docetaxel treatment. *Clin Cancer Res*. 2010;16(1):304-10.
80. Schriewer L, Schutze K, Petry K, Hambach J, Fumey W, Koenigsdorf J, et al. Nanobody-based CD38-specific heavy chain antibodies induce killing of multiple myeloma and other hematological malignancies. *Theranostics*. 2020;10(6):2645-58.
81. Kang YJ, Enger MD. Glutathione content and growth in A549 human lung carcinoma cells. *Exp Cell Res*. 1990;187(1):177-9.
82. Hall AG. Review: The role of glutathione in the regulation of apoptosis. *Eur J Clin Invest*. 1999;29(3):238-45.
83. Ketterer B. Protective role of glutathione and glutathione transferases in mutagenesis and carcinogenesis. *Mutat Res*. 1988;202(2):343-61.
84. Traverso N, Ricciarelli R, Nitti M, Marengo B, Furfaro AL, Pronzato MA, et al. Role of glutathione in cancer progression and chemoresistance. *Oxid Med Cell Longev*. 2013;2013:972913.
85. Mitchell JB, Biaglow JE, Russo A. Role of glutathione and other endogenous thiols in radiation protection. *Pharmacol Ther*. 1988;39(1-3):269-74.
86. Schafer FQ, Buettner GR. Redox environment of the cell as viewed through the redox state of the glutathione disulfide/glutathione couple. *Free Radic Biol Med*. 2001;30(11):1191-212.
87. Meister A. Selective modification of glutathione metabolism. *Science*. 1983;220(4596):472-7.
88. Backos DS, Franklin CC, Reigan P. The role of glutathione in brain tumor drug resistance. *Biochem Pharmacol*. 2012;83(8):1005-12.
89. de Bittencourt Junior PI, Curi R, Williams JF. Glutathione metabolism and glutathione S-conjugate export ATPase (MRP1/GS-X pump) activity in cancer. I. Differential expression in human cancer cell lines. *Biochem Mol Biol Int*. 1998;45(6):1227-41.
90. Wang B, Yang C, Jin X, Du Q, Wu H, Dall'Acqua W, et al. Regulation of antibody-mediated complement-dependent cytotoxicity by modulating the intrinsic affinity and binding valency of IgG for target antigen. *MAbs*. 2020;12(1):1690959.

91. Sanchez L, Wang Y, Siegel DS, Wang ML. Daratumumab: a first-in-class CD38 monoclonal antibody for the treatment of multiple myeloma. *J Hematol Oncol*. 2016;9(1):51.
92. Manier S, Sacco A, Leleu X, Ghobrial IM, Roccaro AM. Bone marrow microenvironment in multiple myeloma progression. *J Biomed Biotechnol*. 2012;2012:157496.
93. Rao L, Giannico D, Leone P, Solimando AG, Maiorano E, Caporusso C, et al. HB-EGF-EGFR Signaling in Bone Marrow Endothelial Cells Mediates Angiogenesis Associated with Multiple Myeloma. *Cancers (Basel)*. 2020;12(1).
94. Podar K, Anderson KC. Inhibition of VEGF signaling pathways in multiple myeloma and other malignancies. *Cell Cycle*. 2007;6(5):538-42.
95. Judd J, Wei F, Nguyen PQ, Tartaglia LJ, Agbandje-McKenna M, Silberg JJ, et al. Random Insertion of mCherry Into VP3 Domain of Adeno-associated Virus Yields Fluorescent Capsids With no Loss of Infectivity. *Mol Ther Nucleic Acids*. 2012;1:e54.
96. Els Conrath K, Lauwereys M, Wyns L, Muyldermans S. Camel single-domain antibodies as modular building units in bispecific and bivalent antibody constructs. *J Biol Chem*. 2001;276(10):7346-50.
97. Cherkasova E, Espinoza L, Kotecha R, Reger N R, Berg M, Aue G, Attar M R, A Sasser K, Carlsten M, Childs W R, Treatment of Ex Vivo Expanded NK Cells with Daratumumab F(ab')₂ Fragments Protects Adoptively Transferred NK Cells from Daratumumab-Mediated Killing and Augments Daratumumab-Induced Antibody Dependent Cellular Toxicity (ADCC) of Myeloma. *Blood* (2015) 126 (23): 4244.

10. Acknowledgements

These acknowledgements go out to everyone, who was swimming with me on my sine wave with all the lab related ups and downs the last 4 years.

First of all, I want to thank my doctor father Prof. Dr. Friedrich Koch-Nolte. Getting to know you first as a cooperation partner; Later on, you “adopted” me into your group. You have given me the chance to continue my PhD in your group, even though the position in that form did not even exist at the beginning. You helped me getting back into my professional career after being forced to pause health-wise. I am deeply grateful for your trust in me and my work and for the scientific freedom you always have given me. I enjoyed all our discussions and I am so thankful for you patiently answering my infinite number of questions □ I also want to thank PD Dr. Peter Bannas for the constructive weekly lab meetings. For your great help and support with all obstacles that had to be overcome, I just want to express my gratitude to both of you.

Additionally, I want to thank Prof. Dr. Mascha Binder for allowing me to perform all EGFR-relevant experiments in her lab. Thank you very much for helping me with any kind of issue, for always being available at every day and nighttime and for your incredible scientific drive. Doing research with you was a lot of fun and I learnt a lot.

Furthermore, I just will name a few colleagues here, but I really want to express my gratitude to every one of the Ifi institute creating this friendly and creative working environment. Julia, you always lift up the energy in the lab. I have never seen a person who is in such good mood and so helpful on a continuous basis, no matter if I had FACS- or AI-issues. Katha, Marie and Marten, you mediated between the Celesta and me until we became friends. My friend Marten, I really appreciate all the time you invested in showing me how to properly use FloJow and for explaining me how to best analyze FACS-data. Thomas, Stephan, and Tobi: thanks for helping me out with molecular issues. Although I only saw a labyrinth of alphabetic letters in the beginning, you helped me translate those patterns into DNA and AA codes. Waldi, thanks for all the fun times, our scientific discussions and our reflected talks about the sense of our “Being”. Fabienne, Josi, Natalie and Gudrun, our TA-angels: You always had answers to questions that I didn’t even know I had. Without you, good research would not be possible.

A big thanks goes out to my cooperation partners Dr. Ralf Fliegert and Prof. Dr. Matthias Peipp. Ralf, I will miss the white board with your drawings. I am really grateful for your help on all levels: experimental set up, data evaluation and scientific discussions. I also thank your TA-angels Frederike and Andreas, who helped me calculate an infinite amount of dilutional series. Matthias, waking up in Hamburg so early to start various ADCC assays in Kiel at 7am was hard, but I was always looking forward to our car rides to Kiel. Thanks for your support during this time and also after our cooperation.

Last, but most importantly I want to thank my family. Mum, dad and Tini, thank you for your continuous support and your understanding, when I got to experience my different frustration levels □ Max, thanks for your daily support and for coming to Hamburg in 98% of the cases ~~and~~ being mad with me that I mostly was lab-related inflexible of coming to Berlin. Sascha, Jörn and Anya, you have become a part of my family. Thank you for bringing me back into amazing physical, mental and vocal health, respectively. Fritzi, I am so grateful for all EGFR-related discussions and our friendship. Thanks to my Ghanaian family: you guys carried me through the most difficult times and prayed for me. And my biggest appreciation is for my little nephew Harro; You made me understand how unconditional love without expectations truly feels: it’s not related to what we do, how we look, what academic title we carry ... You don’t do much yet, but I love you unconditionally, just because of your being. Life and PhD has become so easy, since you arrived.

11. Declaration on oath/Eidesstattliche Versicherung

I hereby declare on oath that I have written the present dissertation independently and have not used further resources and aids than those stated.

Hiermit erkläre ich an Eides statt, dass ich die vorliegende Dissertationsschrift selbst verfasst und keine anderen als die angegebenen Quellen und Hilfsmittel benutzt habe.

I would like to thank Dr. Stephan Menzel and Lynn Dieckow for their support in performing phage display, Katharina Petry, Jana Röckendorf, Julia Hambach and Marten Junge for their assistance with the flow cytometrically analyzed patient samples, Ralf Fliegert, Frederike Kulow and Andreas Bauche for their help with HPLC- and Tecan fluorometric analyses, Prof. Dr. Matthias Peipp and Dr. Thies Rössner for their support with ADCC analyses of HNSCC and mCRC cell lines, and Prof. Dr. Mascha Binder for her support in performing all EGFR-relevant experiments at her laboratory.

Hamburg, 24.11.2020

City, date



Natalie Baum

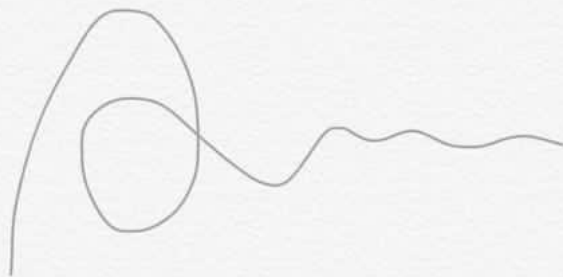
12. Confirmation of accurate language

17 November 2020 at 10:07

11/17/20

To whom it may concern:

I am a native English speaker and certify that I have read Natalie Baum's thesis for English accuracy.

A handwritten signature in dark ink, consisting of a large, stylized 'S' followed by a series of loops and a wavy line extending to the right.

Sarah Pannone, Ed.D
Assistant Professor, School of Education

LIBERTY
UNIVERSITY